PRECISION SELENODESY VIA DIFFERENTIAL VERY-LONG-BASELINE INTERFEROMETRY

by

ROBERT WILSON KING, JR.

B.S., Davidson College

1970

B.S., North Carolina State University

1970

SUBMITTED IN PARTIAL FULFILLMENT
OF THE REQUIREMENTS FOR THE
DEGREE OF DOCTOR OF PHILOSOPHY
IN INSTRUMENTATION

at the

MASSACHUSETTS INSTITUTE OF TECHNOLOGY

June 1975

Signature of Author Signature redacted

Certified by Signature redacted
Thesis Supervisor

Certified by Signature redacted
Thesis Supervisor

Certified by Signature redacted
Thesis Supervisor

Accepted by Signature redacted
Chairman, Departmental Graduate Committee

Archives
MASS. INST. TECH.
OCT 6 1975
LIBRARIES

PRECISION SELENODESY VIA DIFFERENTIAL VERY-LONG-BASELINE INTERFEROMETRY

by

Robert W. King, Jr.

Submitted to the Department of Aeronautics and Astronautics on May 12, 1975, in partial fulfillment of the requirements for the degree of Doctor of Philosophy

ABSTRACT

The technique of differential very-long-baseline interferometry (VLBI) has been used to measure the relative positions of the ALSEP transmitters at the Apollo 12, 14, 15, 16, and 17 lunar landing sites with uncertainties less than 0".005 of geocentric arc. These measurements have yielded improved determinations of the selenodetic coordinates of the Apollo landing sites, and of the physical libration of the moon.

By means of a new device, the Differential Doppler Receiver (DDR), instrumental errors were reduced to less than the equivalent of 0".001. DDRs were installed in six stations of the NASA Spaceflight Tracking and Data Network (STDN) and used in an extensive program of observations beginning in March 1973. Data obtained over a 16-month period were used simultaneously with lunar laser ranging data in least-squares solutions for the 6 elements of the lunar orbit, the mass of the earth-moon system, the 2 lunar moment-of-inertia ratios $\beta[\equiv(C-A)/B]$ and $\gamma[\equiv(B-A)/C]$, 7 third-degree harmonic coefficients of the moon's gravitational potential, 6 initial conditions of the physical libration, and 3 coordinates each of the observing stations, ALSEP transmitters, and laser ranging retroreflectors. The uncertainties in the relative coordinates of the 5 ALSEP transmitters, estimated from the consistency between solutions with independent sets of VLBI data and from the consistency between VLBI and laser ranging results, are 30 m in the radial coordinates and 10 m in the two transverse coordinates. Values determined for the libration parameters

β, C_{31}, and C_{33} have uncertainties smaller than the uncertainties obtained when laser ranging data alone is used in the solution. The rms of the postfit residuals for the VLBI observations is 16° of phase (at 2.3 GHz), about 2 times larger than the random noise level. The systematic components in the residuals may result from unmodeled propagation-medium effects.

Thesis Supervisors:

Charles C. Counselman III, Ph.D.
Title: Associate Professor of Planetary Science

Irwin I. Shapiro, Ph.D.
Title: Professor of Physics and Geophysics

Robert D. Reasenberg, Ph.D.
Title: Research Staff

ACKNOWLEDGEMENTS

The ALSEP differential VLBI experiment described by this thesis could not have been accomplished without the efforts of many people. The impetus for undertaking the observations came from Irwin I. Shapiro, Hans F. Hinteregger, and Charles C. Counselman, III, in 1970, even before I began my work. To Hans Hinteregger and Chuck Counselman belongs the credit for conceiving and building the Differential Doppler Receiver. Without this device the observations made would not have been of high enough quality to warrant the analysis performed in this thesis. I am grateful for the assistance of Irving M. Salzberg, H. Wade Stonesifer, and especially James W. Ryan of Goddard Space Flight Center in arranging the use of the NASA Spaceflight Tracking and Data Network. The observations have continued successfully for over two years as a result of their cooperation and also the efforts of the personnel at the six tracking stations. The task of preparing the data for final processing at M.I.T. has been accomplished with the considerable assistance of William R. Snow, Richard G. Dower, Juanita O. Hope, Robert F. Willson, Sean K.

Collins, Robert C. Burchsted, Frank T. Chang, and J. Lynn Hall.

I have also received valuable assistance from people working at other institutions on the physical libration problem. I wish to thank particularly Drs. James G. Williams and Martin A. Slade of the Jet Propulsion Laboratory, Dr. Donald H. Eckhardt of the Air Force Cambridge Research Laboratories, and Dr. Peter L. Bender of the National Bureau of Standards and the University of Colorado. I am grateful to the NASA Lunar Laser Ranging Experiment (LURE) team for providing me with ranging data covering the period of the VLBI observations.

In my five years as a graduate student at M.I.T. I have received the support of many people, each of whom has taught me, usually by personal example, the methods of good scientific research. I would like to thank Dr. Robert G. Stern, my supervisor in the Measurement Systems Laboratory, for guiding my early work as a graduate student. I also wish to thank Dr. Robert D. Reasenberg for encouraging my early work, for much helpful technical advice, and for teaching me the effective use of the computer. I am grateful to Dr. Michael E. Ash of Lincoln Laboratory for his continuing work in developing the Planetary Ephemeris Program, which I used for all of the data reduction for this thesis. Most of all I wish to thank my thesis advisors, Professors Counselman and Shapiro, who have provided both the inspiration and principal support for my graduate education. I am grateful especially to Chuck Counselman

for the attention, care and criticism he has given to this thesis. Finally, many other people, too numerous to mention, have contributed to my graduate education through helpful discussions over the years; I would like to thank especially Robert A. Preston, Stephen P. Synnott, and R. Denis White for their contributions.

My greatest debt is to my wife and parents, without whose unfailing support none of this work would have been possible.

This research was supported in part by the National Aeronautics and Space Administration, under grants NGL-22-009-187 and NSG 7010 from the Lunar Programs Office, and contract NAS 5-11947 from Goddard Space Flight Center; and by the Air Force Cambridge Research Laboratories, under contracts F19628-20-C-0009, F19628-73-C-0248, and F19628-74-C-0027. The computation was performed at the Charles Stark Draper Laboratory, at the M.I.T. Laboratory for Nuclear Science, and at Goddard Space Flight Center. I am grateful to Dr. Thomas A. Clark of Goddard for arranging the use of that center's computational facilities.

I am grateful to Judith B. Ungermann for the excellent typing of this thesis.

TABLE OF CONTENTS

		Page
CHAPTER I:	INTRODUCTION	10
CHAPTER II:	BASIC CONCEPTS	22
	2.1 Counted-cycle VLBI	22
	2.2 Information Content of the Differential VLBI Observable	28
CHAPTER III:	EXPERIMENTAL EQUIPMENT AND PROCEDURE	41
	3.1 Unified S-Band System of the NASA Spaceflight Tracking and Data Network	41
	3.2 M.I.T. Differential Doppler Receiver	46
	3.3 Observation Procedure	54
	3.4 Scheduling and Data Collection	57
CHAPTER IV:	DATA PROCESSING TECHNIQUES	61
	4.1 Method of Parameter Estimation	61
	4.2 Theoretical Model for the Observable	66
	4.2.1 Basic Formulation	66
	4.2.2 Evaluation of Propagation Delays	72
	4.2.3 Determination of Transmitter Frequencies	75

CHAPTER IV (continued)

		Page
4.3	Model for the Rotation of the Moon	84
4.4	Partial Derivatives of the Observable with Respect to Parameters	93
4.4.1	Partials with Respect to Parameters of the Lunar Orbit	94
4.4.2	Partials with Respect to the ALSEP Selenodetic Coordinates	95
4.4.3	Partials with Respect to Libration Parameters	96
4.4.4	Partials with Respect to Site Coordinates and Precession Quantities	99
4.4.5	Partials with Respect to Bias Parameter	100
4.5	Error Analysis	101
4.5.1	Instrumental Effects	101
4.5.2	Propagation Medium Effects	104
4.5.3	Effect of Errors in the Dynamical Model of the Earth-Moon System	110

CHAPTER V: RESULTS

5.1	Introduction	113
5.2	Libration Parameters	123
5.3	ALSEP Coordinates	130
5.4	Discussion	136

			Page
CHAPTER VI:	CONCLUSIONS		138
	6.1	Summary	138
	6.2	Suggestions for Further Study	139
	6.3	Applications	140
APPENDICES:	A.1	Units and Parameter Values in the Theoretical Model	143
		A.1.1 Units	143
		A.1.2 Parameters of the Lunar Orbit	145
		A.1.3 Parameters of the JPL Libration Model (LLB-5)	146
	A.2	List of Observations	148
	A.3	Derivation of Terms in the Differential VLBI Observable Resulting from the Moon's Horizontal Parallax	163
REFERENCES			168
BIOGRAPHICAL NOTE			173

CHAPTER I

Introduction

The moon has always been a prime object of study by astronomers, and observations of its motion have important uses in many fields, for example to test gravitational theories and to measure variations in the earth's rotation. In order to interpret these observations, theories of both the orbital and the librational motions of the moon are required. However, until recently the development of libration theories [20, 23] received much less attention than did orbital theories, due to the limitations of ground-based passive optical observations, which for a long time were the only observations available. The departure from uniform rotation represented by the forced or "physical" libration is less than 2 seconds of arc as viewed from earth, near the resolution limit imposed by "seeing" fluctuations. Recently, however, the placement on the lunar surface of man-made optical reflectors and radio transmitters and the development of instrumentation allowing extremely accurate earth-based measurements have stimulated a new interest in the theory of lunar librations. This thesis is concerned with the first use of differential very-long-baseline interferometry

(VLBI) to measure the relative positions of radio transmitters on the lunar surface, and to determine the physical libration by observation of the apparent time-variation of the relative transmitter positions.

Radio tracking of objects on or near the moon has been carried out in the U.S. since the first Ranger mission in 1964 and has continued through the Surveyor, Lunar Orbiter, and Apollo programs. However, the tracking transmitters for these missions operated only for short times, and the tracking data were not suitable for the determination of positions on the moon with uncertainties less than 100 meters [44, 36, 29]. The potential for a longer-duration and higher-accuracy program of radio observations was created by the last five Apollo missions, each of which left on the moon a nuclear-powered ALSEP* with an S-band (~2.3 GHz) transmitter (Figure 1.1). These transmitters have only free-running crystal oscillators and are not able to be tracked by the usual two-way Doppler-shift or ranging methods used for spacecraft with transponders. However, they do provide strong signals suitable for angular-position measurements by VLBI.

---

*ALSEP is an acronym for Apollo Lunar Surface Experiments Package.

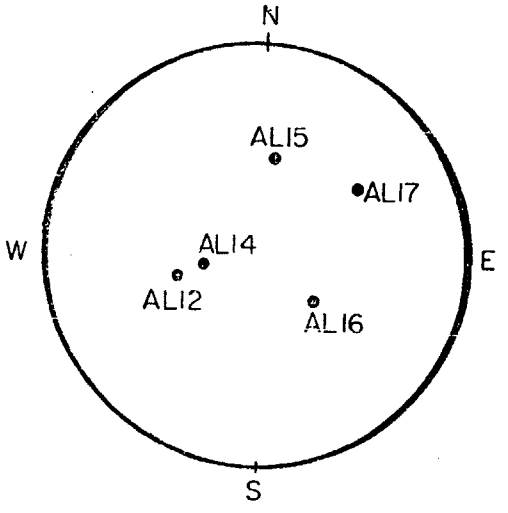


Fig. 1.1 ALSEP transmitters operating in May 1975.

In interferometry, the phases of the signals received from a source simultaneously at two separated ground stations are compared. As the interferometer baseline rotates relative to the source, the difference between the phases changes. The direction of the source with respect to the baseline is determined from this phase variation (see Figure 1.2). The existence of more than one ALSEP transmitter permits the use of the technique of differential interferometry [11], in which the difference in phase of the signal received from one ALSEP at two stations is subtracted from the corresponding difference for another ALSEP. The resulting doubly-

differenced observable is sensitive to the relative right ascension and declination of the two ALSEP transmitters, and is relatively insensitive to those other parameters such as the moon's orbital position, the observing site positions, receiver local oscillator stability and the phase fluctuations introduced by the earth's atmosphere and ionosphere, which tend to affect the observations of both transmitters equally.

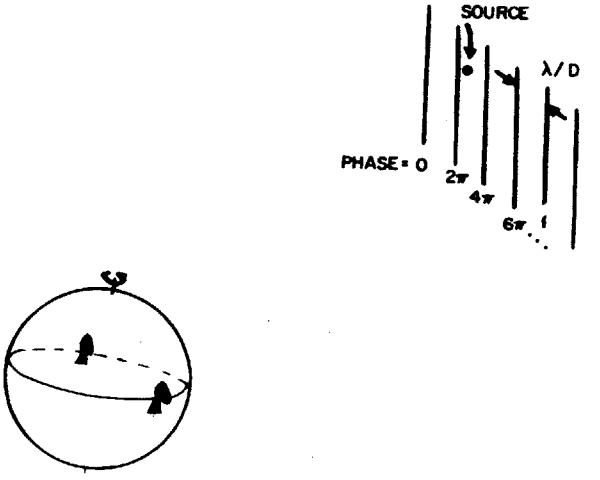


Fig. 1.2 Radio source position determination by VLBI. A change of phase by 2π rad (1 full cycle) corresponds to a source position angle change of λ/D rad, where λ is the wavelength of the radio signal and D is the distance between the stations projected onto a plane perpendicular to the direction of the source. For ALSEP observations such as reported in this thesis ($\lambda \simeq 13.2$ cm, $D \simeq 4000$ km) the phase change can be determined with an uncertainty of less than 10°. Were there no systematic errors present, this phase uncertainty would correspond to an angular uncertainty of less than 10^{-9} rad or a displacement uncertainty of only 40 cm at the distance of the moon [19].

The idea to apply the VLBI technique to study the motions of the moon stems from a 1968 proposal made to the National Aeronautics and Space Administration (NASA) by H. F. Hinteregger and I. I. Shapiro of M.I.T., through the M.I.T. Center for Space Research, to add a wideband ($\simeq$ 50 MHz) noise source, center frequency near 8 GHz, to each ALSEP package. The choice of such an X-band frequency range was based primarily on the desire for the reduction of ionospheric effects on the VLBI observables to a negligible level and for the achievement of compatibility with then-existing ground-based VLBI equipment. The scientific objectives included the determination of the motion of the moon's center of mass through differential VLBI observations of the ALSEPs and compact extragalactic radio sources that are nearly occulted by the moon, as well as the determination of the moon's motion about its center of mass through differential VLBI observations of two or more ALSEPs. This Lunar Radio Beacon proposal was not accepted by NASA. Thereafter, C. C. Counselman III, of M.I.T., along with Hinteregger and Shapiro, elicited the cooperation of I. M. Salzberg of the Goddard Space Flight Center of NASA to attempt to use the narrowband, lower frequency, S-band signals from the ALSEP telemetry system to meet many of the same scientific objectives.

The resultant MIT-GSFC cooperation led to NASA's Space-flight Tracking and Data Network (STDN) undertaking differential VLBI observations of the ALSEPs in early 1971, as soon as two ALSEP transmitters were operating on the moon. The accuracy of these observations was degraded by instrumental errors equivalent to positional uncertainties on the lunar surface of the order of 100 m, due mainly to the fact that the signals from the two ALSEPs did not pass through identically the same receiving equipment and were sampled separately before a difference observable was formed (see Figure 1.3).

In order to reduce these instrumental errors, Hinteregger and Counselman designed and built a new device, called a Differential Doppler Receiver (DDR). Used with the antennas and S-band receivers of the STDN, the DDR extracts the carrier signals of two ALSEPs from the intermediate-frequency passband of a single receiver and mixes them together. The resulting difference frequency, after a constant "bias" is subtracted, is multiplied by a factor of 360 to improve phase resolution, then counted digitally. A differential VLBI observable is obtained by numerical subtraction of the counts recorded simultaneously at two stations.

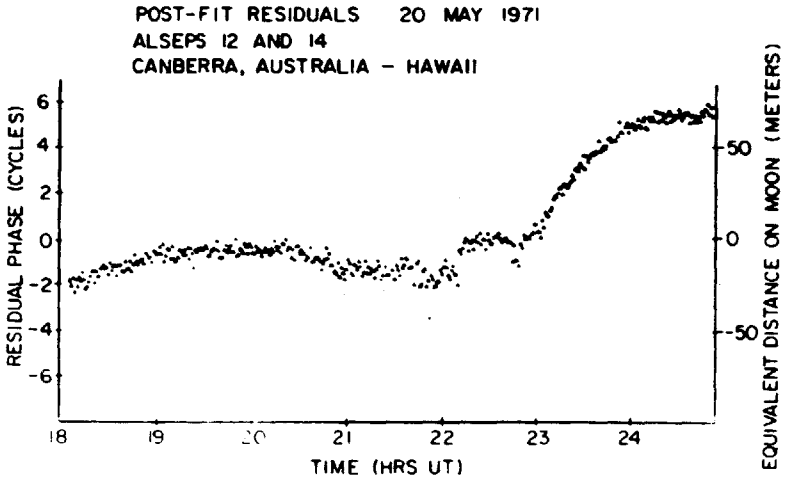


Fig. 1.3 An example of the results of early differential interferometric observations of ALSEP telemetry transmitters. Note the presence of phase noise on the order of a cycle peak to peak and drifts of several cycles, corresponding to tens of meters displacement on the lunar surface.

In October 1972, Hinteregger and I installed prototype models of the DDR in the STDN tracking stations at Merritt Island, Florida, and Goldstone, California, and conducted successful observations of the ALSEP 12 and ALSEP 14 transmitters during a six-hour tracking period. Analysis of the data from this first experiment

indicated that measurement errors had been reduced to the equivalent of less than a meter of displacement on the moon [13] (Figure 1.4).

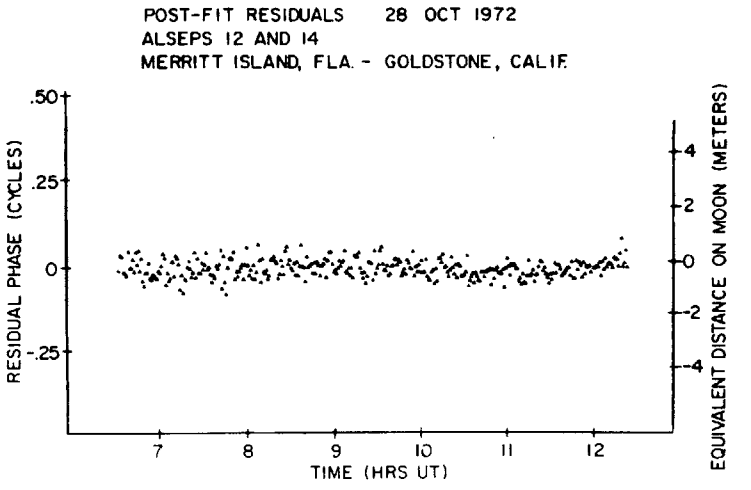


Fig. 1.4 Residuals (observed minus computed values) for differential interferometric phase observations of ALSEP 12 and ALSEP 14, expressed directly as fractions of a cycle at S-band (wavelength, 13.2 cm) and as the equivalent (projected) displacement of an ALSEP transmitter on the surface of the moon.

In early 1973 we installed two DDRs at each of six stations of the STDN (Figure 1.5). Since that time, simultaneous observations have been made of two pairs of ALSEPs an average of twice per week on each of two earth baselines. The data set analyzed in this thesis

consists of the observations during the 16-month period between March 1973 and July 1974.

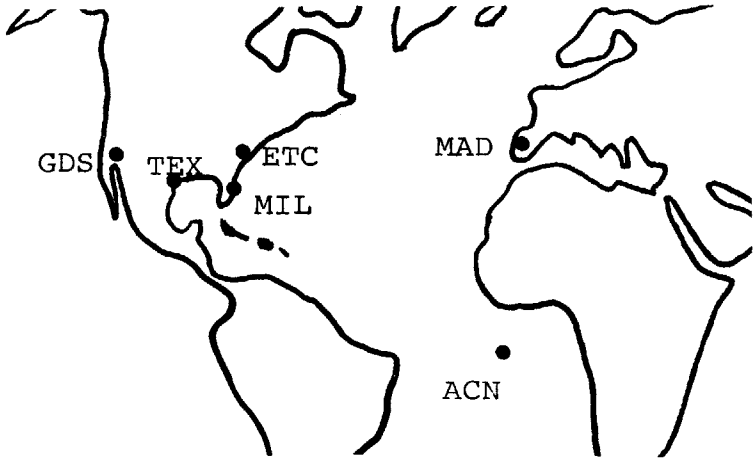


Fig. 1.5 Stations of the NASA Spacecraft Tracking and Data Network that have engaged in VLBI tracking of the ALSEPs are Ascension Island (ACN); Madrid, Spain (MAD); Merritt Island, Florida (MIL); Corpus Christi, Texas (TEX); Goldstone, California (GDS); and the Network Test and Training Facility at Greenbelt, Maryland (ETC).

Analysis of these data has been carried out using the M.I.T. Planetary Ephemeris Program (PEP), a large computer program originally developed at the M.I.T. Lincoln Laboratory under the direction of Michael E. Ash

and Irwin I. Shapiro. PEP is able to utilize data from many types of astronomical observations simultaneously to estimate various physical parameters [2, 6]. Recently, Martin A. Slade, in his M.I.T. thesis research, incorporated into PEP an accurate, numerically-integrated model for the lunar orbit [36]. The use of this model has been essential to my work. I have made the further modifications to PEP necessary to process counted-cycle differential VLBI observations, and to model more accurately the moon's physical libration.

Before and during the period of our observations, members of the NASA Lunar Laser Ranging Experiment (LURE) team [7] have collected and analyzed laser ranging observations from the McDonald Observatory in Texas to the retroreflectors on the moon (principally the reflectors at the Apollo 11, 14, and 15 landing sites). Since differential VLBI observations have little direct sensitivity to the orbital motion of the moon, I have used laser data to improve PEP's lunar ephemeris. In addition, I am indebted to members of the LURE team for the development of much-improved models of the lunar physical libration. In my data reduction I have used

principally a numerically integrated model developed at the Jet Propulsion Laboratory by Williams et al. [40]. The JPL numerical integration derives its initial conditions by fitting to a semi-analytic model developed by D. H. Eckhardt of the Air Force Cambridge Research Laboratories [15,16].

The ALSEP relative coordinates determined from these VLBI observations should be useful in the definition of a unified selenodetic coordinate system that incorporates both the high accuracy of laser ranging and the wide coverage of Apollo orbital photography and earth-based telescopic photography. In particular, the VLBI observations serve to extend to the Apollo 12, 16, and 17 landing sites the positional accuracy obtained from the laser ranging observations of the Apollo 11, 14, and 15 sites. The Apollo 16 and 17 coordinates obtained by VLBI are the most important because these landing sites are covered by the metric photographs taken by the orbiting command module during these two missions. The Apollo 15 laser ranging retroreflector has been located relative to the ALSEP transmitter at that site with an uncertainty of less than one meter by L. A. Schimerman et al. [30] at the Defense Mapping Agency Aerospace Center, using photographs taken on the lunar surface by the astronauts.

In the following chapters I try to document in some detail each major aspect of the ALSEP VLBI experiment. I begin with a basic discussion of counted-cycle VLBI and of the sensitivity of such observations to relative ALSEP positions. In Chapter III, a description is given of the Differential Doppler Receiver and its use with the NASA STDN Unified S-Band tracking system. Chapter IV deals with the software developed to analyze the data, including the special processing algorithms required for the doubly-differenced observable, the documentation of the model used for the lunar rotation, and the method of parameter estimation. The chapter concludes with an analysis of the major sources of error which might degrade the results. The results of my solutions for the ALSEP coordinates and the libration parameters are given in Chapter V. A concluding chapter suggests the likely gains from further analysis of these data and from the application of the differential VLBI technique to other problems in dynamical astronomy.

CHAPTER II

Basic Concepts

2.1 Counted-cycle VLBI

The usual VLBI system consists of two or more stations, each with four key elements: 1) a high-gain antenna with a low-noise radio frequency (RF) amplifier; 2) one or more stages of mixing with "local oscillators" to convert the received RF signals to low "video" frequencies; 3) some means of recording the converted signals; and 4) a stable (1 part in 10^{12} or better) frequency standard to provide a reference for the local oscillators and a time base for the recording. Systems differ in the ways in which the interferometric phase is determined from the recordings made at the two stations. In the conventional technique, the signals are recorded directly on magnetic tape in either analog or digital form at each station. The tapes are later collected, played back together, and the data cross-correlated to determine the differential phase delay. For observations of natural radio sources, which emit essentially random signals, statistical cross-correlation of the signals is necessary to determine the phase difference. This technique also offers the possibility of determining the group delay

difference with useful accuracy if the bandwidth of the system is sufficient.

For observations of artificial radio transmitters which emit phase-coherent signals, an alternative to the relatively expensive process of direct signal recording and cross-correlation is available. An oscillator can be locked in phase to the signal received at each station and a digital counter used continuously to count the cycles of this oscillator. At suitable intervals the numerical value of the continuously-accumulating count can be recorded*. The oscillator can be locked to a multiple, n, of the signal frequency, so that each count represents 1/nth cycle of the signal phase. Thus, a phase resolution of a degree or less is possible. An interferometric phase observable is formed simply by subtracting the counts corresponding to the same time at the two stations. For

---

*Counted-cycle VLBI observations of spacecraft can easily be made between any pair of sites equipped to perform Doppler tracking. Ondrasik and Rourke of JPL have analyzed the technique as a supplement to the two-way Doppler tracking of interplanetary spacecraft [25]. Although some observations were made of Mariner 9 [45], application of this technique has been limited by the lack of sufficiently stable frequency standards at most sites: Atomic hydrogen maser oscillators are required for useful results. If two spacecraft are observable simultaneously, the differential VLBI technique can be employed and the commonly used cesium-beam standards would be adequate since the effects of local-oscillator frequency variations would tend to cancel.

differential observations involving signals from two transmitters, the oscillator may be locked to the difference between the frequencies of the two signals received at a given station.

In present practice, the phase delay observable determined by counting cycles differs from that determined by direct signal recording in two ways. In direct recording VLBI the received signals are compared for common transmission times, since in the cross-correlation one of the recordings is shifted with respect to the other by an amount equal to the propagation time difference, determined from prior knowledge. In all of the cycle-counting systems employed thus far, the counts have been sampled simultaneously at the two receiving sites, so that the phase difference determined by subtraction refers to signals transmitted at different times. One consequence of this transmission-time difference is that short-term (time scale of milliseconds) phase fluctuations of the transmitter that are not filtered out by the phase-locked loops may add noise to the measurement, which cancels in the interferometric observable only when the propagation times to the two stations are equal. An additional problem with sampling simultaneously at both receivers is the possible introduction of systematic errors into the model of the observable due to persistent (over minutes or hours) drifts in the transmitter frequency. This effect in the ALSEP observations will be analyzed in Section 4.5. In principle, both of these errors could be reduced by offsetting the receiver

sampling times during observations using a priori information about the differential delay between stations. The systematic effect of persistent transmitter frequency drift may also be accounted for in the theoretical formulation of the counted-cycle observable, as described in Section 4.2.

The second difference between the two VLBI methods, as now implemented, involves the technique of conversion of the measured phase difference to a corresponding delay difference. This conversion, which is necessary in order to relate the observed quantity to the geometry of the observing and transmitting sites, involves the use of the observed frequency. In conventional VLBI observations there are two possible cases. For a continuum source, there is no characteristic source frequency, and the observed frequency is determined by the characteristics of the receiver: usually, although not necessarily, by the total local oscillator (LO) frequency. For a monochromatic source, however, there is a characteristic frequency associated with the received signal. This signal is recorded within the video band at whatever frequency the source appears relative to the total LO. In this case, the conversion of the measured phase to a delay should be based on a suitably defined signal frequency. If, instead, the measured phase were referred to the LO frequency using the group delay, the derivative of phase with respect to frequency, then a phase

error would be introduced, equal to the product of the error in the value of group delay used, and the offset of the LO frequency from the signal frequency. In a cycle-counting VLBI system, no extrapolation to refer the phase from the received frequency to the LO frequency at a station is necessary, since the local oscillator is variable and continuously tracks the phase, and therefore the frequency, of the received signal. In practice we convert phase to delay using an estimate of the actual transmitted frequency, obtained from a measurement of the received frequency at one site and a priori knowledge of the Doppler shift of the signal received at that site. This procedure is discussed in detail in Section 4.2.

Compared with direct-recording VLBI, cycle counting offers significant simplifications in observation procedure and data processing. Numerical data are obtained directly in real time and can be recorded at a relatively low sampling rate, for example, once per minute. (In fact, the data could be written down by hand, using pencil and paper!) In addition, the differential phase observable may be formed in real time by communicating via the telephone or teletype the numbers recorded at each station, thus allowing the experimenter to check that valid data are being obtained.

2.2 Information Content of the Differential VLBI Observable

The principles underlying the use of differential VLBI observations to determine the relative coordinates of a pair of ALSEP transmitters can be understood by means of a simplified geometric analysis in which the moon is assumed to be infinitely far from the earth and to remain stationary during a single day's tracking period*. The geometry of a pair of stations observing a single such ALSEP is shown in Figure 2.1 where $\vec{b}(t)$ is the baseline vector and $\hat{e}_i$ is the unit vector in the direction of ALSEP i. The difference between the phases

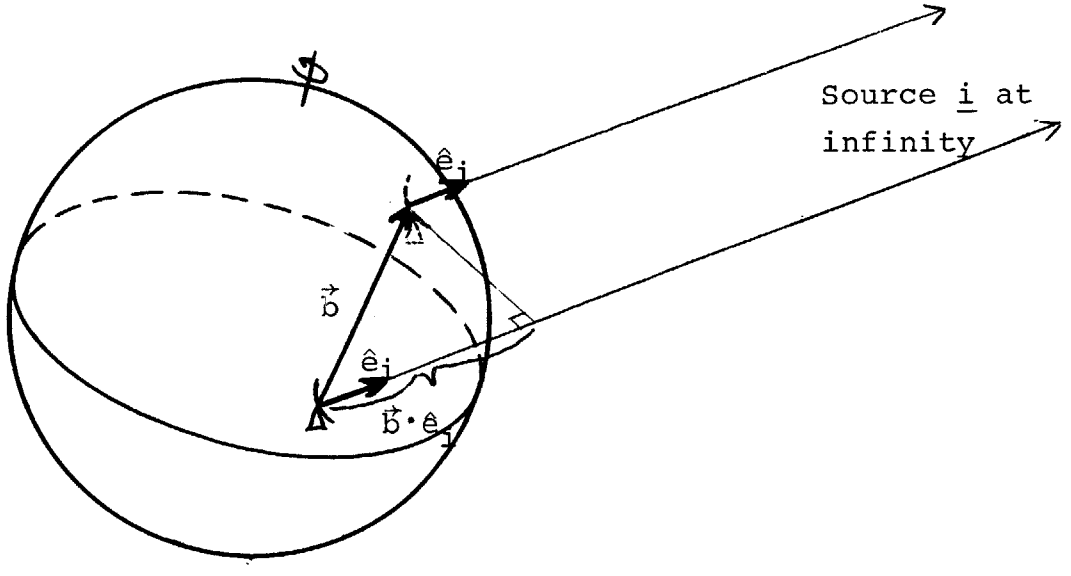


Figure 2.1 Geometry for two stations observing a source at infinity.

*The approximations introduced in this section are not made in the actual data processing. See Chapter IV.

of the signals received simultaneously at the two stations, usually called the interferometric "fringe phase", is simply

$$\phi_i(t) = \frac{\omega}{c} \vec{b}(t) \cdot \hat{e}_i \qquad (2.2.1)$$

where ω is the angular frequency of the transmitted signal, c is the speed of light, and $\vec{b} \cdot \hat{e}_i$ is the path-length difference. The two vectors may be written

$$\vec{b}(t) = B\{\cos D[\cos A(t)\hat{\imath} + \sin A(t)\hat{\jmath}] + \sin D\, \hat{k}\} \qquad (2.2.2)$$

$$\hat{e}_i = \cos \delta_i(\cos \alpha_i\, \hat{\imath} + \sin \alpha_i\, \hat{\jmath}) + \sin \delta_i\, \hat{k} \qquad (2.2.3)$$

where B is the baseline length; $\hat{\imath}$, $\hat{\jmath}$, $\hat{k}$, are unit vectors, $\hat{\imath}$ in the direction of the vernal equinox, $\hat{k}$ in the direction of the earth's angular velocity vector, and $\hat{\jmath}$ orthogonal to $\hat{\imath}$ and $\hat{k}$ so as to complete a right-handed system; A, D, and α_i, δ_i refer to the right ascension and the declination of the baseline and the source, respectively.

If two ALSEP transmitters are observed simultaneously, the <u>differential fringe phase</u> is given by

$$\Delta\phi(t) = \phi_1(t) - \phi_2(t) = \frac{\omega}{c} \vec{b}(t) \cdot (\hat{e}_1 - \hat{e}_2) \qquad (2.2.4)$$

where I have assumed that the two transmitter frequencies are the same. (All of the ALSEPs do in fact have different frequencies, but the frequency differences are small

and do not need to be considered here.) In order to express $\Delta\phi(t)$ in terms of the small differential right ascension, $\Delta\alpha$, and differential declination, $\Delta\delta$, between the directions to the two ALSEPs, we write

$$\alpha_2 = \alpha_1 + \Delta\alpha$$
$$\delta_2 = \delta_1 + \Delta\delta$$

and substitute these expressions in Equations (2.2.3) and (2.2.4). Since the actual geocentric angular separation of the ALSEPs is less than 5×10^{-3} radians, we expand the trigonometric functions in powers of $\Delta\alpha$ and $\Delta\delta$, ignoring terms of order higher than the first in these angles. Expanding yields

$$\hat{e}_1 - \hat{e}_2 \simeq [\Delta\delta \sin\delta_1 \cos\alpha_1 + \Delta\alpha \cos\delta_1 \sin\alpha_1]\hat{i} + [\Delta\delta\sin\delta_1 \sin\alpha_1 - \Delta\alpha\cos\delta_1 \cos\alpha_1]\hat{j} - \Delta\delta \cos\delta_1\hat{k} \qquad (2.2.5)$$

Substituting Equations (2.2.2) and (2.2.5) in Equation (2.2.4) gives

$$\Delta\phi(t) = \frac{\omega B}{c}\{\Delta\delta[\cos D\sin\delta\cos(\alpha - A(t)) - \sin D\sin\delta] + \Delta\alpha[\cos D\cos\delta\sin(\alpha - A(t))]\} \qquad (2.2.6)$$

in which the subscript on α and δ has been dropped.

By counting cycles of the DDR outputs and taking the difference between the counts at the two stations we

can measure the change in the differential fringe phase during the period of observation, but not the "absolute" value at a given time. Hence the constant term in Equation (2.2.6) is not observable. The observable quantity is

$$\Delta\phi_{obs}(t) = \frac{\omega B}{c}\cos D[\Delta\delta\ \sin\delta\cos(\alpha - A(t)) + \Delta\alpha\cos\delta\sin(\alpha - A(t))] + \Delta\phi_o \qquad (2.2.7)$$

where $\Delta\phi_o$ is an unknown constant which accounts both for the constant term in Equation (2.2.6) and for the difference between the arbitrary initial values of the cycle counters at the two stations.

Equation (2.2.7) shows that the coefficients of the sinusoidal and cosinusoidal variations of $\Delta\phi_{obs}(t)$ are proportional, respectively, to $\Delta\alpha$ and $\Delta\delta$. Thus, determining $\Delta\alpha$ and $\Delta\delta$ for an ALSEP pair corresponds to determining the amplitudes of the quadrature (sine and cosine) components of the variation of $\Delta\phi_{obs}(t)$. If the observation period is long enough to allow separate determination of both quadrature components, or, equivalently, of both the amplitude and the phase of the diurnal sinusoid, then both $\Delta\alpha$ and $\Delta\delta$ may be estimated with the uncertainties given by

$$\sigma_{\Delta\alpha} = \sigma_s \frac{c}{\omega B\cos D\cos\delta} \qquad (2.2.8)$$

$$\sigma_{\Delta\delta} = \sigma_c \frac{c}{\omega B\cos D\sin\delta} \qquad (2.2.9)$$

where σ_s and σ_c are the uncertainties in the determination of the sine and cosine coefficients, respectively, in Equation (2.2.7). Typical values with present equipment for the parameters in Equations (2.2.8) and (2.2.9) are $\sigma_s \approx \sigma_c \approx 20°$, $\omega \approx 2\pi \times 2.3 \times 10^9$ radians/sec and BcosD (the equatorial projection of the baseline) $\approx$ 3500 km. If the moon is at a relatively high declination, say $\delta = 20°$, then $\sigma_{\Delta\alpha} \approx 0''.0005$ and $\sigma_{\Delta\delta} \approx 0''.0012$. Of course, at low lunar declinations, $\Delta\delta$ is poorly determined.

These values provide only crude estimates of the uncertainties of the determinations of $\Delta\alpha$ and $\Delta\delta$. In practice, due to the problem of separating the sine and cosine coefficients from the constant component in Equation (2.2.7), the formal standard errors obtained for a particular observation period depend strongly on the time span of the observations and on the characteristics of the earth baseline. To investigate these problems, Frankston [18] has performed a series of three-parameter least-squares solutions based on the model of Equation (2.2.7), using simulated observations for each of the available STDN baselines (see Figure 1.5). For each solution he assumed that the error in each observation was 10° and that observations were made at one- hour intervals throughout

the "observation window" for a particular baseline. This window was defined as the time during which the moon was at least 20° above the horizon for both stations. For each observation period three parameters were estimated: $\Delta\alpha$, $\Delta\delta$, and the constant, $\Delta\phi_o$. For all baselines which had equatorial projections longer than 1500 km and observation windows longer than 3 hours, the solutions yielded formal standard errors for $\Delta\alpha$ between 0".0003 and 0".006, equivalent to 0.5 m to 10 m in distance at the moon. For $\Delta\delta$, considering only observations made when the declination of the moon was at least 10° (about three-fourths of each month), he found that the formal standard errors ranged from 0".0004 to 0".014 or 0.8 m to 30 m in equivalent distance on the surface of the moon.

The type of baseline most useful for determining each of the relevant parameters can be deduced by inspection of Equation (2.2.7). Since observations typically are obtained over only 4-6 hours, the curvature of the diurnal-period sinusoid is rather poorly determined from the observed change in differential fringe phase. The best-determined quantity is the average slope of $\Delta\phi(t)$; consequently, the quadrature component of $\Delta\phi(t)$ which is best determined is the one which has its maximum slope during the period of the observations. The cosine function multiplies $\Delta\delta$ and has its maximum slope when $\alpha - A(t) = \pm 90°$. This implies that for the best deter-

mination of $\Delta\delta$, the baseline should be perpendicular to the direction of the moon at the midtime of the observations, a condition best satisfied by a baseline that is oriented east-west on the earth. Conversely, the sine function which multiplies $\Delta\alpha$ has its maximum slope when $\alpha - A(t) = 0$ or $180°$, so that, for the best determination of $\Delta\alpha$, the baseline vector should be parallel to the meridian plane of the moon at the midtime of the observations. This condition is satisfied by a baseline that is formed by a pair of stations with nearly equal longitudes, but that has a large equatorial projection.

From the foregoing analysis, it is clear that observations should be made with both east-west and north-south baselines in order to obtain optimum determination of both $\Delta\alpha$ and $\Delta\delta$ from the relatively short observing periods available. The application of this strategy in the context of station availability and other scheduling constraints is discussed in Section 3.4.

By combining observations made on different days, when the moon presents different aspects to the earth, we can use this differential VLBI technique to determine the third (radial) component of the separation, or baseline vector, between the ALSEPs. This determination is possible because the moon's geometric, or "optical" libration, which

varies by ±7° in both longitude and latitude, allows the interferometer to view the lunar baseline from different perspectives during the course of a month. The standard error associated with the radial component is greater by a factor of about 3 than the formal errors associated with the transverse components.

The continuation of VLBI observations over a sufficiently long time also enables the moon's physical libration to be determined, through the variations of $\Delta\alpha$ and $\Delta\delta$ which the libration produces. The apparent change in the relative angular position of a pair of ALSEPs produced by the libration depends on the orientation and length of the ALSEP baseline and on the nature of the libration. The libration may be characterized by rotations about three axes, one along the line of sight from earth to moon and two perpendicular to this line. Differential VLBI observations are most sensitive to the librations about the line of sight, since the ALSEPs are all located relatively close to a single plane normal to the line of sight. ALSEPs 12 and 17, for example, are separated by approximately 1300 km along a nearly east-west line (see Figure 1.1). Determination of $\Delta\delta$ with an uncertainty of 0".001 for this pair corresponds to a determination of the libration about the line of sight with an uncertainty of $0".001 \times \frac{384000 \text{ km}}{1300 \text{ km}} \sim 0".3$, where 384000 km is the earth-moon distance. The sensitivity

of VLBI observations to libration about the axes perpendicular to the line of sight is proportional to the component of an inter-ALSEP baseline along the line of sight. The baseline which has the greatest component in this direction is formed by ALSEP 14 (longitude -17°, latitude -4°) and ALSEP 17 (longitude 31°, latitude 20°)*. For this baseline, an uncertainty of 0".001 in the measurement of $\Delta\alpha$ is equivalent to an uncertainty in the libration in longitude (about a north-south axis) of 1".6, and an uncertainty in $\Delta\delta$ of 0".002 corresponds to an uncertainty of 3".2 in the libration in latitude (about an east-west axis). Of course, the libration cannot be determined in all three degrees of freedom from one day's observations of a single pair of ALSEPs. Only two independent quantities, corresponding to $\Delta\alpha$ and $\Delta\delta$, are observable. However, simultaneous observations of a second ALSEP pair may be used to determine the third libration component.

The assumption that the ALSEPs are located at an infinite distance from the receiving stations has led to a relatively simple expression, Equation (2.2.7), which has helped us to see how a single day's observations can

*The ALSEP 14 - ALSEP 17 pair is not directly observable with a single DDR since the frequency difference for this pair is greater than 3.3 MHz (see Section 3.2). However, the baseline may be synthesized in a solution by combining observations from two DDRs; for example, one DDR observing ALSEP 14 with respect to ALSEP 12, the other ALSEP 17 with respect to ALSEP 12.

determine the angular separation of a pair of ALSEPs in both right ascension and declination. There is, however, additional information content in the observable provided by the lunar parallax. (The moon's parallax is defined loosely as the angle subtended at the distance of the moon by the earth's equatorial radius.) The parallax describes the extent to which an observer on the earth can view the moon from different perspectives during the course of a single day. For an interferometer we define the parallax as P/R, where R is the earth-moon distance and P is the distance of the baseline midpoint from the earth's axis of rotation.

In Appendix A.3 I derive an expression for $\Delta\phi_{obs}(t)$ for the two-dimensional case ($D = \delta = 0$), including terms of first order in the parallax:

$$\begin{aligned}\Delta\phi_{obs}(t) = \Delta\phi_o &+ \frac{\omega B \Delta\alpha}{c}\{\sin(\alpha - A(t)) \\ &+ \frac{P}{R}[\sin 2(\alpha - A(t)) - \frac{1}{2}\tan \ell \cos 2(\alpha - A(t))] \\ &+ \frac{r_m}{R}\frac{\cos(\Delta\ell/2)\cos 2\ell}{\cos \ell}[\sin(\alpha - A(t)) \\ &- \frac{1}{2}\tan 2\ell \cos(\alpha - A(t))]\} \qquad (2.2.8)\end{aligned}$$

where r_m is the lunar radius, ℓ is the longitude of the midpoint of the lunar baseline, and $\Delta\ell$ is the separation of the ALSEPs in selenocentric longitude. Note that the first line of Equation (2.2.8) is exactly the same as

Equation (2.2.7) for the case $D = \delta = 0$.

The third and fourth lines in Equation (2.2.8) contribute no additional information since they have the same period as the main term*. However, the term in the second line, proportional to P/R, has a 12-hour period so that its signature is distinct from the signature of the main term. The determination of the amplitude and phase of the semi-diurnal sinusoid allows the determination of two additional parameters, P/R and ℓ, for example. However, the uncertainties for these parameters will be larger than those for $\Delta\alpha$ by a factor of approximately $1/\Delta\alpha$ which is about 400 for an ALSEP pair whose separation, when projected along the right-ascension direction, is about 1000 km.

The simplified geometric analysis presented above is useful for the purpose of gaining qualitative insight into the way in which the observations determine the parameters of interest. However, it fails to answer quantitatively the question of what uncertainties may be expected if the various parameters are estimated from observations extending over several months. The relatively complicated orbital and rotational motions of the moon add significant information content to the data and decorrelate the estimates of parameters which could not be estimated

*The phase of the term in the fourth line differs from the phase of the main term. However, if $\delta \neq 0$, the main term will also have a cosine component [see Equation (2.2.7)].

separately from a single day's observations. Clearly advance knowledge of the parameter-estimation uncertainties obtainable from an experiment is important in planning an experiment. Therefore I used PEP to perform maximum-likelihood estimates of relevant parameters using simulated observations made on two days per week over the period March 1973 to July 1974 [19]. Each day's observations of an ALSEP pair consisted of only five differential-interferometric phase measurements, made one hour apart. The 1-σ uncertainty of each measurement was assumed to be 9°. I estimated simultaneously the six elements of the lunar orbit; the three selenocentric coordinates of each ALSEP; the three geocentric coordinates of each observing station; the two lunar moment-of-inertia ratios, β [$\equiv$ (C-A)/B] and γ [$\equiv$ (B-A)/C], upon which the characteristics of the physical libration mainly depend; and, for each daily tracking session, an additional parameter representing the arbitrary initial value of the differenced phase-counter readings. For the moon's orbital elements I assumed a priori 1-σ uncertainties for a and e equivalent to 2.5 meters in radius, and for the angular elements, to 100 m in the two orthogonal directions. The origin of the selenocentric coordinate system was defined by assuming

that the position of ALSEP 15 was known. The results of the simulation indicated that the coordinates of ALSEPs 12 14, 16, and 17 would be determined with 1-σ uncertainties of approximately 1 meter in longitude and latitude and 3 meters in radius. The uncertainty obtained for β corresponded to an uncertainty of 0".06 in the libration in latitude and node ; at one lunar radius, approximately the distance between the more widely separated ALSEPs, the corresponding displacement uncertainty is about 50 cm. The uncertainty obtained for γ implies an uncertainty of 0".23 in rotation about the spin axis (the libration in longitude). The uncertainties obtained for the tracking station coordinates ranged from 5 to 15 meters in radius and longitude and 15 to 20 meters in latitude. These uncertainties are comparable to the uncertainties in the coordinates derived from other methods, so that the station coordinates should be included among the parameters to be estimated from the actual VLBI observations.

CHAPTER III

Experimental Equipment and Procedure

3.1 Unified S-Band System of the STDN

The NASA Spaceflight Tracking and Data Network (STDN) was created in 1972 by the merger of the Manned Space Flight Network (MSFN), which supported the Mercury, Gemini, and Apollo missions, and the Space Tracking and Data Acquisition Network (STADAN), which provided primary tracking for the extensive NASA earth satellite program. Each of the former MSFN stations is equipped with either a 30-foot- or 85-foot-diameter parabolic antenna (or both) and an S-band tracking and telemetry receiving system capable of providing position determination and communications for spacecraft in the vicinity of the earth or moon. Since 1970 the network has used these stations regularly to observe the ALSEP transmitters on the moon, primarily for the purpose of demodulating and recording the information telemetered from the scientific experiments left on the surface by the astronauts. Because differential VLBI observations of the ALSEPs can be performed simultaneously with telemetry support, an extensive program of VLBI observations

has been conducted with little additional complication for the network.

The central element of the Unified S-Band (USB) system is a Motorola superheterodyne receiver of a type built originally for use by the Deep Space Network* in the early 1960's. A simplified schematic diagram of the receiver and its associated elements is shown in Figure 3.1. For differential Doppler tracking of ALSEPs, the S-band antenna is directed at the moon and the USB receiver is phase-locked to one ALSEP, which we call the "reference ALSEP". The carrier signal of the reference ALSEP appears in the center of the 10 ± 3.3 MHz intermediate frequency (IF) band of the USB receiver, at exactly the same frequency as, and with a fixed phase relationship to, the 10 MHz reference oscillator of the USB system. The signals from other ALSEPs will also appear within this IF band at various frequencies above and below 10 MHz, unless the radio frequency (RF) difference between the reference ALSEP and another exceeds about 3.3 MHz, in which case the latter signal falls outside the IF passband.** The USB

---

*Operated for NASA by the Jet Propulsion Laboratory.

**The antenna beams are sufficiently broad to receive signals from all ALSEPs simultaneously.

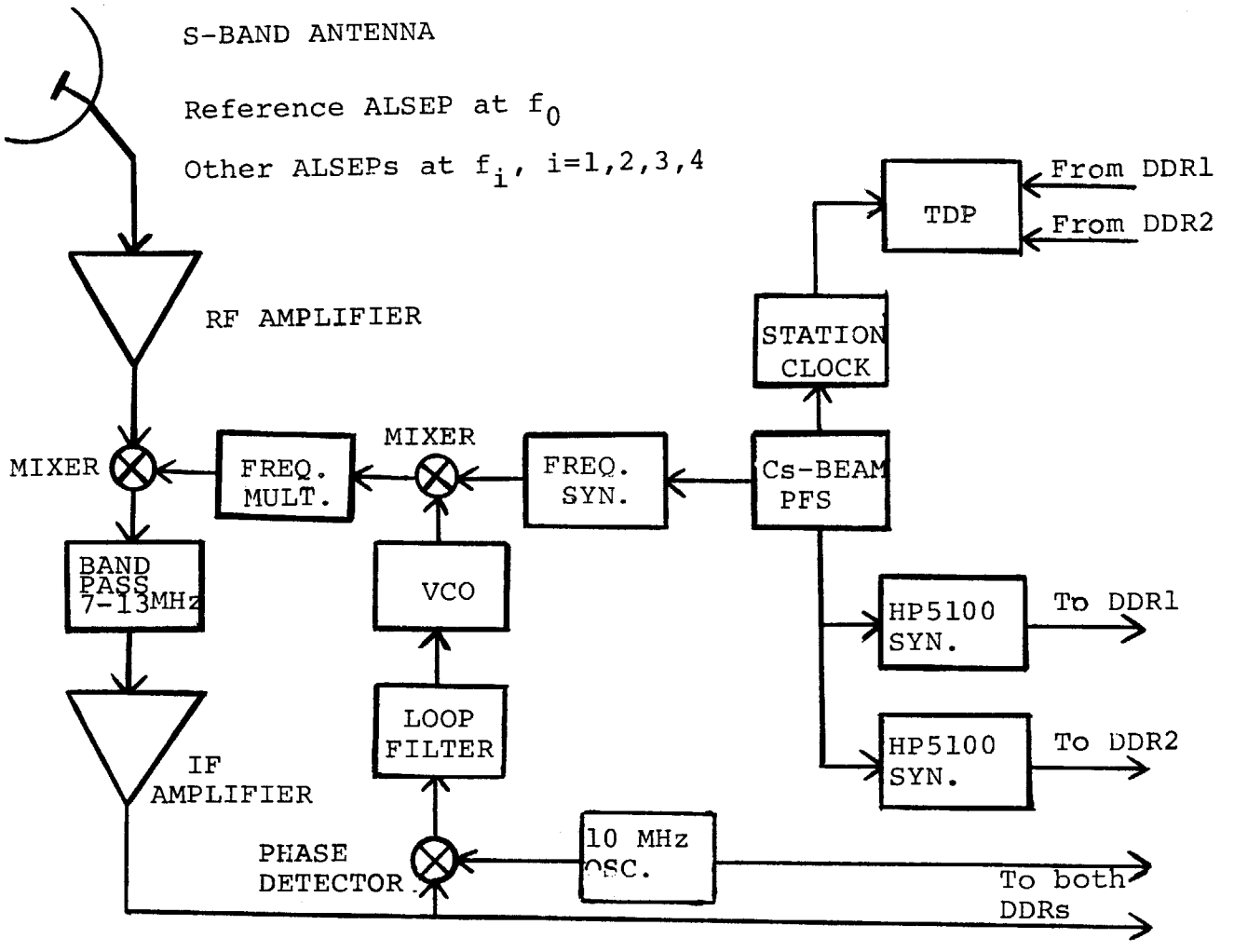


Figure 3.1 Schematic diagram of the STDN USB system. The signal of the reference ALSEP appears at 10 MHz in the output of the IF amplifier; the other ALSEP signals appear at 10 MHz + (f_0-f_i), i = i, 2, 3, 4. (See text.)

receiver, because its frequency conversion stages have "high" local oscillators, reverses the RF spectrum, so that, for example, the signal of an ALSEP whose S-band frequency is 1 MHz above the frequency of the reference ALSEP will appear at 9 MHz in the IF band. Table 3.1 shows the radio frequencies of the five ALSEPs, and the intermediate frequencies for two possible choices of the reference ALSEP.

STDN ALSEP NUMBER	APOLLO MISSION NUMBER	S-BAND RADIO FREQUENCY (MHz)	USB RCVR I.F. (MHz)	
			A1 REF	A2 REF
A1	12	2278.5	10.0	9.5
A2	15	2278.0	10.5	10.0
A3	16	2276.0	12.5	12.0
A4	14	2279.5	9.0	8.5
A5	17	2275.5	13.0	12.5

Table 3.1 Radio frequencies and USB receiver intermediate frequencies of ALSEPs for two possible choices of reference. These are nominal frequencies. Actual frequencies may deviate from the nominal by about 20 kHz.

Several other elements of the USB system are used by the Differential Doppler Receivers (DDRs). The station primary frequency standard (PFS), a cesium atomic-beam device, serves as a reference for

two Hewlett-Packard model HP5100 frequency synthesizers, each of which provides a local-oscillator signal to one of the DDRs (see Section 3.2). The output of each DDR is in turn connected to one of the two input channels of the USB system Tracking Data Processor (TDP). The heart of the TDP is a pair of digital counters which count, continuously, cycles of the input signals. At selected time intervals controlled by the station clock, the readings of these counters are sampled non-destructively and recorded on paper tape. The TDP has two modes of operation. In the "single" mode only one channel is sampled and recorded, with the sampling interval selectable between 6 seconds and 10 minutes. In the "dual" mode, the two channels are sampled alternately, and, in this case, the maximum sampling rate for each channel is once per 12 seconds. For ALSEP differential VLBI observations, the TDP is usually operated in the dual mode in order to count and record the output signal from two DDRs.

3.2 The M.I.T. Differential Doppler Receiver

The Differential Doppler Receiver (DDR) was developed by Hinteregger and Counselman to enable the TDP to count directly the difference between the frequencies received from two ALSEP transmitters. Although it is possible to determine this difference without a DDR by subtracting frequency readings from two USB receivers with one USB receiver locked to each ALSEP signal, the results obtained in this way are much less accurate than those which can be obtained with the DDR (compare Figures 1.3 and 1.4).

The DDR receives as input from the USB receiver the 10 MHz reference signal, which is locked in phase with the reference ALSEP carrier signal, and the wideband (7-13 MHz) IF signal, which contains the carrier signals of all the ALSEPs whose frequencies are within approximately ±3.3 MHz of the frequency of the reference ALSEP (see Section 3.1). In the DDR, one of these ALSEP signals (other than the reference) is selected and is mixed with a local-oscillator signal derived from the USB receiver's 10 MHz reference signal to obtain a beat-frequency signal which has the phase of the reference ALSEP carrier minus the phase of the selected ALSEP carrier. The DDR's output, which is counted by the TDP,

comes from a voltage-controlled-multivibrator which is phase-locked to an integer multiple (360) of the beat-frequency signal. To explain more completely the operation of the DDR, we refer to Figure 3.2.

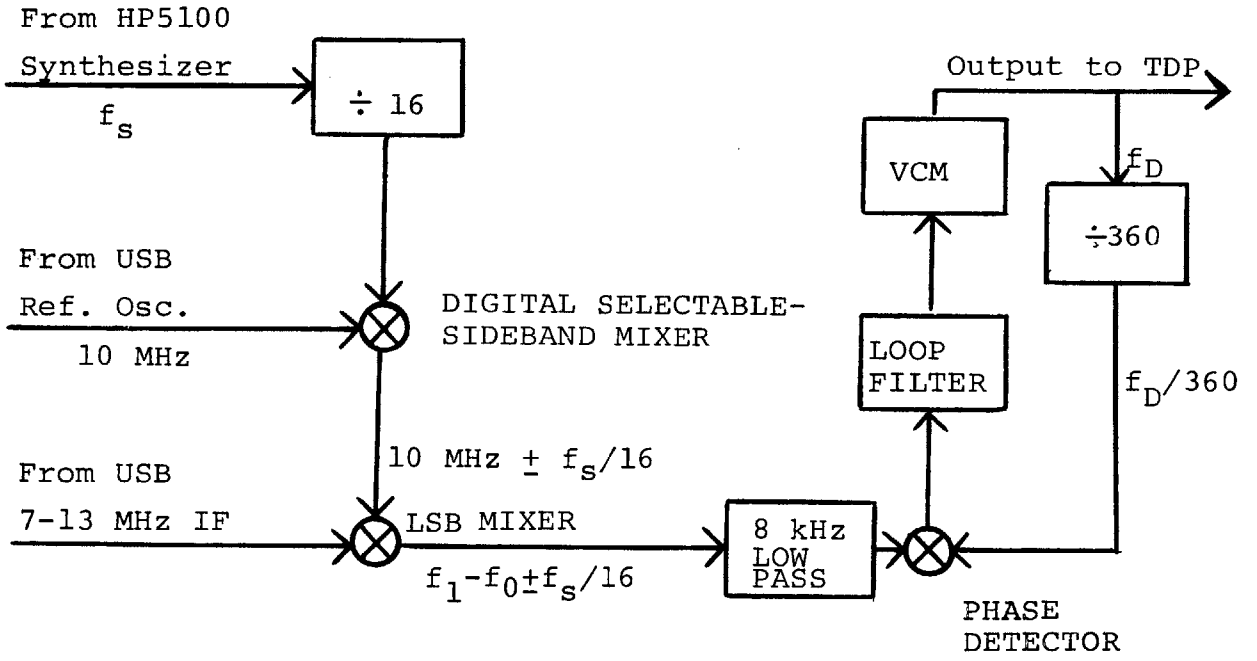


Figure 3.2. Block diagram of the Differential Doppler Receiver (DDR). In the 7-13 MHz wideband IF input from the USB receiver, the ALSEP carrier signal to be tracked differentially by the DDR appears at a frequency of 10 MHz - f_1 + f_0. The HP5100 synthesizer frequency, f_s, is set, and the sideband of the DDR's digital mixer is selected, so that the chosen ALSEP signal emerges from the DDR's LSB mixer between 2.5 and 5.5 kHz. The voltage-controlled-multivibrator (VCM) is phase-locked to this signal in a frequency-multiplying (x 360) loop.

Selection of the desired ALSEP signal for phase-locked tracking by a DDR is accomplished by a human operator who must first have measured, by means of a pair of USB receivers, the approximate difference between the reference and the other ALSEP's carrier frequencies. Based on this measurement, the operator sets the HP5100 synthesizer which is connected to the DDR, and he selects the appropriate sideband for the digital mixer which generates the DDR's local-oscillator (LO) signal, so that the desired ALSEP carrier signal will be converted within the DDR to approximately 4 kHz, near the center of the 2.5 to 5.5 kHz tracking range of the DDR's phase-locked loop. For example, if A1 is the reference ALSEP and it is desired to lock a DDR to A2, Table 3.1 shows that A2's IF carrier frequency will be approximately 10.5 MHz, or 0.5 MHz on the upper side of the 10 MHz reference frequency. Referring to Figure 3.2, we see that the frequency of the HP5100 synthesizer must be set in this case to 8.064 MHz and the upper (+) LO sideband selected, to obtain a DDR local-oscillator frequency of 10 MHz + (8.064 MHz/16) = 10 MHz + 0.504 MHz = 10.504 MHz. The desired ALSEP carrier signal, at 10.5 MHz, is now 4 kHz lower than the LO frequency and will be converted to 4 kHz at the output of the final, lower-sideband (LSB) mixer. The output of this mixer is then

low-pass filtered so that all noise signals farther than ± 4 kHz from the chosen ALSEP's carrier frequency, and all other ALSEP signals, are rejected.

If the ALSEP to be tracked by the DDR has an IF frequency on the lower side of 10 MHz (for example A4 when the reference ALSEP is A1), then the operator must switch the DDR's digital SSB mixer to lower sideband (-). The operator sets the synthesizer, in general, according to one of the following formulas:

$$f_s = 16(f_0 - f_1 + 4\ \text{kHz}) \quad \text{Upper sideband case } (f_1 < f_0) \qquad (3.2.1a)$$

or

$$f_s = 16(f_1 - f_0 - 4\ \text{kHz}) \quad \text{Lower sideband case } (f_1 > f_0) \qquad (3.2.1b)$$

where f_0 and f_1 are the measured S-band frequencies of the reference and the other ALSEP, respectively.

Setting the synthesizer and the sideband-selection switch are the only manual operations required in order to place the desired ALSEP carrier signal within the phase-lock tracking range of the DDR. However, it is usually also necessary for the operator to slew the VCM's frequency manually to the neighborhood of the proper locking point, 360 times the converted ALSEP carrier frequency, or nominally 360 x 4 kHz = 1440 kHz.

A frequency counter is used by the operator to monitor the VCM frequency, which, once having been locked, will track any subsequent ALSEP frequency variations within the limits of 4 ± 1.5 kHz for the input to the phase detector, or 1440 ± 540 kHz for the VCM output. In general the DDR (VCM) output frequency, f_D, in terms of the (constant) offset synthesizer frequency, f_s, and the two (varying) ALSEP frequencies, is given by

$$f_D = 360(f_1 - f_0 + f_s/16) \quad \text{Upper sideband case} \quad (3.2.2a)$$

$$f_D = 360(f_1 - f_0 - f_s/16) \quad \text{Lower sideband case} \quad (3.2.2b)$$

We note that the frequencies of the local oscillators used in the USB receiver to convert the ALSEP signals from S-band (2.3 GHz) to the 10 ± 3.3 MHz band do not appear in this equation because the difference between ALSEP frequencies is not affected by these conversions as long as both ALSEP signals pass through the same mixers, etc. Also, the exact value of the "10 MHz" reference oscillator frequency, which is usually different from 10 MHz by about 50 to 100 Hz, does not matter: By virtue of the USB receiver's phase lock, the reference ALSEP's IF carrier is locked to this reference oscillator, whatever

the latter's frequency is; the first LO of the USB receiver is controlled to maintain this condition. If the frequency of the "10 MHz" reference oscillator is higher than 10 MHz, so will the reference ALSEP's carrier be, and the other ALSEP's carrier frequency in the IF band will be increased by precisely the same amount. But in the DDR the second ALSEP's carrier frequency is subtracted from the frequency of the "10 MHz" reference oscillator, plus or minus $f_{syn}/16$. Thus, any variation in the "10 MHz" reference oscillator's frequency is cancelled out. The only frequencies remaining in Equation (3.2.2) are the ALSEP frequencies (their difference), and $f_{syn}/16$. It is crucial, therefore, that the synthesizer be very stable, and be operating from the station's cesium-beam primary frequency standard.

Since frequency is the time-derivative of phase, it follows that all of the above statements regarding insensitivity and sensitivity to the frequencies of various oscillators apply with equal force to phase variations of the respective signals. The insensitivity of the DDR's output to phase variations within the USB receiver's LO system is the DDR's "secret of success". If we attempted to use separate USB receivers to measure the

frequencies of two ALSEPs separately, in order to determine the frequency (or phase) difference, we would be susceptible to phase instabilities of both USB receivers. With a DDR, we are susceptible to no significant instrumental errors other than those of the DDR, the synthesizer, and prime frequency standard. In practice this has meant a reduction of two orders of magnitude in overall instrumental errors.

The DDR is assembled from 15 integrated circuits, 3 transistors, and associated passive circuit elements on a single board measuring 4 by 6 inches. The digital single sideband mixer is of novel design, using only digital logic devices to generate selectively either the sum or difference of the 10 MHz and offset frequency inputs [12]. The analog lower sideband converter is based on the design of A. E. E. Rogers [27]. The phase-locked loop is a conventional second-order type with lead-lag compensation, but using an exclusive-or logic gate as a phase detector. This type of phase detector, together with the use of differential circuitry in the loop filter, yields excellent performance with both strong and weak signals, with low sensitivity of the output signal phase to the input signal amplitude and to environmental factors. The divide-by-16 in the input cir-

cuit for the offset frequency signal serves to reduce the effect of the phase drift of the synthesizer by that factor.

With a 30-foot-diameter antenna and a 200°K system temperature (typical for an STDN station looking at the moon), the theoretically-calculated ALSEP carrier signal-to-noise ratio is -3 db in the 8-kHz bandwidth input to the phase detector, and +22 db in the ±50 Hz closed-loop bandwidth of the phase-locked loop, which implies that the theoretical rms phase noise in the output of the loop should be 7°. The actually-measured loop performance is in good agreement with this calculated figure. Laboratory measurements that compared the outputs of two prototype DDRs have shown less than 1° of phase drift in 24 hours, including rapid temperature changes of 10°C to one DDR. A field test in which two DDRs using separate synthesizers were locked to the same ALSEP pair showed approximately 1° of relative phase drift in six hours.

3.3 Observation Procedure

The performance of the observations involves a cooperative effort by personnel at two or more STDN stations, at the Network Operations Center (NOC) of Goddard Space Flight Center, and at MIT. The observations are directed from MIT* through NOC. Fifteen minutes before the beginning of each DDR "track", NOC calls the MIT Test Director and connects him to a voice communications network which includes each of the stations scheduled to participate on that day. At this time the Test Director tells the stations which ALSEP is to be used as reference and which ALSEP is to be tracked differentially on each of the two DDRs. At each station the operator then locks a USB receiver to the reference ALSEP and connects the USB IF and 10 MHz reference signals to the DDRs.

Before a DDR can be locked to its assigned ALSEP, the S-band frequencies must be measured for this ALSEP and the reference ALSEP, and the HP5100 frequency synthesizer setting calculated as described in Section 3.2. The two ALSEP frequency measurements are performed simultaneously using two USB receivers with their associated frequency counters at the same station. As soon as the

---

*From the initial installation of the DDRs in March 1973 until July 1974, the period covered by the data included in this thesis, I directed most of the observations, assisted from time to time by Counselman and Hinteregger.

synthesizer frequency has been calculated, the (same) value is set into the synthesizers at both stations, and the operators lock the DDRs by slewing the VCMs to the anticipated locking frequency, usually 1440 kHz (see Section 3.2). Occasionally the DDRs will be found to lock at a frequency significantly different from that anticipated, due to drift of at least one ALSEP frequency between the time of the original measurement and the time the DDR is locked. In this case, a verification is always made that the lock is correct by again reading the two ALSEP S-band frequencies and the DDR output frequency and using Equation (3.2.2) to calculate the theoretical value of the DDR output frequency, which should agree with the measured value to within 3.6 kHz, i.e. to within 360 times the 10-Hz resolution of the USB frequency counters. If the ALSEP frequency drift is so rapid that an extrapolation indicates that the upper or the lower limit of the DDR's tracking range would be reached before the scheduled end of the observing period, the Test Director can instruct the station operators to change their frequency synthesizer settings and to re-lock the DDRs at a lower or higher frequency, in order to accommodate the drift. Alternatively, he can re-assign

that DDR to track a different ALSEP relative to the reference ALSEP. He may also choose a different ALSEP as reference. The frequency drift rate of an ALSEP is usually considerable only when the sunrise or sunset terminator is crossing the ALSEP, or for ~2 days thereafter. Tracking assignments are therefore rotated to avoid tracking an ALSEP near its twice-monthly terminator-crossing times.

After all of the stations have locked their DDRs and have begun recording data, the Test Director performs three additional checks to ensure that the data will be valid. First, he compares the stations' DDR output frequencies to see that the frequency for a given DDR at one station agrees with the frequency for the corresponding DDR at each of the other stations to within a few kHz. This comparison is particularly reassuring if the ALSEP transmitter frequency is drifting significantly, because the Test Director can then see that the DDR frequencies at all of the stations are changing in exactly the same way. As a second check, the Test Director performs a verification calculation similar to that which may have been done by one of the stations using Equation (3.2.2), but in this case he obtains ALSEP S-band frequency readings from a station <u>other than</u> the one which performed the original calculation of synthesizer frequency. This check

is useful, for example, to determine that the DDRs are not locked on a sideband of the ALSEP carrier signal as a result of a mistake in the calculation of f_s. Finally, an operator at each station reads to the Test Director two successive values of the TDP output on each channel. By subtracting successive N-counts and dividing by the time interval between them, the Test Director can determine if the rate of increase of the recorded N-count matches the output frequency of the DDR which should be connected to that input channel of the TDP. The entire process of locking the DDRs and checking the output for two or three stations usually takes about one-half hour. Once this procedure has been completed, the MIT Test Director is disconnected from the communications network, but remains on call in case a problem arises later. The stations remain in contact throughout the observation period in order to compare DDR frequencies once each hour.

3.4 Scheduling and Data Collection

Since their inception in March of 1973, the ALSEP differential VLBI observations have been scheduled by Goddard Space Flight Center* on the basis of non-interference with other NASA tracking requirements. In spite of

---

*Network support for the experiment was arranged at Goddard by I. M. Salzburg, J. W. Ryan, and H. W. Stonesifer, with the general support of Dr. J. M. Clark, Director.

this restriction, observations have been obtained at least twice per week during most of this period. There have been several times when no observations were made for two- or three-week periods, but the only extended gap was from mid-April to the first of July in 1973 during the first Skylab mission. A complete list of observations is given in Appendix A.2.

Because of the uncertainty of scheduling, our philosophy during the first year of the experiment was to observe at any time that two or more stations could be scheduled for four or more hours. During this year, data were recorded on paper tape at the maximum TDP sampling rate, once per 12 seconds on each channel. The paper tapes were mailed by the stations directly to MIT where the data were transcribed onto magnetic tape for processing.

By the spring of 1974, when a large volume of data had been collected and the frequency of the observation periods had become consistent (and none of the ALSEP transmitters had died), we felt able to choose the observing times and stations on a more scientific basis, following the geometrical analysis of Section 2.2. This analysis demonstrates the importance of performing observations with both north-south and east-west baselines

to obtain maximum sensitivity to right ascension and declination separations, respectively, of the ALSEPs. The station pair of Madrid, Spain, and Ascension Island in the South Atlantic fits the north-south baseline criterion very well (see Figure 1.5). The best east-west station pair of those available would be Merritt Island, Florida, and Goldstone, California, if these stations could be scheduled for the entire period during which the moon is mutually visible, often ten hours or more. However, when other NASA tracking requirements limit the scheduled period to less than six hours, a baseline of Madrid or Ascension paired with either Merritt Island or Corpus Christi, Texas, is better by virtue of having a larger equatorial component [see Equation (2.2.7)]. In light of this analysis, and in an effort to optimize the expenditure of resources by both the STDN and the MIT group, in May 1974 we reduced our schedule request to two tracks per week, one using Ascension and Madrid, the other using the east-west baseline which was available for the longest track during the week. The TDP sampling rate was also reduced to one observation per minute from each DDR. The lower sampling rate still provides enough samples during an observation period to ensure that short-period fluctuations will not be the dominant source of error

in the final parameter estimates. The reduction of the sampling rate also allowed the data to be transmitted from the stations via teletype to Goddard Space Flight Center and recorded there on magnetic tape, thus decreasing significantly the time and effort required for us to prepare the data for processing in PEP.

CHAPTER IV

Data Processing Techniques

4.1 Methods of Parameter Estimation

The estimation of parameter values from the observations is accomplished in PEP by weighted least-squares fitting. The theoretical basis for this method may be found in several texts (see [38], for example), and is not repeated here. The reader is also referred to Ash [6] for a discussion of the implementation of this estimation scheme in PEP. In this section I will describe briefly the equations used and discuss their application to the data from this experiment.

Suppose we have the vector of observations $\underline{y}_o$, of dimension n, and a mathematical model which gives the theoretical value of the observations as a function of the parameter vector $\underline{x}$, of dimension $m(\leq n)$. Then the vector of the observed values $\underline{y}_o$ may be written as a sum of the theoretically computed vector $\underline{y}_c$, and the measurement-error vector $\underline{\varepsilon}$:

$$\underline{y}_o = \underline{y}_c(\underline{x}) + \underline{\varepsilon} \qquad (4.1.1)$$

In weighted least-squares fitting, the estimate of the parameter vector, denoted by $\hat{\underline{x}}$, is the value of $\underline{x}$ that

minimizes the scalar quantity

$$[\underline{y}_o - \underline{y}_c(\underline{x})]^T \underline{\underline{W}} [\underline{y}_o - \underline{y}_c(\underline{x})] \qquad (4.1.2)$$

where $\underline{\underline{W}}$ is the (n x n) weighting matrix. The diagonal elements of $\underline{\underline{W}}$ are given by $1/\delta_i^2$, where δ_i is the assumed standard error in measurement i, and the off-diagonal elements are zero (see below).

A closed-form solution for $\hat{\underline{x}}$ exists if the dependence of $\underline{y}_c$ on $\underline{x}$ is linear in $\underline{x}$. If $\underline{y}_c$ is nonlinear, but well-enough behaved for small variations in $\underline{x}$, the problem can be linearized. Then if *a priori* values of the parameters, denoted by $\underline{x}^o$, are available which are sufficiently close to the true values, we can write

$$\underline{y}_o = \underline{y}_c(\underline{x}^o) + \underline{\underline{A}}(\underline{x} - \underline{x}^o) + \underline{\varepsilon} \qquad (4.1.3)$$

where $\underline{\underline{A}}$ is the n x m matrix of partial derivatives with elements $a_{ij} = [\partial y_i/\partial x_j]_{\underline{x}^o}$. If Equation (4.1.3) is valid and the columns of $\underline{\underline{A}}$ are linearly independent, then the least-squares estimate of $\underline{x}$ is given by

$$\hat{\underline{x}} = \underline{x}^o + (\underline{\underline{A}}^T \underline{\underline{W}} \underline{\underline{A}})^{-1} \underline{\underline{A}}^T \underline{\underline{W}} [\underline{y}_o - \underline{y}_c(\underline{x}^o)] \qquad (4.1.4)$$

If $\underline{x}^o$ is not sufficiently close to $\hat{\underline{x}}$ at the outset, then one must iterate, replacing $\underline{x}^o$ with the right side of Equation (4.1.4), then re-evaluating that

side. The solution is said to be converged when substitution of the estimated values of the parameters back into the model produces no significant further decrease in the sum of weighted squared residuals defined by Equation (4.1.2). It is possible, in principle, that the solution so obtained will correspond to a relative, rather than to the absolute, minimum of Equation (4.1.2). In practice the parameter values are sufficiently well known *a priori* that the solution will converge to the proper values.

The statistical properties of the weighted-least-squares estimate depend mainly on the statistics of the errors of observation, $\underline{\varepsilon}$. In particular, if the elements of $\underline{\varepsilon}$ are samples of zero-mean, Gaussian, independent random variables, and if each observation is weighted inversely with its associated error variance, then the weighted-least-squares estimate is the maximum-likelihood estimate. In this case the covariance matrix of the error in $\underline{\hat{x}}$ is given by

$$\underline{\underline{P}} = (\underline{\underline{A}}^T \underline{\underline{W}} \underline{\underline{A}})^{-1} \qquad (4.1.5)$$

If, further, we denote the elements of $\underline{\underline{P}}$ by p_{ij}, the so-called formal standard error of the estimate of parameter $\underline{i}$ is

$$\sigma_i = \sqrt{p_{ii}} \tag{4.1.6}$$

and the correlation coefficient between the errors in the estimates of x_i and x_j is

$$\rho_{ij} = \frac{p_{ij}}{\sqrt{p_{ii}}\sqrt{p_{jj}}} \tag{4.1.7}$$

In practice, σ_i in Equation (4.1.6) can usually be considered only a lower bound on the uncertainties in the parameter estimates. The actual observation errors are most often dominated by processes with significant systematic components. The effect of such systematic errors on the parameter estimates is discussed in Section 4.5.

One source of significant measurement-error correlations in most counted-cycle observations has been eliminated in this experiment by the way in which the observed quantity has been defined. It has been conventional in Doppler tracking to define the observable as the difference between successive counter readings divided by the time interval between them. The resultant from this operation is the average frequency over the interval, a quantity which can be interpreted in coherent Doppler tracking as the average (two-way) Doppler shift of the signal between transmission and reception. However, because the error in a given sample of the counter

contributes in an equal and opposite manner to each of two neighboring average Doppler values, the errors in successive measurements will have a correlation of -0.5 if other noise sources are ignored. Using the simple three-parameter model described in Section 2.2 of this thesis, Shapiro et al. [32] have shown that the neglect of this correlation leads to a significant overestimate of the error in lunar baseline determination. The formal standard errors obtained from a single six-hour observation period will be too large by a factor of n, where n is the number of observations, and the actual error standard deviation will be too large by a factor of $\sqrt{n}$. If the observable is chosen to be the accumulated N-count, formed by subtracting the counter reading at the beginning of the observation period from each successive reading, this problem of correlated sampling errors can be easily avoided (see Section 4.2.1). The -0.5 correlation between the error in each measurement and the error in the initial counter reading is eliminated by solving for an unknown constant for each series of uninterrupted observations. This "bias" parameter will absorb a number of errors which are constant throughout a tracking period (see Section 4.5).

4.2 Theoretical Model for the Observable

4.2.1 Basic Formulation

By counting cycles of the output signal of the voltage-controlled multivibrator (VCM) of the DDR, the tracking data processor (TDP) at each station measures the phase of this signal as a function of time. As described in Section 3.2, the change in the phase over a given time interval is just 360 times the change in the phase difference between the carrier signals received from the two ALSEPs, plus a known bias which is introduced by the frequency synthesizer. Some random measurement noise is also present. Since the initial reading of the TDP is arbitrary, without loss of generality we may define this reading to be zero. Then the reading of the TDP at station j at time t_j is

$$N_j(t_j) = [\phi_{r2j}(t_j) - \phi_{r1j}(t_j) + \phi_{Bj}(t_j) + \phi_{Nj}(t_j)] - [\phi_{r2j}(t_j^0) - \phi_{r1j}(t_j^0) + \phi_{Bj}(t_j^0) + \phi_{Nj}(t_j^0)] \tag{4.2.1}$$

where $\phi_{rij}(t_j)$ is the phase of the signal received from the $\underline{i}^{th}$ ALSEP at the $\underline{j}^{th}$ station at time t_j; ϕ_{Bj} is the known bias; and ϕ_{Nj} is the random noise. Note that, by definition $N_j(t_j^0) \equiv 0$, where t_j^0 is the time of

the initial reading of the TDP. The TDP counts whole cycles of the signal from the VCM, so that in Equation (4.2.1) the unit of N_j is 1/360th of a cycle, or 1° of phase. The error due to the integer-degree truncation is included in the noise term, ϕ_{Nj}.

The times in Equation (4.2.1) are the coordinate times, rather than the station clock readings, when the cycle-count is sampled by the TDP. The relationship between coordinate time and the station time is given in Appendix A1 and discussed in some detail by Ash [6]. Briefly, coordinate time is the independent variable in the equations of motion which we integrate to obtain the positions and velocities of the moon, the earth, and the planets. Coordinate time and atomic time differ by small diurnal, monthly, and annual periodic terms. The station clocks are set, within 10 to 20 μsec, to Coordinated Universal Time (UTC), which has a well-known (defined) relationship with atomic time.

The signal received at the time t_j was transmitted by the i^{th} ALSEP at the time t_i given by

$$t_i = t_j - \tau_{ij} \qquad (4.2.3)$$

where τ_{ij} is the propagation time delay. The phase of the received signal, ϕ_{rij}, is related to the

phase of the transmitted signal, ϕ_{ti}, by

$$\phi_{rij}(t_j) = \phi_{ti}(t_j - \tau_{ij}) \qquad (4.2.4)$$

Thus, the TDP reading at station j may be expressed in terms of the transmitted phases:

$$N_j(t_j) = [\phi_{t2}(t_j - \tau_{2j}) - \phi_{t1}(t_j - \tau_{1j}) + \phi_{Bj}(t_j) + \phi_{Nj}(t_j)] - [\text{similar terms for } t_j^0] \qquad (4.2.5)$$

The <u>differenced N-count observable</u>* is defined as the simple arithmetic difference between the TDP readings, or N-counts, at two stations, taken at identical readings of the two station clocks. Suppose

---

* This observable might equally well have been termed the "doubly-differenced N-count", since the phase is differenced both between stations and between ALSEPs. I have chosen the simpler term inasmuch as the difference between ALSEPs is taken in the DDR before the counting is performed.

that when these clock readings both equal T^m, the coordinate times are t_j^m and t_k^m at station j and station k, respectively. Then the differenced N-count at this "$\underline{m}^{th}$ sample time" is

$$\Delta N_{jk}^m \equiv N_j(t_j^m) - N_k(t_k^m) \qquad (4.2.6)$$

Substituting Equation (4.2.5) into Equation (4.2.6), we obtain

$$\begin{aligned}\Delta N_{jk}^m = \{&[\phi_{t2}(t_j^m - \tau_{2j}^m) - \phi_{t2}(t_k^m - \tau_{2k}^m)] \\ &-[\phi_{t1}(t_j^m - \tau_{1j}^m) - \phi_{t1}(t_k^m - \tau_{1k}^m)] \\ &+ [\phi_{Nj}^m - \phi_{Nk}^m]\} - \{\text{similar terms} \\ &\text{for } m = 0\}\end{aligned} \qquad (4.2.7)$$

where the superscript $\underline{m}$ on τ_{ij} and ϕ_{Nj} denotes that the coordinate time argument is t_j^m. The ϕ_{Bj} and ϕ_{Bk} "bias" terms are omitted deliberately. These terms cancel since the synthesizers that determine the bias frequencies at both stations have the same setting : the synthesizer and the clock at a given station use the same reference frequency standard.

We assume that the transmitter frequency as a function of time can be represented by

$$\phi_{ti}(t + \Delta t) = \phi_{ti}(t) + \dot{\phi}_{ti}(t)\Delta t + \frac{1}{2}\ddot{\phi}_{ti}(t)\Delta t^2 + \ldots \tag{4.2.8}$$

where Δt is some as yet unspecified interval. Using Equation (4.2.8) we expand Equation (4.2.7):

$$\begin{aligned}\Delta N^m_{jk} = \{&[\phi_{t2}(t^m_j-\tau^m_{2j}) - \phi_{t2}(t^m_j-\tau^m_{2j}) - \dot{\phi}_{t2}(t^m_j-\tau^m_{2j})(t^m_k-t^m_j-\tau^m_{2k}+\tau^m_{2j}) \\ &- \tfrac{1}{2}\ddot{\phi}_{t2}(t^m_j-\tau^m_{2j})(t^m_k-t^m_j-\tau^m_{2k}+\tau^m_{2j})^2 - \ldots] \\ &- [\phi_{t1}(t^m_j-\tau^m_{1j}) - \phi_{t1}(t^m_j-\tau^m_{1j}) - \dot{\phi}_{t1}(t^m_j-\tau^m_{1j})(t^m_k-t^m_j-\tau^m_{1k}+\tau^m_{1j}) \\ &- \tfrac{1}{2}\ddot{\phi}_{t1}(t^m_j-\tau^m_{1j})(t^m_k-t^m_j-\tau_{1k}+\tau^m_{1j})^2 - \ldots] \\ &+ [\phi^m_{Nj}-\phi^m_{Nk}]\} - \{\text{similar terms for } m = 0\}\end{aligned} \tag{4.2.9}$$

or

$$\begin{aligned}\Delta N^m_{jk} = \{&\dot{\phi}_{t1}(t^m_j-\tau^m_{1j})(\tau^m_{1j}-\tau^m_{1k}) - \dot{\phi}_{t2}(t^m_j-\tau^m_{2j})(\tau^m_{2j}-\tau^m_{2k}) \\ &+ [\dot{\phi}_{t1}(t^m_j-\tau^m_{1j})-\dot{\phi}_{t2}(t^m_j-\tau^m_{2j})](t^m_k-t^m_j) \\ &- \tfrac{1}{2}\ddot{\phi}_{t2}(t^m_j-\tau^m_{2j})(t^m_k-t^m_j-\tau^m_{2k}+\tau^m_{2j})^2 \\ &+ \tfrac{1}{2}\ddot{\phi}_{t1}(t^m_j-\tau^m_{1j})(t^m_k-t^m_j-\tau^m_{1k}+\tau^m_{1j})^2 + \ldots \\ &+ [\phi^m_{Nj}-\phi^m_{Nk}]\} - \{\text{similar terms for } m = 0\}\end{aligned} \tag{4.2.10}$$

The terms in Equation (4.2.10) have been listed in descending order of magnitude. The geometric information in the observable is contained primarily in the terms in the first line. The main computational task in the determination of the theoretical value of the observable is the evaluation of the propagation delays in the expressions of line 1. Subsection 4.2.2 deals with this evaluation. A second task, much simpler but equally important, is to determine the transmitter frequencies, $\dot{\phi}_{t1}(t_j^m - \tau_{1j}^m)$ and $\dot{\phi}_{t2}(t_j^m - \tau_{2j}^m)$, which are used to convert the calculated delays to phase. Subsection 4.2.3 deals with the evaluation of these quantities.

The terms in line 2 of Equation (4.2.10) account for the non-simultaneity of the receive times. The only effect modeled here is the approximately 1 μsec diurnal variation of the atomic-to-coordinate time difference. We have not attempted to account for constant errors in clock synchronization, or for offsets of the rates of the clocks at the stations from UTC. The errors introduced into our model of the observable by the neglect of these effects are discussed in Section 4.5.

The third and fourth lines of Equation (4.2.10) contain terms involving variations in the transmitter

frequencies. We shall see in the discussion of transmitter frequency characteristics in Subsection 4.2.3 that the effect of these terms is insignificant.

Finally, the random measurement noise term is not included in the theoretical model of the observable except for the initial observation (m = 0). For a given series of observations, the same unknown (solved-for) constant is added to the value of ΔN_{jk}^{m} for all $m \geq 1$, to represent the constant contribution to ΔN_{jk}^{m} of the error in the {m = 0} term in Equation (4.2.10), as discussed in Section 4.1.

4.2.2 Evaluation of Propagation Delays

Each of the propagation delays, τ_{ij}^{m}, in Equation (4.2.10) can be considered, with sufficient accuracy, to be the sum of a geometric (free-space) delay plus a small additional delay representing the effect of the propagation medium on the signal. The geometric delay is the magnitude of the vector

$$\frac{1}{c}\vec{R}_{ij} \triangleq \frac{1}{c}\vec{R}(t_i,t_j) \equiv \vec{r}_m(t_i) + \vec{r}_{ti}(t_i) - \vec{r}_e(t_j) - r_{sj}(t_j) \qquad (4.2.11)$$

where

c is the speed of light;

$\vec{r}_m(t_i)$ is the position of the moon's center of mass with respect to the solar-system barycenter at the time of transmission t_i;

$\vec{r}_{ti}(t_i)$ is the position of transmitter $\underline{i}$ with respect to the moon's center of mass* at t_i;

$\vec{r}_e(t_j)$ is the position of the earth's center of mass with respect to the solar-system barycenter at the time of reception t_j;

and

$\vec{r}_{sj}(t_j)$ is the position of the observing site with respect to the earth's center of mass* at t_j.

The solar-system barycenter is used as the origin of the coordinate system used for the calculation of $\vec{R}_{ij}$ so that our coordinate system may be indistinguishable from an inertial system. The directions of the coordinate axes of the system are defined in theory by the mean equator

---

*Strictly speaking the vectors $\vec{r}_{ti}$ and $\vec{r}_{sj}$ should be expressed properly in the solar-system-barycentric system. I ignored this refinement and added the coordinates (even though expressed in the body-fixed systems) directly in Equation (4.2.11). The resulting errors should be completely negligible.

and equinox of 1950.0. Operationally, the definition of the coordinate system is provided by the models used for the orbits of the planets and the moon and the motions of the earth and moon about their respective centers of mass. The planetary ephemerides which I used were generated at MIT by adjusting the system of planetary masses and the initial conditions of a numerical integration of the planetary orbits to fit many years of optical, radar, and spacecraft tracking data [2, 4, 5]. The particular ephemeris tape employed in processing the data for this thesis is named NBODY311, dated 16 August 1969. My lunar ephemeris resulted from fitting a numerical integration to four and one-half years of laser ranging data [1 , 33 , 34], using the equations originally developed at MIT by M. A. Slade [36]. The model for the motion of a transmitter on the lunar surface with respect to the moon's center of mass included both the mean rotation and the physical libration. This model is of particular interest for this thesis and is described in detail in Section 4.3. Finally, the calculation of the positions of the observing sites in the earth-centered 1950.0 coordinate system, including precession, nutation, variation of UT.1, and polar motion, has been documented by Ash [6].

Given the coordinate time, t, of reception of a signal, the geometric delay $\tau'_{ij}(t)$ is determined iteratively:

$$\tau'_{ij}(t) = \lim_{k\to\infty} \tau'^{(k)}_{ij}(t) \qquad (4.2.12)$$

where

$$\tau'^{(k+1)}_{ij}(t) = \frac{1}{c} R_{ij}(t - \tau'^{(k)}_{ij}(t),\ t)$$

$$k = 0,\ 1,\ \ldots \qquad (4.2.13)$$

and

$$\tau'^{(0)}_{ij}(t) = 1.25 \text{ seconds} \qquad (4.2.14)$$

The additional propagation delay due to the atmosphere was not included in the light-time iteration but was added as a small correction to $\tau'_{ij}(t)$ to yield $\tau_{ij}(t)$. The amount of propagation delay due to the neutral atmosphere was calculated for each site from the monthly-average data for the zenith delay compiled at the Goddard Space Flight Center [28], using a model developed by Chao [10] for the effect of elevation angle. No attempt was made to model the effect of the ionosphere on the propagation delays. Estimates of the errors from both the neutral atmosphere and the ionosphere are given in Section 4.5.

4.2.3 Determination of Transmitter Frequencies

For the evaluation of the theoretical value of the observable by means of Equation (4.2.10) we also

require the values of the transmitter frequencies and their rates of change. The accuracy with which these frequencies must be known, for a given uncertainty in the calculated value of ΔN^m_{ij}, is set by the magnitude of the propagation-delay difference $(\tau_{ij} - \tau_{ik})$ in the first line of Equation (4.2.10). This difference depends on the rotation of the earth, the positions of the stations, etc., but is usually on the order of a few msec and is rarely greater than 10 msec. For the theoretical observable to have an uncertainty of less than 1°, or 0.003 cycles, the transmitted frequency must be known to within (0.003 cycles) ÷ (.01 sec) = 0.3 Hz, or to about 1 part in 10^{10}.

The ALSEP frequencies are not known a priori with nearly this accuracy. These frequencies can vary unpredictably by several kHz from one day to the next, by several hundred Hz to about 1 kHz over 1 hour, and by about 1 Hz in 1 sec, representing even in the last instance a change of 5 parts in 10^{10}. Thus it is necessary to monitor the frequencies of the signals received from the ALSEPs at one (or more) of the tracking stations, and to calculate the transmitted frequencies from the measurements of the received frequencies by accounting for the Doppler shift between the transmitter

and the receiver. How accurate can this procedure be? The accuracy of the cesium-beam reference frequency standard at the station exceeds our requirement of 1 part in 10^{10}. The uncertainties of the a priori positions of the tracking stations, the geocentric ephemeris of the moon, etc., which are needed to calculate the Doppler shift, are smaller than the equivalent of 1 second of arc, which corresponds to an uncertainty in the determination of the transmitter frequency of less than 1 part in 10^{11}. Evidently, then, there are no fundamental difficulties involved in using measurements of the frequency of the signal received at a tracking station as a function of time to determine the transmitted frequency as a function of time, with the accuracy desired for the calculation of Equation (4.2.10). However, a significant practical difficulty for the observations analyzed in this thesis has been that the only available received-frequency measurements have been relatively crude.

At one tracking station, the operator uses a digital counter to measure the received frequency of the reference ALSEP approximately every 15 minutes. The uncertainty in these measurements, including the uncertainty associated with interpolation of the frequency within the 15-minute intervals between measurements, is about 100 Hz. From the foregoing discussion it would appear that the

uncertainty of 100 Hz in this frequency measurement would lead to an uncertainty of a full cycle, or 360° of phase, in the evaluation of Equation (4.2.10). Fortunately, a much more accurate measurement is available of the difference between the received frequencies of the two ALSEPs -- from the output of the DDR. As long as the difference is known accurately, a relatively large common error in the two frequencies can be harmless, because the error introduced in the term in Equation (4.2.10) involving $\dot{\phi}_{t2}$ is very nearly cancelled by the error introduced in the term involving $\dot{\phi}_{t1}$. In fact, since generally

$$\left|(\tau^m_{2j} - \tau^m_{2k}) - (\tau^m_{1j} - \tau^m_{1k})\right| \lesssim 50\ \mu\text{sec} \qquad (4.2.15)$$

a simple common-mode frequency error of 100 Hz results in less than a 2° error in the evaluation of Equation (4.2.10). But a much smaller error in the measurement of the frequency difference can be much more serious because no comparable cancellation occurs. How well is the difference between the received frequencies known? For the observations analyzed in this thesis, the uncertainty associated with the difference-frequency measurement was of the order of 1 to 10 Hz,

due mainly to the fact that it was not possible to record measurements of the difference frequency with good time-resolution. The phase of the output of the DDR, which alone contains the needed information, was usually sampled and recorded by the TDP only at 60-second intervals. In fact, for most of the observations only every third sample was actually processed, in order to conserve computer time. Thus the frequency-measurement interval in most cases was 180 sec long. For historical reasons it was most convenient to use the difference-received-frequency measurement derived from the interval immediately preceding t_j^m, to remove the a priori Doppler shift from the received frequency, and to use the resulting value of transmitted frequency, assumed constant, in the evaluation of Equation (4.2.10). Usually the ALSEP transmitters were sufficiently stable that, even though the frequency-measurement time interval was centered ~90 sec before t_j^m, the error in Equation (4.2.10) due to the use of an inexact value of transmitter frequency was less than 5° (rms). However, in some cases the drift of the transmitter frequency was rapid and systematic, with a drift rate of ~0.5 Hz sec^{-1} persisting over several minutes or more. In such a case the just-described procedure would yield a frequency which was incorrect by ~45 Hz, and an error in Equation (4.2.10)

possibly as great as (~45 Hz)·(360°/cycle)·(0.01 sec) ≈ 160°, which would be intolerable. In cases of such rapid drift, I usually processed every data point instead of every third one so that the frequency-measurement time interval was centered only 30 sec before t_j^m; I also used a slightly more complicated algorithm to determine the transmitted frequencies, based on the use of three successive TDP readings to estimate the drift rate of the transmitted frequency.

In all cases, I programmed PEP to print out the rates of change of the transmitted frequencies and the calculated effect of those rates on the observable. If the error in a series of observations due to erratic behavior of the transmitter seemed likely to exceed a few degrees of phase, the observations were deleted from the later fits.

The specific algorithms used for the calculation of transmitter frequencies are as follows. We calculate the average transmitted frequency of the reference ALSEP over the transmit-time interval corresponding to the receive time interval t_j^{m-1} to t_j^m, by

$$\bar{f}_{tl}^{(m-\frac{1}{2})} = \frac{\bar{f}_{rlj}^{(m-\frac{1}{2})}}{(1 - \beta_{lj}^{m-\frac{1}{2}})} \qquad (4.2.16)$$

where $\bar{f}_{rlj}^{(m-\frac{1}{2})}$ is the received frequency of the reference ALSEP at the midpoint of the receive-time interval, deter-

mined by linear interpolation from the digital counter readings recorded by the operator at 15-minute intervals, and

$$\beta_{ij}^{m-\frac{1}{2}} = \frac{\tau_{ij}^{m} - \tau_{ij}^{m-1}}{t_j^{m} - t_j^{m-1}} \qquad (4.2.17)$$

is the average first-order Doppler shift over the interval t^{m-1} to t^{m}. A more precise calculation of $\bar{f}_{t1}^{(m-\frac{1}{2})}$ is not warranted since the accuracy of the result is limited at present by the accuracy with which the received frequency can be determined for the reference ALSEP.

As indicated previously, the transmitted frequency of the second ALSEP is calculated from the frequency of the reference ALSEP using the DDR output, so that the large error in $\bar{f}_{t1}^{(m-\frac{1}{2})}$ due to the crude measurement of $\bar{f}_{rlj}^{(m-\frac{1}{2})}$ is present equally in $\bar{f}_{t2}^{(m-\frac{1}{2})}$. From Equation (3.2.2), the average frequency of the DDR output at station j over the interval t^{m-1} to t^{m} is given by

$$\bar{f}_{Dj}^{(m-\frac{1}{2})} \triangleq \frac{N_j(t_j^m) - N_j(t_j^{m-1})}{t_j^m - t_j^{m-1}}$$

$$= 360[\bar{f}_{r2j}^{(m-\frac{1}{2})} - \bar{f}_{r1j}^{(m-\frac{1}{2})} + f_{Bj}] \qquad (4.2.18)$$

where f_{Bj} is the bias frequency which can be either positive or negative depending on the setting of the digital sideband selection switch in the DDR (see Section 3.2). Rearranging terms, we obtain an expression for the average received frequency of the second ALSEP:

$$\bar{f}_{r2j}^{(m-\frac{1}{2})} = \bar{f}_{r1j}^{(m-\frac{1}{2})} + \frac{\bar{f}_{Dj}^{(m-\frac{1}{2})}}{360} - f_{Bj} \qquad (4.2.19)$$

From this value, the average transmitted frequency is calculated using

$$\bar{f}_{t2}^{(m-\frac{1}{2})} = \frac{\bar{f}_{r2j}^{(m-\frac{1}{2})}}{(1-\beta_{2j}^{m-\frac{1}{2}})} \qquad (4.2.20)$$

where $\beta_{2j}^{m-\frac{1}{2}}$ is defined by Equation (4.2.17).

The rates of change of the transmitter frequencies are determined from the changes in $\bar{f}_{t1}^{(m-\frac{1}{2})}$ and $\bar{f}_{t2}^{(m-\frac{1}{2})}$ between successive TDP sampling intervals. It is assumed that the rate of change of frequency is constant over

two adjacent sampling intervals. Thus the transmitter frequency drift rate is calculated from

$$\dot{\bar{f}}_{ti}^{(m-1)} = \frac{(\bar{f}^{(m-\frac{1}{2})} - \bar{f}^{(m-\frac{3}{2})})}{\frac{1}{2}[(t^m - t^{m-1}) + (t^{m-1} - t^{m-2})]} \qquad (4.2.21)$$

If this rate is significant, as discussed previously, then the transmitted frequencies used for the calculation of the theoretical observable in Equation (4.2.10) are extrapolated to correspond to the time of reception, t^m, rather than to the midpoint of the previous sampling interval. That is, we use

$$\bar{f}_{ti}^{m} = \bar{f}_{ti}^{(m-\frac{1}{2})} + \frac{1}{2}\dot{\bar{f}}_{ti}^{m}(t^m - t^{m-1}) \qquad (4.2.22)$$

In any case, the value of $\bar{f}_{ti}^{m}$, expressed in degrees of phase per unit time, is substituted for $\dot{\phi}_{ti}(t_j^m - \tau_{ij}^m)$ in the evaluation of Equation (4.2.10). The terms involving $\ddot{\phi}_{ti}$ and higher derivatives in Equation (4.2.10) are ignored.

4.3 Model for the Rotation of the Moon

The dynamical equations of motion for the moon's rotation about its center of mass are the well-known Euler equations for rigid-body rotation:

$$\begin{aligned} A\dot{\omega}_1 + (C-B)\omega_2\omega_3 &= T_1 \\ B\dot{\omega}_2 - (C-A)\omega_1\omega_3 &= T_2 \\ C\dot{\omega}_3 + (B-A)\omega_1\omega_2 &= T_3 \end{aligned} \qquad (4.3.1)$$

in which ω_1, ω_2, ω_3, are the angular velocities of the moon about its principal axes; $A \leq B \leq C$ are the moments of inertia about these axes; and T_1, T_2, and T_3 are the corresponding components of the external torque, $\vec{T}$, exerted by the gravitational fields of the earth and sun on the asymmetries of the moon's figure. The rotation is usually parameterized by writing Equations (4.3.1) in the form

$$\begin{aligned} \dot{\omega}_1 &= -\alpha\omega_2\omega_3 + \frac{1}{A}T_1 \\ \dot{\omega}_2 &= \beta\omega_1\omega_3 + \frac{1}{B}T_2 \\ \dot{\omega}_3 &= -\gamma\omega_1\omega_2 + \frac{1}{C}T_3 \end{aligned} \qquad (4.3.2)$$

in which $\alpha = (C-B)/A$, $\beta = (C-A)/B$, and $\gamma = (B-A)/C$. These three ratios are not independent, but

$\alpha = (\beta - \gamma)/(1 - \beta\gamma)$. The torques are functions of β and γ, and also of coefficients of the moon's gravitational potential above the second degree (see below).

In principle one could generate a model of the lunar rotation by directly integrating Equations (4.3.2), expressing, with three Euler angles, the orientation of the moon's principal axes with respect to a set of axes fixed in inertial space (for example, the axes of the 1950.0 equator-equinox system). In fact, from the standpoint of modern numerical methods, this straightforward approach has many advantages. All models which have been developed thus far, however, introduce intermediate quantities in order to take advantage of the fact that the moon's rotation may be characterized by small-amplitude librations about a quasi-uniform "mean" rotation. This mean rotation was first described in 1693 by Cassini [9], in terms of two "laws":

(i) The moon rotates uniformly about its axis of maximum moment of inertia with a rotational angular velocity equal to its mean orbital angular velocity around the earth.

(ii) The lunar equator maintains a constant inclination with respect to the ecliptic; the planes of the lunar equator, lunar orbit and the ecliptic intersect

along a common line, and the plane of the ecliptic lies always in between the planes of the equator and the orbit.

As a consequence of these "laws", it has been customary to describe the moon's rotation with respect to the rotating set of axes defined by the so-called mean ecliptic and mean equinox of date: the conventionally defined mean-of-date (MOD) ecliptic coordinate system (see below). Usually the orientations of the moon's principal axes of inertia with respect to the MOD ecliptic coordinate axes are specified by three Euler angles, ψ, θ, and ϕ, as shown in Figure 4.1. The angular velocities ω_1, ω_2, and ω_3 are related to the time-derivatives of these Euler angles by

$$\begin{aligned} \omega_1 &= -\dot{\psi}\,\sin\theta\sin\phi - \dot{\theta}\cos\phi \\ \omega_2 &= -\dot{\psi}\,\sin\theta\cos\phi + \dot{\theta}\sin\phi \\ \omega_3 &= \dot{\psi}\,\cos\theta + \dot{\phi} \end{aligned} \qquad (4.3.3)$$

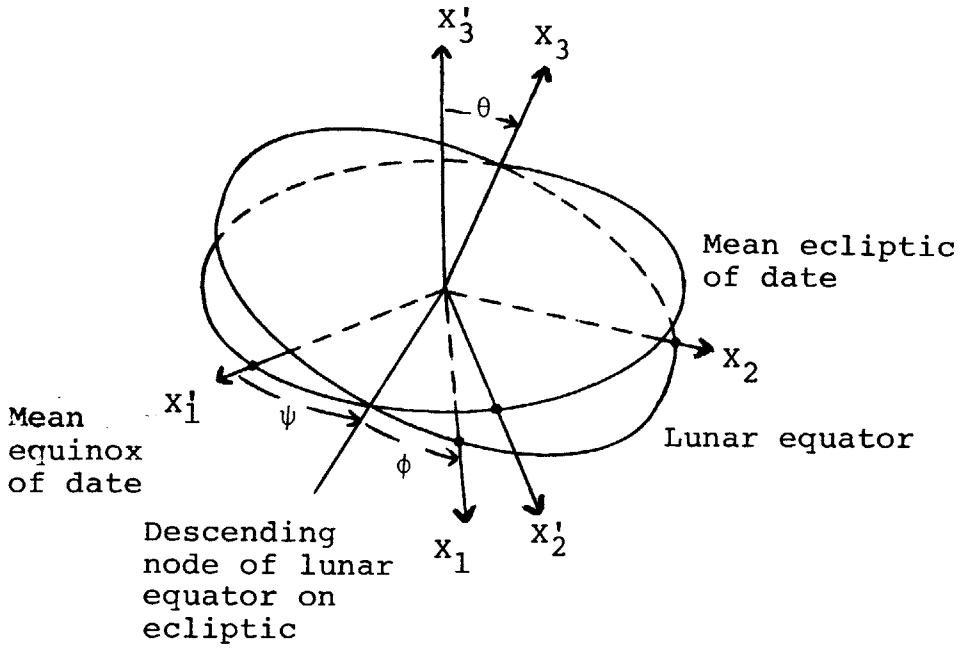


Figure 4.1 Orientation of the selenodetic coordinate system with respect to the mean-of-date ecliptic system. X_1, X_2, and X_3 designate the moon's principal axes of inertia. X_1', X_2' and X_3' represent the axes of the MOD ecliptic system.

The physical libration is defined as the deviation of the moon's rotation from that predicted by Cassini's laws, and is described by the three small angles σ, ρ, and τ, which are defined by

$$\sigma = \psi - \Omega$$
$$\rho = \theta - I \qquad (4.3.4)$$
$$\tau = \psi + \phi - \text{☾} - \pi$$

where Ω is the longitude of the ascending node of the moon's mean orbit on the mean ecliptic of date, measured from the mean equinox of date along the ecliptic; I is the inclination of the lunar equator with respect to the mean ecliptic of date; ℓ is the mean orbital longitude of the moon measured from the mean equinox of date; $\pi = 3.14159...$; σ, ρ, and τ are the angles describing the physical librations in node, latitude, and longitude, respectively. The angles Ω and ℓ are obtained conventionally from the Improved Lunar Ephemeris (see [17]).

$$\Omega = 259°10'59\overset{''}{.}79 - 5^{r}134°08'31\overset{''}{.}23T + 7\overset{''}{.}48T^2 + 0\overset{''}{.}008T^3 \qquad (4.3.5a)$$

$$\ell = 270°26'02\overset{''}{.}99 + 1336^{r}307°52'59\overset{''}{.}31T - 4\overset{''}{.}08T^2 + 0\overset{''}{.}0068T^3 \qquad (4.3.5b)$$

where T is measured in Julian centuries of 36525 ephemeris days from Julian Day 2415020.0 (1900 Jan 0.5 E.T.).

The libration model used for this thesis resulted from a numerical integration, performed by W. S. Sinclair, M. A. Slade, and J. G. Williams of the Jet Propulsion Laboratory, of the equations of motion for the quantities $I\sigma$, ρ, and τ. These equations were derived from Equation (4.3.2) by means of Equations (4.3.3) and (4.3.4), with the torque given by

$$\vec{T} = M_e \vec{r}_e \times (\nabla U)_e + M_s \vec{r}_s \times (\nabla U)_s \qquad (4.3.6)$$

where M_e, M_s are the masses of the earth and sun, $\vec{r}_e$ and $\vec{r}_s$ are the positions of the earth and sun relative to the moon, and $(\nabla U)_x$ is the gradient of the moon's gravitational potential at the center of mass of body x. The potential is represented by an expansion in spherical harmonics:

$$U = \frac{k^2 M_m}{r} \{1 - \sum_{n=2}^{\infty} J_n (\frac{R_m}{r})^n P_n(\sin L)$$

$$+ \sum_{n=2}^{\infty} \sum_{h=1}^{n} (\frac{R_m}{r})^n [C_{nh} \cos h\ell + S_{nh} \sin h\ell] P_{nh}(\sin L) \} \qquad (4.3.7)$$

where r, L, and ℓ are, respectively, the radius, latitude, and longitude referred to the principal-axis system; k^2 is the gravitational constant (see Appendix A.1); M_m is the mass of the moon; R_m is an adopted value for the moon's equatorial radius; J_n are the zonal-harmonic coefficients; C_{nh} and S_{nh} are the tesseral cosine and sine harmonic coefficients, respectively; and P_n and P_{nh} are the Legendre polynomials and generalized Legendre functions, respectively.

The gravitational harmonic coefficients enter Equation (4.3.2) multiplied by factors of $M_m R_m^n$ and divided by A, B, or C. If the value of either J_2 or C_{22}

is known independently, e.g. from observations of spacecraft orbiting the moon, then this value may be combined with the values of β and γ to determine $C/M_m R_m^2$. Thus, the measurements of the third- and higher-degree harmonic coefficients derived from the physical libration will be uncertain by a common scale factor, with the uncertainty in scale set by the uncertainty in the independent determination of J_2 or C_{22} or, equivalently, in $C/M_m R_m^2$. The relationships among these quantities and their uncertainties are discussed by Williams et al. [40]. In the JPL libration model, J_2 has been fixed at a value of 2.03822×10^{-4}, determined from an analysis of Lunar Orbiter data. The adjustable parameters in the model are β, γ, J_3, C_{31}, C_{32}, C_{33}, S_{31}, S_{32}, and S_{33}. Values for C_{22} and $C/M_m R_m^2$ may be derived from the adopted value of J_2 and from the values for β and γ determined from the observations. A description of the procedure used at JPL to generate the integrated libration model is also given in [40]. The numerical values of the parameters in the particular model I have used are listed in Appendix A.1.

The values of τ, ρ, and σ determined from the libration model, in combination with the conventionally defined values of ℓ and Ω, define the relationship between the

selenodetic coordinates of an ALSEP, $\underline{X}$, and the corresponding MOD ecliptic coordinates, $\underline{X}'$ [see Figure 4.1 and Equations (4.3.4)].

$$\underline{X} = \underline{\underline{U}}\,\underline{X}' \tag{4.3.8}$$

where

$$\underline{\underline{U}} = \begin{bmatrix} \cos\psi\cos\phi-\sin\psi\cos\theta\sin\phi & \sin\psi\cos\phi+\cos\psi\cos\theta\sin\phi & -\sin\theta\sin\phi \\ -\cos\psi\sin\phi-\sin\psi\cos\theta\cos\phi & -\sin\psi\sin\phi+\cos\psi\cos\theta\cos\phi & -\sin\theta\cos\phi \\ -\sin\psi\sin\theta & \cos\psi\sin\theta & \cos\theta \end{bmatrix} \tag{4.3.9}$$

The transformation from MOD ecliptic coordinates to 1950.0 coordinates, $\underline{x}$, is defined by Ash [3]:

$$\underline{x} = \underline{\underline{A}}^{T}\underline{X}' \tag{4.3.10}$$

where

$$\underline{\underline{A}} = \begin{bmatrix} p_{11} & p_{21}\cos\varepsilon_o+p_{31}\sin\varepsilon_o & p_{31}\cos\varepsilon_o-p_{21}\sin\varepsilon_o \\ p_{21} & p_{22}\cos\varepsilon_o+p_{32}\sin\varepsilon_o & p_{32}\cos\varepsilon_o-p_{22}\sin\varepsilon_o \\ p_{31} & p_{23}\cos\varepsilon_o+p_{33}\sin\varepsilon_o & p_{33}\cos\varepsilon_o-p_{23}\sin\varepsilon_o \end{bmatrix} \tag{4.3.11}$$

In Equation (4.3.11), ε_o is the conventional value for the mean obliquity of the earth's equator to the ecliptic, given by [17]

$$\varepsilon = 23°27'08\overset{''}{.}26 - 46\overset{''}{.}845T - 0\overset{''}{.}0059T^2 + 0\overset{''}{.}00181T^3 \qquad (4.3.12)$$

and p_{ij} are the elements of the precession matrix. The precession matrix used in PEP is derived from the conventional representation [17]; in addition, the matrix includes the possible effects of small additional angular rates about the three axes of the 1950.0 system. These rates may be adjusted in the least-squares solution. For a complete definition of the precession matrix, see Ash [6].

Using the fact that $\underline{\underline{U}}$ is orthogonal (hence, $\underline{\underline{U}}^{-1} = \underline{\underline{U}}^T$), we can combine Equations (4.3.8) and (4.3.10) to give the complete transformation from the selenodetic system to the 1950.0 mean equator-equinox system:

$$\underline{x}(t) = \underline{\underline{A}}^T(t)\underline{\underline{U}}^T(t)\underline{X} \qquad (4.3.13)$$

where the time dependence of $\underline{x}$, $\underline{\underline{A}}$, and $\underline{\underline{U}}$ has been denoted explicitly.

4.4 Partial Derivatives of the Observable with Respect to Parameters

Using Equations (4.2.10) and (4.2.22), we can write the differenced N-count observable as

$$\Delta N^m_{jk} = \bar{f}^m_{t1}(\tau^m_{1j} - \tau^m_{1k}) - \bar{f}^m_{t2}(\tau^m_{2j} - \tau^m_{2k}) - [\text{similar terms for } m = 0] \qquad (4.4.1)$$

Changes in the values of the parameters in our model of the earth-moon system affect the propagation delays, $\tau_{ij}(t^m)$. If we ignore the weak dependence of $\bar{f}^m_{t1}$ and $\bar{f}^m_{t2}$ on the delays, the partial derivative of ΔN^m_{jk} with respect to a parameter, p, may be written

$$\frac{\partial \Delta N^m_{jk}}{\partial p} = \bar{f}^m_{t1}\left[\frac{\partial \tau^m_{1j}}{\partial p} - \frac{\partial \tau^m_{1k}}{\partial p}\right] - \bar{f}^m_{t2}\left[\frac{\partial \tau^m_{2j}}{\partial p} - \frac{\partial \tau^m_{2k}}{\partial p}\right] - [\text{similar terms for } m = 0] \qquad (4.4.2)$$

From the discussion above Equation (4.2.11),

$$\frac{\partial \tau^m_{ij}}{\partial p} = \frac{1}{c} \frac{\partial |\vec{R}_{ij}(t^m_i, t^m_j)|}{\partial p} \qquad (4.4.3)$$

where $|\vec{R}_{ij}(t_i, t_j)|$ is the magnitude of the vector pointing from receiving site j to transmitter i on the

moon. We will denote the Cartesian coordinates of $\vec{R}_{ij}(t_i,t_j)$ in the 1950.0 system by the mathematical vector (3 x 1 column matrix of the coordinates) $\underline{x}_{ij}$. The unit of $\underline{x}_{ij}$ is the light-second, the fundamental distance unit of the observations. Then Equation (4.4.3) can be written

$$\frac{\partial \tau_{ij}}{\partial p} = \frac{\partial |\underline{x}_{ij}|}{\partial p} = \frac{\underline{x}_{ij}^T}{|\underline{x}_{ij}|} \cdot \frac{\partial \underline{x}_{ij}}{\partial p}$$

$$= \frac{\underline{x}_{ij}^T}{|\underline{x}_{ij}|} \cdot \left[\frac{\partial \underline{x}_m}{\partial p} + \frac{\partial \underline{x}_{ti}}{\partial p} - \frac{\partial \underline{x}_e}{\partial p} - \frac{\partial \underline{x}_{sj}}{\partial p}\right] \qquad (4.4.4)$$

where $\underline{x}_m$, $\underline{x}_{ti}$, $\underline{x}_e$, and $\underline{x}_{sj}$ give the 1950.0 Cartesian coordinates of the vectors $\vec{r}_m(t_i)$, $\vec{r}_{ti}(t_i)$, $\vec{r}_e(t_j)$, and $\vec{r}_{sj}(t_j)$, which represent the positions of the moon, ALSEP transmitter, earth, and observing site, respectively, as defined in Section 4.2.2.

4.4.1 Partials with Respect to Parameters of the Lunar Orbit

ALSEP differential VLBI observations are relatively insensitive to the orbital motion of the moon. However, partials of the theoretical differenced N-count observable with respect to the 6 initial conditions of the lunar orbit and the mass of the earth-moon system were calculated, in addition to the partials of the theoretical laser ranging observable. The latter observable is, of course,

highly sensitive to the orbital motion. For any one of the 6 orbital and 1 mass parameter(s), the derivative $\frac{\partial \underline{x}_{ij}}{\partial p}$ in Equation (4.4.4) is simply

$$\frac{\partial \underline{x}_{ij}}{\partial p} = \frac{\partial}{\partial p}(\underline{x}_m - \underline{x}_e) \tag{4.4.5}$$

I integrated these partials numerically, simultaneously with the orbit of the moon, using the equations described by Ash [3] and Slade [36]. The components of the partials at a particular epoch are determined by interpolation from values written on the integration tape.

4.4.2 Partials with Respect to the ALSEP Selenodetic Coordinates

From Equation (4.3.13) the selenocentric coordinates of an ALSEP transmitter expressed in the 1950.0 system, $\underline{x}_{ti}$, are related to the principal-axis (selenodetic) coordinates $\underline{X}_{ti}$, by

$$\underline{x}_{ti}(t) = \underline{\underline{A}}^T(t)\underline{\underline{U}}^T(t)\underline{X}_{ti} \tag{4.4.6}$$

If p represents the selenodetic radius r, longitude ℓ, or latitude L of an ALSEP, then

$$\frac{\partial \underline{x}_{ij}}{\partial p} = \frac{\partial \underline{x}_{ti}}{\partial p} = \underline{\underline{A}}^T\underline{\underline{U}}^T \frac{\partial \underline{X}_{ti}}{\partial p} \tag{4.4.7}$$

Since

$$\underline{X}_{ti} = \begin{pmatrix} r \cos \ell \cos L \\ r \sin \ell \cos L \\ r \sin L \end{pmatrix} \tag{4.4.8}$$

we have

$$\frac{\partial \underline{X}_{ti}}{\partial r} = \frac{\underline{X}_{ti}}{r} \tag{4.4.9a}$$

$$\frac{\partial \underline{X}_{ti}}{\partial \ell} = \begin{pmatrix} -r \sin\ell \cos L \\ r \cos\ell \cos L \\ 0 \end{pmatrix} \tag{4.4.9b}$$

$$\frac{\partial \underline{X}_{ti}}{\partial L} = \begin{pmatrix} -r \cos\ell \sin L \\ -r \sin\ell \sin L \\ r \cos L \end{pmatrix} \tag{4.4.9c}$$

4.4.3 Partials with Respect to Libration Parameters

For physical libration parameters, Equation (4.4.6) may again be used, since the libration affects the observable through the lunar rotation matrix $\underline{\underline{U}}(t)$.

$$\frac{\partial \underline{x}_{ij}}{\partial p} = \frac{\partial \underline{x}_{ti}}{\partial p} = \underline{\underline{A}}^T \frac{\partial \underline{\underline{U}}^T}{\partial p} \underline{X}_{ti} \tag{4.4.10}$$

The elements of $\underline{\underline{U}}^T$ are functions of the Euler angles ψ, θ, and ϕ, which describe the orientation of the

selenodetic system with respect to the mean-of-date ecliptic system (see Section 4.3). Thus,

$$\frac{\partial \underline{\underline{U}}^T}{\partial p} = \frac{\partial \underline{\underline{U}}^T}{\partial \psi}\frac{\partial \psi}{\partial p} + \frac{\partial \underline{\underline{U}}^T}{\partial \theta}\frac{\partial \theta}{\partial p} + \frac{\partial \underline{\underline{U}}^T}{\partial \phi}\frac{\partial \phi}{\partial p} \qquad (4.4.11)$$

and, from Equation (4.3.9),

$$\frac{\partial \underline{\underline{U}}}{\partial \psi} = \begin{pmatrix} -\sin\psi\cos\phi-\cos\psi\cos\theta\sin\phi & \cos\psi\cos\phi-\sin\psi\cos\theta\sin\psi & 0 \\ \sin\psi\sin\phi-\cos\psi\cos\theta\cos\phi & -\cos\psi\sin\phi-\sin\psi\cos\theta\cos\phi & 0 \\ -\cos\psi\sin\theta & -\sin\psi\sin\theta & 0 \end{pmatrix}$$

$$= \begin{pmatrix} -u_{12} & u_{11} & 0 \\ -u_{22} & u_{21} & 0 \\ -u_{32} & u_{31} & 0 \end{pmatrix} \qquad (4.4.12a)$$

$$\frac{\partial \underline{\underline{U}}}{\partial \theta} = \begin{pmatrix} \sin\psi\sin\theta\sin\phi & -\cos\psi\sin\theta\sin\phi & -\cos\theta\sin\phi \\ \sin\psi\sin\theta\cos\phi & -\cos\psi\sin\theta\cos\phi & -\cos\theta\cos\phi \\ -\sin\psi\cos\theta & \cos\psi\cos\theta & -\sin\theta \end{pmatrix} \qquad (4.4.12b)$$

$$\frac{\partial \underline{\underline{U}}}{\partial \phi} = \begin{pmatrix} -\cos\psi\sin\phi - \sin\psi\cos\theta\cos\phi & -\sin\psi\sin\phi + \cos\psi\cos\theta\cos\phi & -\sin\theta\cos\phi \\ -\cos\psi\cos\phi + \sin\psi\cos\theta\sin\phi & -\sin\psi\cos\phi - \cos\psi\cos\theta\sin\phi & \sin\theta\sin\phi \\ 0 & 0 & 0 \end{pmatrix}$$

$$= \begin{pmatrix} u_{21} & u_{22} & u_{23} \\ -u_{11} & -u_{12} & -u_{13} \\ 0 & 0 & 0 \end{pmatrix} \qquad (4.4.12c)$$

in which u_{ij} is the element of the $\underline{i}^{th}$ row and $\underline{j}^{th}$ column of $\underline{\underline{U}}$.

The physical libration parameters affect the Euler angles through the libration angles τ, σ and $(I + \rho)$. From Equation (4.3.4),

$$\begin{aligned} \psi &= \Omega + \sigma \\ \theta &= I + \rho \\ \phi &= \text{(} + \pi - \Omega + \tau - \sigma \end{aligned} \qquad (4.4.13)$$

so that

$$\frac{\partial \psi}{\partial p} = \frac{\partial \sigma}{\partial p} \qquad (4.4.14a)$$

$$\frac{\partial \theta}{\partial p} = \frac{\partial I}{\partial p} + \frac{\partial \rho}{\partial p} \qquad (4.4.14b)$$

$$\frac{\partial \phi}{\partial p} = \frac{\partial \tau}{\partial p} - \frac{\partial \sigma}{\partial p} \qquad (4.4.14c)$$

The JPL libration tape includes the quantities I $\frac{\partial \sigma}{\partial p}$, $\frac{\partial \rho}{\partial p}$, and $\frac{\partial \tau}{\partial p}$ for the parameters β, γ, C_{30}, C_{31}, C_{32}, C_{33}, S_{31}, S_{32}, S_{33}, and the 6 initial conditions τ_o, ρ_o, $I\sigma_o$, $\dot{\tau}_o$, $\dot{\rho}_o$, and $I\dot{\sigma}_o$. We note that the quantity $\underline{I}$, which in Eckhardt's and other analytic theories is the time-average or "mean" value of θ, does not have the same significance in the numerically integrated theory. For the numerical integration, $\underline{I}$ was set equal to the mean inclination obtained by evaluating Eckhardt's theory with the nominal parameter values. With $\underline{I}$ fixed, the variables $\rho(\equiv \theta - I)$, $I\sigma$, τ, and the partial derivatives of these variables with respect to the various parameters were integrated. Thus, a partial $\partial\rho/\partial p$ given on the libration tape is, identically, $\partial\theta/\partial p$, and $\partial I/\partial p \equiv 0$. The partials given for $(I\sigma)$ and $(I\dot{\sigma})$ are just $I(\partial\sigma/\partial p)$ and $I(\partial\dot{\sigma}/\partial p)$, respectively. Note also that, by virtue of the definition of I, the mean value of ρ will be non-zero if the parameters are adjusted from their nominal values.

4.4.4 Partials with Respect to Site Coordinates and Precession Quantitites

For parameters which affect the 1950.0 coordinates of the observing sites, $\frac{\partial \underline{x}_{ij}}{\partial p}$ in Equation (4.4.4) becomes

$$\frac{\partial \underline{x}_{ij}}{\partial p} = -\frac{\partial \underline{x}_{sj}}{\partial p} \qquad (4.4.15)$$

The partials $\frac{\partial \underline{x}_{sj}(t_j)}{\partial p}$ for the geocentric radius, longitude, and latitude of a site, and for the three angular rates which represent corrections to the precession matrix are given in detail by Ash [6].

4.4.5 Partials with Respect to Bias Parameter

Finally, for the constant "bias" which is added to the theoretical value of the observable,

$$\frac{\partial \Delta N^m_{jk}}{\partial p} = 1 \qquad (4.4.16)$$

for all $m > 0$. There are no observations processed for which $m \leq 0$.

4.5 Error Analysis

Any physical process which affects the observations and is not properly accounted for in the theoretical model of the observable can introduce errors into the parameter estimates obtained from analysis of the observations. The main sources of these errors may be grouped into three general categories: 1) instrumental effects, 2) propagation medium effects, and 3) deficiencies in the dynamical model used to determine the relative motions of the ALSEP transmitters and the observing sites.

4.5.1 Instrumental Effects

In the class of instrumental effects I include those associated with both the transmitters and the receiving systems. Of these, the more important effects for the observations analyzed in this thesis have been the fluctuations of the transmitter frequencies. We saw in Section 4.2.3 that under some conditions transmitter frequency drift could lead to a systematic error in the calculation of the theoretical observable exceeding 100° of phase. However, in the estimation of parameters I have not included any data for which the errors due to frequency drift exceeded 5° of phase when averaged over 10 minutes or more.

There is one mode of transmitter frequency fluctuation which seems to have affected almost all of the observations: a quasi-periodic oscillation, with a period of 6 to 8 minutes and an amplitude up to 5 Hz*. This transmitter-frequency oscillation causes an oscillating error in the differenced N-count observable; the amplitude of the latter oscillation is proportional to the propagation-delay difference between the receiving stations (see Section 4.2.3). At the beginning or end of the tracking period, when the delay difference is largest, the amplitude may be as large as 50° of phase, but is usually smaller than 25°. Near the mid-time of the observation period, the oscillation is imperceptible. Since the oscillation is very nearly periodic, it should average out in the data even better than errors that are completely random. If transmitter-frequency drift is included in the calculation of the theoretical observable by means of Equation (4.2.22), then the 6- to 8-minute oscillation will be accounted for, provided that the data sampling interval is much shorter ($\lesssim$1 minute) than the oscillation period. However, in

---

* The origin of this oscillation is still being investigated. It may be related to cycling of a temperature controller for the crystal which determines the transmitter frequency.

most of the data processing for this thesis the sampling interval was 3 minutes, and Equation (4.2.22) was not used. (But see page 83.)

The dominant sources of error in the receiving systems are rate variations of the station clocks*. If the clock at one station runs faster than the clock at a second station, then the first station will count fewer cycles of the ALSEP frequency-difference signal in a given interval of station-clock time. The rate of the clock at each station is governed by a Cesium-beam primary frequency standard. Tests performed prior to the Apollo 16 mission [39] indicated that the frequencies of these standards (or rates of the clocks) may differ by at most 1 to 2 parts in 10^{12} between different stations. If the ALSEP frequency difference is 3 MHz, then a rate offset of 2 parts in 10^{12} will cause a variation in the differential N-count in 6 hours of $(3 \times 10^{6}$ Hz$) \times (2 \times 10^{-12}) \times (2.16 \times 10^{4}$ sec$) = 0.13$ cycles, or 47° of phase. Since the effect of a clock rate error is proportional to the transmitter-frequency difference, it may be possible to identify errors stemming from this source by comparing the results of simultaneous observations made

---

*See also Section 3.2 for a discussion of receiving system errors.

on the same earth baseline of two ALSEP pairs having widely different frequency separations.

The theoretical observable may also be in error as a result of an epoch offset in one of the station clocks. The main effect of such an epoch error is to cause an error in the calculation of the propagation delays. The size of the latter error is equal to the epoch error multiplied by the rate of change of the difference in delay from two ALSEP transmitters to the receiving station. Since the epoch error is unlikely ever to exceed 20 μsec, and the differenced delay-rate is never more than 5×10^{-9}, the error in the calculated delay difference must be less than 10^{-13} sec, equivalent to less than 0.1° of phase.

4.5.2 Propagation-Medium Effects

As discussed in Section 4.2.2, the effect of the neutral atmosphere on the propagation delays is modeled using monthly average values of the zenith delay. The actual atmospheric delay at a station may differ from the value calculated from the model by as much as 20% as a result of variations in temperature, pressure, and water vapor content. We may estimate the magnitude of the effect of this error in the ob-

servable by using a simple secant law for the dependence of the delay on the zenith angle, θ:

$$\tau_{atm} = \tau_{atm(zenith)}/\cos\theta \qquad (4.5.1)$$

and

$$\frac{d\tau_{atm}}{d\theta} = \tau_{atm(zenith)}\sin\theta/\cos^2\theta \qquad (4.5.2)$$

so that the difference in atmospheric delay between two ALSEPs separated by $\Delta\theta$ in zenith angle is $\Delta\tau_{atm} \approx \tau_{atm(zenith)}(\sin\theta/\cos^2\theta)\Delta\theta$. In general the effect on the differenced N-count observable depends on both the orientation of the lunar baseline with respect to the horizon at each of the tracking stations, and on the elevation of the moon at each station during the observing period. However, an estimate of the maximum effect can be obtained by calculating the change in $\Delta\tau_{atm}$ at one station as the moon rises (or sets), assuming that the other station views the ALSEPs always at high elevations, and that the ALSEP baseline appears nearly vertical at the former station. The maximum possible elevation difference for the most widely separated ALSEP pair is 5×10^{-3} radians. At 10° elevation, the value of $\sin\theta/\cos^2\theta$ is ~33, so that the amount of differential phase introduced by the atmosphere, if we assume

a zenith delay of 7 ns, is $(2.3 \times 10^{9}$ Hz) x $(7 \times 10^{-9}$ sec) x (33) x (5×10^{-3}) x (360°/cycle) ≈ 1000°. The effect of a 20% error in the model zenith delay is thus about 200°. However, at 30° elevation, the effect of a 20% model error is only 20° of phase. Since the neutral-atmospheric delay increases so rapidly near the horizon, errors from this source may often be detected from data obtained at low elevations.

Variations of the propagation delay introduced by the earth's ionosphere are much more difficult to model than those introduced by the neutral atmosphere, because the density of the ionosphere fluctuates widely on the timescale of hours and days. In order to estimate the magnitude of the effect of the ionosphere on the differenced N-count observable, I will use a simple model for the elevation-angle dependence of the ionospheric delay, together with crude estimates of the time-variability of the ionosphere. I will ignore the detailed dependences of the ionospheric density on magnetic latitude, etc.

The contribution to the phase delay of a signal due to the ionosphere is given by

$$\tau_{ion} = -\frac{k}{f^2} \int_{path} N(S)dS \qquad (4.5.3)$$

where f is the frequency of the signal, N(S) is the electron density as a function of position S along the propagation path, and $\underline{k}$ is a constant numerically equal to 1.35×10^{-7} if τ_{ion} is in seconds, f in Hz, S in meters, and N in electrons/meter^3. Using a modified Chapman model of the ionospheric density due to Kazantsev and Nanozov, and assuming a characteristic scale height of 350 km, Pfeiffer [26] has obtained the expression for τ_{ion} as a function of the zenith angle θ, and of the integrated content at the zenith, N_T:

$$\tau_{ion} = -\frac{1.35 \times 10^{-7} N_T}{f^2} H(\theta) \qquad (4.5.4)$$

in which the function $H(\theta)$ takes different forms for high and low elevations. With sufficient accuracy for this analysis,

$$H(\theta) = 1 + 0.8(\sec\theta - 1) \qquad 0 < \theta \lesssim 1 \qquad (4.5.5a)$$

$$(35° \lesssim \text{elevation} < 90°)$$

$$H(\theta) = 2\theta - 0.3 \qquad 1 \lesssim \theta \lesssim 1.5 \qquad (4.5.5b)$$

$$(5° \lesssim \text{elevation} \lesssim 35°)$$

where θ is measured in radians.

From Equation (4.5.4) it is evident that there is an effect on the observable due both to the frequency difference between the ALSEPs and to their geometric separation. We will calculate first the geometric effect. For nighttime observations, an upper bound on N_T is 10^{17} el/m^2. Then for two ALSEPs separated by $\Delta\theta$ in zenith angle

$$(\Delta\tau_{ion})_{geom} = - \frac{1.35 \times 10^{10}}{f^2} \frac{dH}{d\theta}\Delta\theta \qquad (4.5.6)$$

For elevations between 5° and 35°, $dH/d\theta \approx 2$, so that an ALSEP pair with an apparent vertical separation of 5×10^{-3} radians has

$$\left|(\Delta\tau_{ion})_{geom}\right| = \frac{(1.35 \times 10^{10})}{(2.3 \times 10^{9})^2} (2)(5 \times 10^{-3})$$

$$= 25 \text{ psec}$$

equivalent to 21° of phase. The error introduced into the differenced N-count observable at a given time is just the <u>difference</u> between the ionospheric effect at that time and the effect at the beginning of the track (see Section 4.2). However, this difference may be expected to be of the order of 100% of the effect calculated for low elevation.

The frequency effect may be calculated in a similar manner. Using Equation (4.5.4),

$$\frac{d\tau_{ion}}{df} = + \frac{2.7 \times 10^{-7} N_T}{f^3} H(\theta)$$

or

$$(\Delta\tau_{ion})_{freq} = \frac{2.7 \times 10^{-7} N_T}{f^3} H(\theta) \Delta f$$

The maximum frequency separation Δf for observations with the DDR is 3 MHz. For this frequency separation, we find for θ = 1.2 rad (20° elevation), that $(\Delta\tau_{ion})_{freq} \approx$ 15 psec, equivalent to 12° of phase. When the moon is more than 60° above the horizon, $H(\theta) \approx 1$ and $(\Delta\tau_{ion})_{freq} \approx$ 7 psec. Thus the <u>change</u> in delay which affects the differenced N-count, is ~ 8 ps, equivalent to 7° of phase.

We may expect that ionospheric effects will be more serious for observations of the ALSEP 12-ALSEP 17 pair, which has a large geometric separation (5×10^{-3} rad) as well as the maximum possible frequency separation (3 MHz), than for other pairs. For observations of the 12-17 pair, the total error introduced by the nighttime ionosphere may be as great as 30° of phase. However,

in the daytime, the total ionospheric electron content may rise to 10 times the nighttime value, with most of the increase taking place over a period of 4 hours following sunrise. For daytime observations especially, and for the ALSEP pairs which have the greatest geometrical and frequency separations, the ionospheric effect on the observable may produce errors of the order of hundreds of degrees of phase.

Any model for the ionosphere which is not based on direct measurements of the electron content on an approximately hourly basis seems likely to be in error by 50% or more on most days. Consequently, I have chosen not to use the relatively crude model available in PEP in the processing of the data for this thesis. However, in Chapters V and VI I discuss the probable effect on the parameter estimates of errors introduced by the ionosphere and how eventual reprocessing of the data with an improved model might reduce the effect of these errors.

4.5.3 Effect of Errors in the Dynamical Model of the Earth-Moon System

There are two obvious requirements for the proper use of a dynamical model in fitting a set of observations: first, the model itself must

accurately represent the dynamics, and second, all the parameters in the model which affect the observations must be adjusted simultaneously in the least-squares estimation procedure. For ALSEP differential VLBI observations, these two requirements apply primarily to the model of the moon's physical libration, but also to the models for the moon's orbital motion and the earth's rotation.

In considering possible errors in PEP's model of the dynamics of the earth-moon system, I have relied heavily on the results of fits I have made to the lunar laser ranging data. In these fits I adjusted the moon's 6 orbital elements, the mass of the earth-moon system, up to 15 parameters affecting the physical libration, and 3 corrections to the adopted precession matrix. These fits are useful because the laser ranging data are more sensitive than the differential VLBI data to most of the dynamics, especially the orbital motion of the moon and the earth's rotation. An indication of the size of the errors in the latter models is afforded by the fact that I have been able to fit the laser data with rms residuals of 60 cm in (one-way) range. It is possible, of course, that errors much greater than 60 cm exist in the model but are being masked in the fitting process. Since the laser observations measure range, and are relatively insensitive to rotational motions of the moon about the line of sight, there may be particularly large orientation

errors in libration models which are derived from fits to laser data alone.

The ALSEP differential VLBI data are more sensitive to the moon's libration than to the orbital motion. The model which I used for the libration was the JPL LLB-5 numerical integration. Williams et al. [41] have tested for errors in the integration by comparing it with a semi-analytic libration model developed independently by Eckhardt [15,16]. When a 7-year integration of the libration angles ρ, $I\sigma$, and τ is fit by least-squares to the Eckhardt series "300" libration model, the rms difference between the two models for these angles is less than 0".2, equivalent to approximately 1.6 m at the lunar surface.

CHAPTER V

RESULTS

5.1 Introduction

In this chapter I present the results of solutions for the libration parameters and the ALSEP coordinates. All of these solutions used combinations of data from differential VLBI observations of the five ALSEP transmitters, together with data from laser ranging observations of the Apollo 11, 14, and 15 Lunar Ranging Retroreflectors (LRRRs). The laser ranging observations were performed at the Mc Donald Observatory under the auspices of the NASA Lunar Laser Ranging Experiment (LURE) [7]. The data obtained from the laser observations are in the form of 1194 normal points constructed at the University of Texas from ranges obtained between January 1970 and June 1974 [1 , 33 , 34].

The VLBI data were selected from observations made between March 1973 and June 1974 at the six STDN stations which are equipped with DDRs (see Figure 1.5)*. These observations involved all five ALSEP transmitters, in 8 pair-wise combinations.**

---

*One of these 6 stations, the Network Test and Training Facility at Greenbelt, Md., was actually used for ALSEP DDR observations on only 2 days: 7 and 8 March 1973.

** Of the 10 pairs which can be formed from the 5 ALSEPs, 2 pairs (AL14-AL17; AL14-AL16) cannot be observed by the DDR because the transmitter-frequency separations are more than 3.3 MHz (see Section 3.2).

Since the VLBI observations are sensitive primarily to the relative positions of the different ALSEPs, I have used an independent photogrammetric determination of the coordinates of the Apollo 15 ALSEP with respect to the nearby LRRR, in order to tie the system of ALSEP coordinates to that of the laser retroreflectors. The photogrammetric determination was done by Schimerman et al. of the Defense Mapping Agency Aerospace Center, using the photographs of the landing site taken by the astronauts. The azimuth and the distance of the Apollo 15 ALSEP from the LRRR were obtained with uncertainties of about 1 meter [30].

In Appendix A.2, I have listed all of the ALSEP observations made through June 1974 and have designated those which were used in the solutions. The observations are grouped into series, each consisting of a sequence of observations of a pair of ALSEPs by a pair of tracking stations during which the cycle-count at both stations was uninterrupted. Since each STDN station is equipped with two DDRs, and since more than two stations often observe at the same time, several observation series were often obtained on a single day. As discussed in Sections 2.2, 4.1, and 4.2, each observation series has associated with it an adjustable bias parameter

which accounts for the error in the initial observation in the series. At present, PEP can accommodate only 130 biases, and hence only 130 observation series, in a single solution. For this reason, as well as to provide a check of my results, I divided the ALSEP data into two groups.

The first group consists of 10,602 observations (100 observation series) of ALSEP 15 with respect to other ALSEPs. These observations have been combined with the 1194 laser normal points to form the data set which I will designate A (DS A). The second group consists of the remaining observations (10,123) and includes observations of all pairs which can be formed from the other four ALSEPs. This group, combined with the laser normal points, comprise Data Set B (DS B). The particular division of the data which I have chosen has several advantages. First, the inclusion of all observations of ALSEP 15 in DS A allows a determination of the coordinates of ALSEPs 12, 14, 16, and 17 with respect to the Apollo 15 retroreflector. Second, because ALSEP 15 is absent from DS B the geometry of the VLBI observations in this data set is significantly different from that of DS A (see Figure 5.1), so that a meaningful consistency

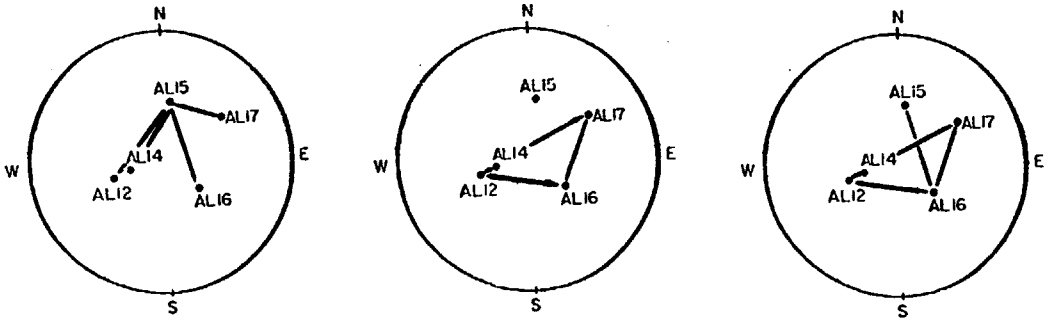


Figure 5.1 Geometry of ALSEP pairs for observation in Data Sets A, B, and C.

check is possible. The origin of the ALSEP coordinate system for the DS B solutions was defined arbitrarily by fixing the coordinates of ALSEP 16 at values which had been determined by preliminary solutions and which are probably accurate to within 30 m. The disadvantage of this grouping of the data is that the parameter estimates obtained using DS B may have errors introduced by the errors in the assumed ALSEP 16 coordinates. For this reason, a third data set was formed, DS C, consisting of DS B plus 1569 observations of ALSEP 16 with respect to ALSEP 15 taken from DS A. A summary of the observations contained in each of the three data sets is given in Table 5.1.

With each of these three data sets I performed a series of solutions. In every solution I estimated the 6 elements of the lunar orbit, the mass of the earth-moon system; three angular rates representing corrections to the earth's precession matrix; 3 coordinates each for the McDonald Observatory, the STDN stations*, the Apollo

---

*A priori information was included for each of the STDN station coordinates as shown in Table 5.2.

Table 5.1

Differential VLBI Observations Contained in the Data Sets*

ALSEP Pair	No. Obs.	No. Obs. Series	No. Diff. Tracking Days	Period Covered
Data Set A				
AL 12-AL 15	3418	34	24	Mar 73-Jun 74
AL 14-AL 15	2153	20	14	Mar 73-Jun 74
Al 16-AL 15	2719	29	18	Jul 73-May 74
AL 17-Al 15	2312	17	11	Apr 73-Jun 74
Totals:	10,602	100	49	Mar 73-Jun 74
Data Set B				
AL 12-AL 14	3509	36	27	Jul 73-Jun 74
Al 12-AL 16	2281	23	18	Aug 73-Jun 74
AL 12-AL 17	2781	18	14	Jul 73-Feb 74
AL 16-AL 17	1552	8	7	Nov 73-May 74
Totals:	10,123	85	48	Jul 73-Jun 74
Data Set C				
From Data Set B	10,123	85	48	Jul 73-Jun 74
AL 16-Al 15 from Data Set A	1569	17	12	Sep 73-May 74
Totals:	11,692	102	53	Jul 73-Jun 74

*Each Data Set also contains 1194 laser ranging normal points covering the period Jan 1970 - June 1974.

Table 5.2

Nominal STDN Station Coordinates*

Station	Geodetic Coordinates**		
	Height (m)	Longitude (deg)	Geodetic Lat. (deg.)
Ascension Is. (ACN)	527.0	14.327058	-7.954794
Madrid, Spain (MAD)	763.0	4.168453	40.454892
Merritt Is., Fla. (MIL)	-54.0	80.693469	28.508272
Merritt Is., Fla. - System 2 (MILW)	-54.0	80.693469	28.507753
Greenbelt, Md. (ETC)	-22.0	76.842914	38.998481
Corpus Christi, Tex. (TEX)	-39.0	97.378622	27.653750
Goldstone, Calif. (GDS)	921.0	116.873597	35.341594

*The a priori standard deviations for Ascension and Madrid were 15 m in geocentric radius, and 1.5×10^{-4} deg in longitude and latitude; for all other stations, 10 m in radius, and 1.0×10^{-4} deg in longitude and latitude were used.

**Referred to an ellipsoid with equatorial radius 6378.166 km and degree of flattening 1/298.3. See [6].

retroreflectors, and the ALSEP transmitters; a bias parameter for each VLBI observation series; the lunar moment-of-inertia parameters β and γ; certain third-degree-harmonic coefficients in the lunar gravitational potential; and the 6 initial conditions of the lunar libration. Different combinations of the third-degree-harmonic coefficients were solved for in the different solutions.

Figure 5.2 shows examples of the postfit residuals obtained from the solutions. The best fits of the VLBI data were obtained for observations of ALSEPs 12 and 14 [graph (a)]. These ALSEPs are separated by only 180 km on the moon, so that the observations are relatively insensitive to the physical libration and also to the effects of the earth's atmosphere and ionosphere. Graph (b) shows one of the worst-fitting series (186D) and two others (186F and 186E) whose r.m.s. residuals were also larger than the average for all of the VLBI data (16°). Since a bias parameter was adjusted for each series, errors in the theoretical model tend to show up primarily as a slope in the postfit residuals. The slope in the residuals for series 186D (~40°/hour) is approximately equivalent to a 10 meter error in ALSEP relative position.

The laser residuals shown in the bottom graph of Figure 5.2 are typical for these solutions. The r.m.s. of the residuals for this 8-day span is 2.7 ns, compared with 3.5 ns for all of the laser data. The random noise level for the normal points in this span, based on the scatter in individual photon returns, is ~0.8 ns. The residuals shown in the graph illustrate the results of three different types of model error. The 1-2 ns trend which is common to all three reflectors results from lunar orbit errors which affect the earth-moon center-to-center

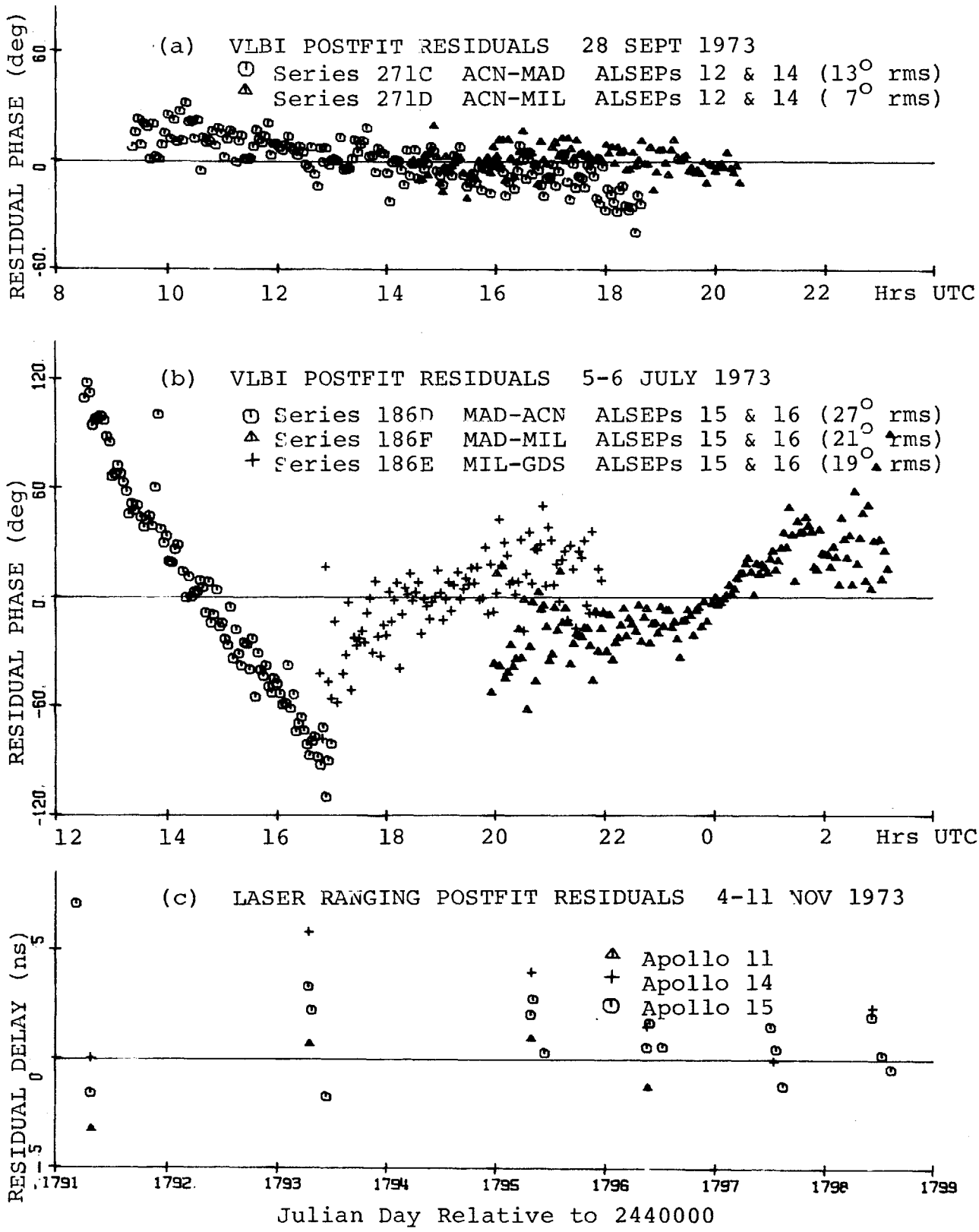


Figure 5.2 Typical postfit residuals from solutions combining both VLBI and laser ranging data. The upper two graphs are examples of the best (a) and worst (b) fits of VLBI series. The overall rms of the VLBI residuals was 16°. The bottom graph (c) is typical of the laser ranging residuals throughout. (See text.)

distance. Differences in the residuals between different reflectors at the same time, also about 2 ns, can be attributed mainly to errors in the physical libration model. Finally, a spread in the residuals obtained from a single reflector over one day may result from an error in the model for earth rotation. On two of the days shown, the spread exceeds 5 ns.

5.2 Libration Parameters

The values of the libration parameters used by Williams et al. at JPL to generate the numerically-integrated libration model, LLB-5, were derived partially from fits to laser ranging data and partially from the results of solutions performed by other groups using Doppler tracking data from the Lunar Orbiter spacecraft [43]. In particular, the values used for J_2, C_{31}, C_{33} and S_{31} were calculated from an average of the Lunar Orbiter results of Michael and Blackshear [22], Liu and Laing [21], and Sjogren [35]; β, γ, and the remaining third degree harmonics were determined from solutions performed at JPL using essentially the same set of laser normal points as I have used in my solutions*. Prior to

---

*The time period covered by the normal points used at JPL and at MIT is identical. Minor differences exist between the two data sets as a result of different editing criteria and the fact that the JPL data set includes some ranges to Lunakhod II [43].

performing solutions with the ALSEP differential VLBI data, I used the laser ranging data alone in an effort to duplicate the solutions performed at JPL. The estimates obtained for libration parameters are given in columns 3 and 4 of Table 5.3. With a nondegenerate set of harmonic coefficients estimated (column 3 of the table, PS-1), most of my results are consistent with the nominal values of LLB-5.

The first solutions I performed with Data Set A indicated that the addition of the VLBI data to the laser data improves substantially the formal errors obtained for C_{31} and C_{33}, which were poorly determined with laser data alone. (Results with laser data alone are shown for two parameter sets, one [PS-1] in which C_{31}, C_{33}, and S_{31} were fixed and one [PS-2] in which all harmonics were estimated.) The improvement in the formal error for C_{31} is by a factor of 100, and for C_{33}, a factor of 25. These improvements are also reflected in the parameter correlations. With the laser data alone, the correlation coefficient between C_{33} and γ is -.997. The addition of the VLBI data reduces the correlation to -0.92. With laser data alone, C_{31} has a correlation of 0.97 with β; with VLBI data added, the correlation coefficient is 0.003.

The formal errors shown in Table 5.3 do not necessarily reflect the true uncertainties in the parameter estimates. The postfit residuals for both laser and ALSEP data are not

Table 5.3

Comparison of Libration Parameter Values and Formal Standard Errors* Obtained with Laser and VLBI Data Sets

(Units of 10^{-6})

Parameter	Nominal Value (LLB-5)	Laser Data Alone		Laser + VLBI Data (DS A)	
		PS-1†	PS-2††	PS-1†	PS-2††
β	631.26	631.28±0.01	629±1	631.266±0.003	631.261±0.003
γ	227.37	227.39±0.03	224±1	227.42±0.01	227.34±0.04
J_3	10.44	5±2	7±2	5.6±0.8	1±1
C_{31}	28.6†††	28.6	21±20	28.6	28.3±0.2
C_{32}	4.82	4.75±0.04	4.70±0.05	4.83±0.02	4.70±0.03
C_{33}	2.7	2.7	9±2	2.7	2.82±0.08
S_{31}	8.8	8.8	12±7	8.8	-8±4
S_{32}	1.71	1.66±0.06	1.45±0.08	1.72±0.03	1.79±0.04
S_{33}	-1.14	0.0±0.2	0.0±0.2	-0.2±0.1	-0.4±0.1

*Formal standard errors (based on the r.m.s. values of the postfit residuals) are given here for the purpose of comparing the sensitivities of the two data sets to the parameters. The actual uncertainties of the parameter values are typically much larger (see Table 5.5).

†Parameter Set 1 included 6 initial conditions of the lunar orbit, mass of earth + moon, 3 adjustments to the earth's precession matrix, 3 coordinates each of McDonald Observatory and the Apollo 11, 14, and 15 LRRRs, β, γ, J_3, C_{32}, S_{32}, S_{33} and 6 initial conditions of the libration. When VLBI data were used the parameter set also included 3 coordinates each of the 6 tracking stations (with 10-15 m *a priori* σ's) and 4 ALSEP transmitters (AL 15 fixed to AP 15 LRRR), and a bias parameter for each of 100 observation series.

††Parameter Set 2 is the same as PS-1 with the addition of S_{31}, C_{31}, and C_{33}.

†††Underlined values were not adjusted to fit either laser or VLBI data but were fixed from an average of Lunar Orbiter results (see Table 5.5).

random. In order to obtain a fairer estimate of the uncertainties in the parameter values, I performed a series of solutions in which different combinations of parameters were estimated with different data sets. For each parameter set a solution was first made with laser data alone, then with Data Sets A, B, and C, each of which includes combinations of laser and VLBI data. Table 5.4 shows a comparison of the results obtained with Data Sets A, B, and C when all the libration parameters were adjusted. The agreement among the three solutions is poorest (inconsistency on the order of 20 times the formal standard error) for the three parameters (γ, C_{31}, and C_{33}) which are most highly correlated, possibly reflecting a larger influence on these parameters of systematic errors.

My best estimates of the values of the libration parameters and their uncertainties are summarized in Table 5.5. For comparison, I have also included in the table three determinations of the third-degree harmonic coefficients from Lunar Orbiter Doppler tracking data, and the determinations from lunar laser ranging data reported recently by J.G. Williams of JPL. The VLBI results listed are averages of the values obtained from the DS A and DS C solutions.* The uncertainties

---

*The DS C solution is believed to be more reliable than the DS B solution because, in the former, VLBI observations of the Apollo 15 ALSEP were included in order to relate the ALSEP positions to those of the laser retroreflectors.

Table 5.4

Comparison of Solutions for Libration Parameters with Data Sets A, B, and C

(units of 10^{-6})

Parameter	DSA	DSB[++]	DSC
β	631.261±0.003[+]	631.273±0.003	631.277±0.003
γ	227.34±0.04	228.09±0.04	228.05±0.04
J_3	1±1	6±1	5±1
C_{31}	28.3±0.2	24.4±0.2	24.5±0.2
C_{32}	4.70±0.02	4.84±0.02	4.77±0.02
C_{33}	2.8±0.1	1.3±0.1	1.3±0.1
S_{31}	-8±4	26±3	5±4
S_{32}	1.79±0.04	1.79±0.03	1.76±0.03
S_{33}	-0.4±0.1	-1.0±0.1	-0.2±0.1

[+]Formal standard error

[++]ALSEP 16 coordinates fixed: Radius = 1737.447 km, Long. = 15.43625°, Lat. = -8.95541°

Table 5.5

Estimates of Lunar Gravity and Libration Parameters

(units of 10^{-6})

	Lunar Orbiter Doppler			Laser Ranging	
Parameter	Michael & Black-Shear [22]	Liu & Laing [21]	Sjogren [35]	Williams [42]*	+VLBI*
β	---	---	---	631.26±0.3	631.27±0.03
γ	---	---	---	227.37±0.6	227.7±0.7
J_2	2071.	1996±2	2048±3	2038.22+	2038.22+
C_{22}	22.4	23.6±5.3	22.1±0.5	22.4++	22.4++
J_3	-28.4	5.9±2.9	10.7±9	10.44±4	3±20
C_{31}	24.1	30.0±3.7	31.6±5	28.6+	26±4
C_{32}	7.6	4.7±2.8	5.5±1	4.82±0.15	4.7±0.2
C_{33}	1.4	4.8±2.2	1.8±0.3	2.7	2 ±2
S_{31}	20.8	1.4±3.2	4.3±12	8.8	-1±30
S_{32}	2.27	0.6±1.7	2.7±1	1.71±0.15	1.8±0.3
S_{33}	-0.3	-0.9±1.3	-1.0±0.2	-1.14±0.7	-0.3±1.0

*Estimated uncertainties are provisional

+Underlined values for laser and VLBI solutions were fixed from an average of the Lunar Orbiter determinations

++Derived from β, γ, and J_2

assigned to most of my results are a factor of 20 larger than the corresponding formal standard errors. This factor is based on the observed disagreements among the DS A, B, and C solutions in Table 5.4. For C_{32}, S_{31}, S_{32}, and S_{33} I have used 10σ rather than 20σ uncertainties since these coefficients are determined almost entirely by the laser data (see Table 5.3), which I believe to be less corrupted than the VLBI data by systematic errors.

5.3 ALSEP Coordinates

The coordinates of the ALSEP transmitters were adjusted in all solutions which included VLBI data. The results to be presented in this section were obtained from the solutions with PS-2, for which all of the libration parameters were estimated. Since the third-degree harmonics produce offsets of the mean directions of the moon's principal axes from the mean direction of the earth, the selenodetic (principal-axis) coordinate systems defined by solutions obtained using different data sets tend to differ. In an effort to define a consistent selenodetic coordinate system for the comparison of results from solutions with Data Sets A, B, and C, in all of these solutions I fixed the coordinates of the Apollo 15 LRRR at the values determined from the laser-only solution. Fixing the Apollo 15 LRRR coordinates in this way reduces substantially the correlations among the retroreflector and the ALSEP coordinates, but has only a negligible effect on the r.m.s. of the post-fit residuals.

Since the primary tie between the ALSEPs and the laser retroreflectors is at the Apollo 15 site (see Section 5.1), Data Set A (which includes all of the data from observations of ALSEP 15) was used in a solution to determine the coordinates of the other ALSEPs with respect to the Apollo 15 LRRR. The results of this solution are given in Table 5.6. These results were then checked by performing additional solutions for the relative coordinates of the Apollo 12, 14, 16, and 17 ALSEPs using Data Sets B and C. For solutions with

Table 5.6

Relative Coordinates (ALSEP-Apollo 15 LR^3) Using Adjusted Libration Model*

ALSEP	ΔX_1 (km)	ΔX_2 (km)	ΔX_3 (km)	ΔRadius (km)	ΔLong. (deg)	ΔLat. (deg.)
12	35.287	-787.824	-855.543	0.503	-27.05296	-29.14417
14	97.589	-619.135	-874.730	0.860	-21.10591	-29.77784
15**	- 0.012	0.038	0.020	0	0.00143	0.00074
16	99.611	359.859	-494.678	1.944	11.86812	-35.10912
17	-155.057	734.404	-165.681	-0.695	27.13959	- 5.94397

*From solution with Data Set A. The Apollo 15 LR^3 selenodetic coordinates were fixed at the following values: Radius = 1735.5087 km, Long. = 3.56822°, Lat. = 26.15404°. The estimated libration parameters are β = 631.259, γ = 227.40, J_3 = 4.2, C_{31} = 28.2, C_{32} = 4.81, C_{33} = 2.7, S_{31} = 12.2, S_{32} = 1.82, S_{33} = -1.0, τ_o = 257".49, ρ_o = -20".81, $I\sigma_o$ = 26".12, $\dot{\tau}_o$ = -5".492/day, $\dot{\rho}_o$ = -1".938/day, $I\dot{\sigma}_o$ = -5".044/day.

**Fixed in the solution. These values are from the photogrammetric determination by Schimerman et al. [30]. The uncertainty in each coordinate is 1 m.

DS B, which contains no data from observations of ALSEP 15, the ALSEP coordinate system was fixed relative to the retroreflectors by fixing the 3 coordinates of ALSEP 16, as described in Section 5.1. The ALSEP relative coordinates determined from the three solutions, with Data Sets A, B, and C, are in Table 5.7. For the short (180 km) ALSEP 12 - ALSEP 14 lunar baseline, the agreement among the 3 determinations is within 3 meters in all 3 coordinates. For the other baselines, the results of the 3 solutions disagree by up to 20 m in the radial (X_1) coordinate and by up to 8 m in the 2 transverse coordinates (X_2 and X_3).

An important external check of the VLBI results is also available. The relative coordinates of the Apollo 14 ALSEP and LRRR determined from the landing-site photographs may be compared with the coordinate differences determined from the earth-based observations. The coordinates of the Apollo 14 LRRR with respect to the Apollo 15 LRRR have been determined by laser ranging, and the coordinates of ALSEP 14 with respect to ALSEP 15 have been determined via differential VLBI*. If we

---

*These two determinations are not entirely independent inasmuch as both were based on the use of the same libration model.

Table 5.7

Comparison of Solutions for ALSEP Relative Coordinates with Adjusted Libration Model

ALSEPS	Data Set	ΔX_1 (km)	Diff. from Soln. A (m)	ΔX_2 (km)	Diff. from Soln. A (m)	ΔX_3 (km)	Diff. from Soln. A (m)
12-14	A	- 62.304	---	-168.688	---	19.190	---
	B	- 62.306	- 2	-168.688	0	19.192	2
	C	- 62.304	0	-168.689	-1	19.192	2
16-14	A	2.013	---	978.995	---	-160.704	---
	B	1.994	-19	979.000	5	-160.708	-4
	C	1.994	-19	979.002	7	-160.708	-4
17-14	A	-252.619	---	1353.535	---	709.061	---
	B	-252.618	1	1353.542	7	709.054	-7
	C	-252.611	8	1353.542	7	709.053	-8
17-16	A	-254.632	---	374.541	---	869.765	---
	B	-254.612	20	374.542	1	869.762	-3
	C	-254.614	18	374.542	1	869.761	-4

assume that the relative coordinates of the ALSEP transmitter and LRRR at the Apollo 15 site are well determined (uncertainties less than 1 m) from photogrammetric analysis, then a comparison of the relative coordinates of the LRRR and ALSEP at the Apollo 14 site determined by laser ranging and VLBI with the relative coordinates determined from the landing site photographs constitutes an excellent check on the accuracy of both earth-based observation types. The results of this comparison are given in Table 5.8. The disparity between the coordinates determined by earth-based and moon-based methods is only 8 m and may in fact include errors at the level of 5 m in the as yet preliminary photogrammetric determination at the Apollo 14 site.

Table 5.8

Comparison of Earth-based and Moon-based Determinations of the Relative Coordinates of the ALSEP Transmitter with Respect to the LRRR at the Apollo 14 Landing Site

Method	Difference (ALSEP-LRRR)			Distance
	Longitude	Latitude	Radius	
Laser Ranging + VLBI*	0°.00101	0°.00047	7 m	34 m
Apollo 14 Landing Site Photographs**	0°.00132	0°.00023	---	41 m
Difference (Laser/VLBI - Photo.)	-0°.00031 (-8 m)	0°.00024 (7 m)	---	-7 m

*from solution with Data Set A. In this solution the relative coordinates of ALSEP 15 with respect to the Apollo 15 LRRR were taken from the photogrammetric determination by Schimerman et al. [30]. See Table 5.6.

**from preliminary results with uncertainties of the order of 5 m [8].

5.4 Discussion

The estimates of uncertainty which have been derived in the preceding sections from comparisons of different solutions with different data sets and parameter sets may not be completely reliable. Such comparisons do not necessarily uncover every kind of systematic error that might be present. One reason for caution is the presence of obvious systematic trends in both the VLBI and laser residuals (see Figure 5.2). My results may also have been affected significantly by errors in the partial derivatives on the libration tape. These partials were generated from earlier numerical integrations, which were based on different values of the parameters. Consequently, the errors in some of the partials may be of the order of 1% [43]. Errors in the partial derivatives tend to affect most seriously the estimates of parameters which are highly correlated with other parameters. However, because I was unable to re-integrate the libration using the adjusted parameter values, I cannot say just how serious the effects of partial-derivative errors were.

Additional questions have arisen as a result of comparing my laser-only solutions with similar solutions performed at JPL by J.G. Williams and W.S. Sinclair [43]. With the libration model fixed (i.e., LLB-5, unadjusted), I obtain retroreflector coordinates which differ from those obtained at JPL by 10-15 m. The coordinates estimated for the McDonald Observatory also differ, by 0.°0013 (12 m) in

longitude, 0.1 m in cylindrical radius, and 2 m in the z coordinate. The discrepancy for McDonald may be due to differences between the JPL and MIT planetary ephemerides, which effectively determine the orientations of our respective coordinate systems. I attempted to absorb possible orientation errors by adjusting three angular-rate corrections to the precession matrix (see Section 4.2.2 and also Ash [6], p. 60). The estimated rates were of the order of 1"/century about all three axes. The STDN station coordinates were also adjusted (with 10-15 m a priori σ's), partly to account for any errors in orientation of the network with respect to McDonald. However, the adjustments to these coordinates were sometimes excessive (up to 200 m in the radii and latitudes of Ascension and Madrid) and showed little consistency between the DSA and DSB solutions. This inconsistency may indicate that the STDN station coordinates were more sensitive than other parameters to unmodeled effects of the ionosphere and atmosphere.

I expect that many of the problems considered in this section will be better understood, if not eliminated, as the relevant models are improved and additional data become available. Work on the models is continuing at MIT and elsewhere. The observations also continue, with certain improvements as discussed in Chapter 6.

CHAPTER VI

CONCLUSION

6.1 Summary

Earth-based radio observations have been used for the first time to determine the positions of transmitters on the surface of the moon with uncertainties less than 30 m, and to determine the moon's physical libration. In these observations a new phase-locked differential tracking technique was employed, and an interferometric observable was formed by subtracting simultaneous measurements at widely separated ground stations.

The differential interferometric data were combined with lunar laser ranging data to estimate parameters of the moon's physical libration and to determine the relative selenocentric coordinates of the 5 Apollo Lunar Surface Experiments Package (ALSEP) transmitters. The parameter estimation was carried out within the framework of the MIT Planetary Ephemeris Program, using a numerically-integrated physical libration model developed at the Jet Propulsion Laboratory. The estimate obtained for the lunar moment-of-inertia ratio β is believed to be more accurate than any previous determination. The uncertainties of the estimates obtained for 2 of the third-degree harmonic coefficients of the moon's gravitational potential are smaller than those obtained using laser ranging data alone and are comparable to the uncertainties obtained by other investigators using Lunar Orbiter Doppler data. The values obtained for all

of the harmonics are consistent with the Lunar Orbiter results. The relative coordinates of the ALSEP transmitters were determined with uncertainties of about 30 m in the radial (X_1) coordinates and about 10 m in the two orthogonal coordinates (X_2 and X_3). The dominant sources of error in all of the parameter estimates may have been unmodeled effects of the propagation medium.

6.2 Suggestions for Further Study

Future work should be directed toward both the improvement of dynamical models and the reduction of observational errors. The modifications necessary to enable PEP to integrate directly the equations of motion for the rotation of the moon are already in progress. The completion of these modifications will provide an independent check of the JPL integration. Further, it will be possible to re-integrate the libration using adjusted parameter values, in order to minimize the effects of errors in the partial derivatives (see Section 5.4). The moon's elasticity (and inelasticity) should be accounted for in the equations of motion for the rotation.

The three sources of error believed to be most serious for the VLBI observations analyzed in this thesis - the ionosphere, the neutral atmosphere, and variations in the rates of the station clocks - may be significantly reduced for the observations now being made with improved equipment. A new device, called the Differential Doppler Processor (DDP), allows

the use of multiple DDRs at a station, so that all 5 ALSEPs may be observed simultaneously. The additional information available at each sample time may be used to construct a new observable, a linear combination of the 4 differenced N-counts, which has minimum sensitivity to certain carefully defined effects; for example, effects which are dependent on elevation above the horizon at a station (atmosphere and ionosphere) and effects which are dependent on frequency (ionosphere and station clock rate variations).

For the existing VLBI data, additional study is needed to determine whether reprocessing with improved modeling of the ionosphere would yield significantly improved estimates of the libration parameters and the ALSEP coordinates.

6.3 Applications

The results of this work have immediate or near-term application in at least four areas of astronomical research: 1) lunar mapping, 2) studies of the moon's gravitational field, 3) astrometry, and 4) radio tracking of future lunar and planetary spacecraft.

The ALSEP relative positions presented in Table 5.6 are of sufficient accuracy (10-30 m) to be of immediate use in providing calibration points for combining orbital metric photography from three different Apollo missions (15, 16, and 17) [31]. Errors in the models for the Apollo spacecraft orbits have limited the accuracy with which photographic features could be located

in a selenocentric coordinate system to the level of several hundred meters, an order of magnitude larger than the resolution limit of the photographs. The inclusion of the accurate coordinates for the ALSEPs in the photogrammetric solutions should help to bring the uncertainties closer to the resolution limit.

The values estimated in this thesis for β, γ, and the third-degree gravitational harmonic coefficients (Table 5.5) represent only a slight improvement over the results from lunar-orbiter tracking and laser ranging. However, the sensitivity of the VLBI observations to β, C_{31}, and C_{33}, indicated by the formal errors, suggests that the values of these parameters will be improved further as more data become available.

The results of this experiment may be important in future uses of the moon for astrometric and geodetic purposes. With lunar laser ranging and with the photogrammetric tie between the Apollo 15 retroreflector and ALSEP transmitter, the VLBI results determine the positions of the ALSEPs with respect to the moon's center of mass. The uncertainty in the selenodetic positions, set mainly by the uncertainty in parameters in the libration model, is approximately 30 m, corresponding to an angular uncertainty of 0".015 of geocentric arc. With this tie to the lunar center of mass, the ALSEPs may be used in differential VLBI observations between the moon and extragalactic radio sources in order to determine the orientation of the lunar orbit with respect to an inertial

reference frame [11]. A program of such observations is presently being carried out by M.A. Slade and R.A. Preston at JPL [37].

Finally, the cycle-counting differential VLBI technique demonstrated in the ALSEP experiment has potential application for a number of future lunar and planetary missions [11]. For any mission in which transmitters on two or more spacecraft are operating at nearly the same frequency, a DDR could be used for differential observations. If the spacecraft are equipped with transponders or stable oscillators, Doppler tracking may be done. In any case, differential interferometry may be used. The Viking project, in which two orbiters and two landers will be sent to Mars later this year, will provide several important applications for the techniques discussed in this thesis.

APPENDICES

A. 1 Units and Parameter Values in the Theoretical Model

A.1.1 Units

The physical units of time, mass, and length used in the Planetary Ephemeris Program are defined as follows [6]:

Time - The A.1 second; defined as 9,192,631,770 cycles at the terrestrial transition frequency of cesium at zero magnetic field [6].

Coordinate time (CT), the independent variable of the equations of motion, is related theoretically to A.1 time by

CT = A.1 + 32.15 sec + periodic general relativistic terms.

The theoretical derivation of the relativistic terms is discussed by Ash [6]. The definition presently implemented in PEP is

$$CT = A.1 + 32.15\ \text{sec} + (1.658 \times 10^{-3}\ \text{sec})\sin M + (1.672 \times 10^{-6}\ \text{sec})\sin D + \frac{1}{c^2}(\vec{r}_s \cdot \dot{\vec{r}}_e)$$

where M is the earth's mean anomaly, D is the elongation of the moon from the sun, c

is the speed of light, $\vec{r}_s$ is the position of the observing site with respect to the earth's center of mass, and $\dot{\vec{r}}_e$ is the velocity of the earth's center of mass with respect to the sun. The coefficients of the annual and monthly terms are from Moyer [24], and the expressions used for M and D are conventional [17]. The vectors in the last (diurnal) term are evaluated using PEP's planetary ephemeris (NBODY311).

Mass - The solar mass

Length - The astronomical unit (AU), defined as the radius of a heliocentric circular Keplerian orbit in which a body of negligible mass would have a period of $2\pi\sqrt{G}$ days, where the gravitational constant, G, is assumed to be fixed at the Gaussian value, $(.01720209895)^2 AU^3/day^2$ (1 day = 86400 A.1 seconds). The accuracy of PEP's ephererides depends mainly on the measurements of the echo time delays of radar signals reflected from the inner planets. Simultaneously, one also obtains the speed of light (i.e., of the radar signals) measured in AU/day; this result can be written corveniently as:

1 AU = 499.004780 ± 3 x 10^{-6} light seconds

The conversion to metric units is accomplished using the adopted value of the speed of light:

c = 299792.458 km/sec

A.1.2 Parameters of the Lunar Orbit. The orbit of the moon was determined by fitting to laser ranging data [1, 33, 34] a numerical integration of the fundamental equations of motion, as described by Ash [3] and Slade [36]. The parameter values determined from or used in this fit are as follows (not all digits given are necessarily significant):

Mass Ratio (sun)/(earth+moon) = 328900.5011220281

Mass ratio (earth/moon) = 81.3007

Planetary masses and ephemerides - from NBODY311

Osculating Keplerian elements at epoch JED 2440000.5 (0 Hrs, CT on Julian Day Number 2440001), with respect to 1950.0 equator and equinox:

Semimajor axis, a = 0.002571513220080629

Eccentricity, e = 0.05561587179127649

Inclination, i = 28°39685642497140

Right ascension of ascending node, Ω = 3°31291959239597

Argument of perigee, ω =226°271133323205

Initial mean anomaly, M_0 = 154°.885673245178

Earth parameters:

J_2 = 1.082628×10^{-3}

J_3 = -2.538×10^{-6}

Radius used with harmonics, R_e = 6378.166 km

Tidal friction parameter, sin 2δ = 0.0755 (see Slade [36].)

Moon parameters:

J_2 = 2.03822×10^{-4}

C_{22} = $2.239570773993590 \times 10^{-5}$

Radius used with harmonics, R_m = 1738.09 km

Inclination of lunar equator to ecliptic, I = 5552.71"

Model of physical libration - Koziel, 1962 [20]

A.1.3 Parameters of JPL Lunar-Libration Model (LLB-5)

The libration model was generated by Williams and Sinclair of the Jet Propulsion Laboratory by fitting a numerical integration [40] to laser ranging data. The detailed characteristics of the fit are described in a memo [41], available to the user. The nominal values of the parameters of the model are listed below for reference:

Moment of inertia ratios: $\beta = 631.26 \times 10^{-6}$

$\gamma = 227.37 \times 10^{-6}$

Inclination of lunar equator to ecliptic = 5552".71

Harmonics (units of 10^{-6}):

	$J_2 = 203.822$
$C_{30} = -10.44$	$C_{22} = 22.396$
$C_{31} = 28.6$	$S_{31} = 8.8$
$C_{32} = 4.82$	$S_{32} = 1.71$
$C_{33} = 2.7$	$S_{33} = -1.14$

Radius used with harmonics, R_m = 1738.09 km

Harmonics consistent with $C/MR^2 = 0.394$

Mass of earth + moon = 328900.526 inverse solar mass units

Mass ratio earth/moon = 81.3007

Lunar ephemeris: LURE-2

Initial conditions at epoch JED 2440400.5:

$\tau_o = 1.245172332504406 \times 10^{-3}$ rad

$\rho_o = -0.070227621267468 \times 10^{-3}$ rad

$I\sigma_o = 0.1703911685703775 \times 10^{-3}$ rad

$\dot{\tau}_o = -2.656265725254470 \times 10^{-5}$ rad/day

$\dot{\rho}_o = -1.948246963467498 \times 10^{-5}$ rad/day

$I\dot{\sigma}_o = -1.651226963560306 \times 10^{-5}$ rad/day

A. 2 List of Observations

The following list shows all of the differential VLBI observations of ALSEP transmitters which were made with MIT differential Doppler receivers at NASA Spacecraft Tracking and Data Network (STDN) stations between Oct 1972 and June 1974. Date is the UTC date of the start of a continuous series of observations, that is, a series within which the differential Doppler counts are uninterrupted at both stations. The times are the UTC start and stop times; if the listed stop time of a series is numerically less than the start time, it is understood that the series stopped on the following UTC day. Stations are: GDS: the 85' "Apollo" station at Goldstone, California; TEX: the 30' station, now closed, at Corpus Christi, Texas; MIL: the original 30' station on Merritt Island, Florida; ETC: the original 30' station at Greenbelt, Maryland; MAD: the 85' station at Madrid, Spain; and ACN: the 30' station on Ascension Island in the South Atlantic Ocean. The first ALSEP listed is the "reference" ALSEP, that is, the one to whose carrier signal the S-band receiver was phase-locked. The second ALSEP is the one to whose carrier

signal the DDR was locked. The ALSEPs are designated by their Apollo mission numbers. A number in the Obs. Lib. Tape column identifies the MIT observation library tape on which the data from a series is written. The Series Name is formed from the day of the year and an identifying letter (series in 1973 end in A through L, those in 1974 end in M through Z).

The Notes indicate whether or not the observation series was included in the data sets processed for this thesis. If a series was not included, the reason is indicated. The key to the notes is as follows:

1 - The series was included in Data Set A.

2 - The series was included in Data Sets B and C.

3 - The series was included in Data Set C (as well as DS A).

4 - An error was made in preparing the data tapes to be used by PEP. The data are recoverable unless an error (not yet detected) of the type described by Note 5 also occurred.

5 - Valid data were not obtained due to operator error or equipment malfunction.

6 - All data taken at GDS between 22 Aug and 20 Sept 1973 were corrupted by severe fluctuations (~ 1 part in 10^{10}) in the primary frequency standard.

Date (mm/dd)	Times (hhmm)	Stations	ALSEPS	Obs.Lib. Tape	Series Name	Notes
1972						
10/28	0634-1330	MIL-GDS	12-14	10	302A	Omitted from these solutions
1973						
03/7	1350-2045	MAD-ETC	15-14	11	066G	1
03/8	1352-2048	ACN-ETC	15-14	11	067G	1
	1130-2048	ACN-MAD	15-14	11	067H	1
	1352-2214	ETC-MAD	15-14	11	067I	4
	1352-2048	ACN-ETC	15-12	12	067J	1
	1130-2048	ACN-MAD	15-12	12	067K	1
	1352-2214	ETC-MAD	15-12	12	067L	1
03/15	2038-0335	MAD-MIL	15-14	11	074G	4
	0146-0330	MAD-ACN	15-14	11	075H	5
	0146-0330	MIL-ACN	15-14	11	075I	5
	2045-0335	MAD-MIL	15-12	12	075J	5
	2045-0335	MAD-ACN	15-12	12	075K	1
	2045-0335	MIL-ACN	15-12	12	075L	5
03/22	2348-0404	ACN-MAD	15-14	11	081B	1
03/24	0215-0545	ACN-MAD	15-14	11	083B	5
	0215-0447	ACN-MAD	15-17	13	083A	5
03/28	1115-1915	GDS-TEX	15-14	11	087B	1
03/30	1135-1415	ACN-MAD	15-14	11	089D	5
	1135-1415	ACN-MAD	15-17	13	089B	5
04/3	1336-1639	TEX-MAD	15-14	11	093G	4
04/4	1454-1627	MAD-TEX	15-14	11	094G	4
04/9	1815-2330	ACN-TEX	15-17	13	099A	5
	2351-0400	ETC-TEX	15-17	13	099B	5
04/12	2115-0059	MAD-ACN	15-14	11	102A	4
	2110-0059	MAD-TEX	15-14	11	102B	4
04/13	1925-0245	ACN-MAD	15-14	49	103A	1
	1635-0245	ACN-MAD	15-16	48	103B	5

Date (mm/dd)	Times (hhmm)	Stations	ALSEPS	Obs. Lib. Tape	Series Name	Notes
04/17	2040-0300	ACN-MAD	15-14	11	107A	5
	0228-0520	MAD-TEX	15-14	11	107B	5
	0435-1215	TEX-GDS	15-14	11	107C	5
04/18	2100-0300	ACN-MAD	15-14	11	108D	5
	2100-0300	ACN-MAD	15-17	13	108A	5
	0230-0545	MAD-TEX	15-17	13	108B	1
	0435-1300	TEX-GDS	15-17	13	108C	1
07/2	1450-2035	ACN-TEX	15-14	21	183A	1
	1600-2030	TEX-GDS	15-14	21	183B	1
	2035-2335	TEX-GDS	15-14	21	183D	1
	2335-0305	TEX-GDS	15-14	21	183E	1
	2115-2330	GDS-MIL	15-17	22	183C	5
07/3	1815-0200	MIL-GDS	15-14	21	184A	1
	2015-0200	MIL-TEX	15-14	21	184B	1
	1530-2000	TEX-MAD	15-14	21	184C	5
	2005-0345	TEX-GDS	15-14	21	184D	1
	1815-0200	MIL-GDS	15-17	22	184E	4
07/5	1230-1600	MAD-ACN	15-17	22	186A	4
	1955-0315	MIL-GDS	15-12	24	186B	4
	0000-0500	GDS-TEX	15-16	23	186C	1
	1230-1700	MAD-ACN	15-16	25	186D	1
	1830-2200	MAD-ACN	15-16	25	186H	5
	1645-2200	MAD-MIL	15-16	25	186E	1
	1955-0315	MIL-GDS	15-16	25	186F	1
	1800-2315	MIL-TEX	15-16	25	186G	1
07/6	1410-2140	ACN-MAD	14-15	21	187A	5
	1715-0015	ACN-MIL	14-15	21	187B	1
	2050-0245	MIL-GDS	14-15	21	187C	5
	1410-2140	ACN-MAD	14-12	23	187D	4
	1715-0015	ACN-MIL	14-12	23	187E	4
	2050-0245	MIL-GDS	14-12	23	187F	4
07/9	2145-0245	ACN-TEX	15-16	25	190A	4
	2225-0315	MIL-TEX	15-16	25	190B	5
	0325-0730	TEX-GDS	15-16	25	190C	1
	0245-0545	MIL-GDS	15-17	22	190D	4
	2225-0235	ACN-MIL	15-17	22	190E	1

Date (mm/dd)	Times (hhmm)	Stations	ALSEPS	Obs. Lib. Tape	Series Name	Notes
07/10	2100-0115	MAD-MIL	15-14	11	191A	5
	0015-0330	MIL-GDS	15-14	11	191B	5
	2100-0115	MAD-MIL	15-16	25	191C	4
	0015-0600	MIL-GDS	15-16	25	191D	1
	0015-0600	TEX-GDS	15-16	25	191E	4
07/11	2200-0145	MAD-MIL	15-17	22	192A	4
	0200-0600	MIL-TEX	15-17	22	192B	4
	0115-0600	MIL-GDS	15-17	22	192C	4
	0115-0600	MIL-GDS	15-12	24	192D	4
07/12	1845-0050	ACN-MAD	15-16	25	193A	1
	2245-0515	ACN-MIL	15-16	25	193B	1
	0200-0630	MIL-GDS	15-16	25	193C	5
	0000-0430	MIL-TEX	15-16	25	193D	4
	0115-0515	ACN-MIL	15-12	24	193E	4
	1845-0050	ACN-MAD	15-12	24	193F	4
	0150-0630	MIL-GDS	15-12	24	193G	
07/13	1946-0330	ACN-MAD	15-17	22	194A	1
	2355-0300	ACN-MIL	15-17	22	194B	4
	0240-0553	ACN-GDS	15-17	22	194C	4
	1946-0330	ACN-MAD	15-12	24	194D	4
	2355-0300	ACN-MIL	15-12	24	194E	4
	0240-0600	ACN-GDS	15-12	24	194F	4
07/17	0220-0630	MAD-ACN	15-17	22	198A	1
	0230-0730	ACN-TEX	15-17	22	198B	1
	0415-0730	ACN-GDS	15-17	22	198C	1
	0415-1030	TEX-GDS	15-17	22	198D	4
	0220-0630	MAD-ACN	15-16	25	198E	1
	0415-0730	ACN-GDS	15-16	25	198F	5
07/18	0315-0735	TEX-MAD	15-12	24	199A	4
	0452-1415	TEX-MAD	15-12	24	199B	4
	0500-0735	GDS-MAD	15-17	22	199C	4
07/19	0345-0810	MAD-TEX	15-12	24	200A	4
	0530-1205	TEX-GDS	15-12	24	200B	4
	0530-0810	MAD-GDS	15-16	25	200C	4

Date (mm/dd)	Times (hhmm)	Stations	ALSEPS	Obs. Lib. Tape	Series Name	Notes
07/20	0000-0700	MAD-ACN	15-14	49	201A	4
	0620-0930	ACN-GDS	15-14	49	201B	4
	0620-0930	ACN-GDS	15-16	48	201C	4
	0000-0700	MAD-ACN	15-16	48	201D	4
07/23	0615-1150	TEX-ACN	12-17	26	204A	4
	1425-1850	GDS-TEX	12-17	26	204B	2
	0930-1225	ACN-GDS	12-14	21	204C	2
07/24	0230-0730	ACN-MAD	12-17	26	205A	2
	0820-1400	MAD-GDS	12-17	26	205B	4
	0820-1745	TEX-GDS	12-17	26	205C	2
	0230-0730	ACN-MAD	12-14	23	205D	4
	0820-1400	MAD-GDS	12-14	23	205E	4
07/25	0745-0912	MAD-TEX	12-17	26	206A	5
	0850-1700	GDS-TEX	12-17	26	206C	2
	1000-1515	MAD-GDS	12-14	23	206D	2
08/6	2315-0415	GDS-MIL	12-14	23	218A	4
	2318-0415	TEX-GDS	12-14	23	218B	4
	2315-0415	GDS-MIL	12-17	26	218C	5
08/8	0015-0500	MIL-GDS	15-17	22	220A	1
	0015-0500	TEX-GDS	15-17	22	220B	1
	0015-0500	MIL-GDS	15-16	25	220C	4
	0000-0330	MIL-GDS	15-17	22	220D	4
	2213-0330	MIL-TEX	15-16	25	220E	5
	0000-0330	TEX-GDS	15-16	25	220F	5
08/9	1800-2055	MAD-ACN	12-17	26	221A	4
	0055-0630	MIL-GDS	12-17	26	221B	2
	2330-0500	MIL-TEX	12-15	24	221C	1
	0240-0630	MIL-GDS	12-15	24	221F	4
	1800-2055	MAD-ACN	12-15	24	221E	4
08/14	0105-0600	MIL-ACN	12-15	24	226A	4
	0105-0600	MIL-ACN	12-14	23	226B	5
08/17	0240-0700	MIL-ACN	12-15	24	229A	4
	0240-0700	MIL-ACN	12-14	23	229B	4
08/21	0600-1305	MAD-MIL	12-14	23	233A	4
	1435-1730	MIL-GDS	12-15	24	233B	6
	0600-1100	MAD-MIL	12-17	26	233C	4
	1405-1800	GDS-TEX	12-17	26	233D	6
	1325-1730	MIL-TEX	12-17	26	233E	4

Date (mm/dd)	Times (hhmm)	Stations	ALSEPS	Obs. Lib. Tape	Series Name	Notes
08/22	0603-1400	MAD-MIL	16-17	47	234A	4
	1300-1830	MIL-GDS	16-17	47	234B	6
	0603-1400	MAD-MIL	16-15	25	234C	1
	1300-1830	MIL-GDS	16-15	25	234D	6
	1316-2000	GDS-TEX	16-15	25	234E	6
08/23	1440-1620	TEX-GDS	12-17	26	235A	6
	1700-2115	TEX-GDS	12-17	26	235B	6
08/24	0932-1440	ACN-MIL	12-15	24	236A	5
	1300-1945	MIL-GDS	12-15	24	236B	6
	0932-1440	ACN-MIL	12-14	23	236C	2
	1300-1945	MIL-GDS	12-14	23	236D	6
08/27	1502-2200	MIL-GDS	12-14	23	239A	6
	1502-2200	MIL-GDS	12-17	26	239B	6
	1502-2028	GDS-TEX	12-17	26	239C	6
08/28	1508-2300	MIL-GDS	12-14	23	240A	6
	1508-2300	MIL-GDS	12-15	24	240B	6
	1508-2130	TEX-GDS	12-15	24	240C	6
08/29	1600-2230	MIL-GDS	12-14	23	241A	6
	1600-2230	MIL-GDS	12-15	24	241B	6
	1600-2100	TEX-GDS	12-15	24	241C	6
08/30	1633-2130	MIL-GDS	12-17	26	242A	6
	1636-2130	MIL-GDS	12-16	34	242B	6
	1508-2000	MIL-TEX	12-16	34	242C	2
09/3	1830-2400	ACN-MIL	12-15	24	246A	1
	1830-2400	ACN-MIL	12-14	23	246B	2
09/10	0005-0400	MIL-MAD	15-16	48	253A	1,3
	2352-0400	MIL-MAD	15-14	49	253B	5
09/11	2345-0450	MAD-MIL	15-16	48	254A	1,3
	0600-1015	MIL-GDS	15-16	48	254B	6
	0605-1200	TEX-GDS	15-16	48	254C	6
	2345-0445	MAD-MIL	15-17	46	254D	1
	0600-1015	MIL-GDS	15-17	46	254E	6
09/13	0015-0530	MAD-MIL	15-17	46	256A	1
	0500-1030	MIL-TEX	15-17	46	256B	1
	0630-1255	GDS-TEX	15-17	46	256C	6
	0015-0530	MAD-MIL	15-14	49	256D	1
	0620-1030	MIL-GDS	15-14	49	256E	6

Date (mm/dd)	Times (hhmm)	Stations	ALSEPS	Obs. Lib. Tape	Series Name	Notes
09/14	0125-0550	MAD-ACN	12-15	32	257A	1
	0034-0630	MIL-MAD	12-15	32	257B	1
	0605-1200	MIL-GDS	12-15	32	257C	6
	0125-0550	MAD-ACN	12-14	33	257D	2
	0100-0630	MIL-MAD	12-14	33	257E	2
	0605-1200	MIL-GDS	12-14	33	257F	6
09/15	0115-0700	ACN-MAD	12-16	34	258A	4
	0115-0700	ACN-MAD	12-17	31	258B	5
09/17	0640-1200	MIL-TEX	12-15	32	260A	5
	0858-1330	GDS-TEX	12-15	32	260B	6
	0858-1200	MIL-GDS	12-14	33	260C	6
09/18	0510-1200	MIL-TEX	12-17	31	261A	2
09/19	0540-0930	MIL-TEX	12-17	31	262A	4
	0935-1500	MIL-GDS	12-17	31	262B	6
	0630-1500	MIL-GDS	12-14	33	262C	6
09/20	1126-1340	MIL-GDS	12-15	32	263A	6
	1013-1230	MIL-GDS	12-16	34	263B	6
	1235-1430	MIL-GDS	12-16	34	263C	6
09/24	0930-1530	ACN-MIL	12-15	32	267A	1
	0930-1530	ACN-MIL	12-17	31	267B	4
09/26	1230-1645	MAD-MIL	12-17	31	269A	4
	1352-2200	MIL-TEX	12-17	31	269B	2
	1230-1645	MAD-MIL	12-15	32	269C	1
09/27	0830-1730	ACN-MAD	12-17	31	270A	2
	1350-1900	ACN-MIL	12-17	31	270B	2
	0830-1730	ACN-MAD	12-16	34	270C	2
	1350-1900	ACN-MIL	12-16	34	270D	2
09/28	0916-1800	ACN-MAD	12-16	34	271A	2
	1402-2000	ACN-MIL	12-16	34	271B	4
	0916-1800	ACN-MAD	12-14	33	271C	2
	1402-2000	ACN-MIL	12-14	33	271D	2
10/1	1720-2245	ACN-MIL	12-16	34	274A	4
	2235-0130	MIL-TEX	12-16	34	274B	2
	1720-2245	ACN-MIL	12-15	32	274C	1
10/2	1720-2100	MIL-MAD	12-15	32	275A	1
	2100-0230	MIL-TEX	12-15	32	275B	1
	1720-2100	MIL-MAD	12-16	34	275C	2

Date (mm/dd)	Times (hhmm)	Stations	ALSEPS	Obs. Lib. Tape	Series Name	Notes
10/3	1820-2200	MIL-MAD	12-15	32	276A	1
	2010-0300	MIL-TEX	12-15	32	276B	1
	1835-2200	MIL-MAD	12-14	33	276C	4
10/4	1930-2300	ACN-MAD	12-16	34	277A	4
	1930-2300	ACN-MIL	12-16	34	277B	4
	0025-0400	MIL-TEX	12-16	34	277C	5
	1930-2300	ACN-MAD	12-14	33	277D	2
	1930-2300	ACN-MIL	12-14	33	277E	2
10/5	1730-2200	ACN-MAD	12-17	31	278A	2
	1923-2400	MAD-MIL	12-17	31	278B	5
	1730-2200	ACN-MAD	12-14	33	278C	2
	1923-2400	MAD-MIL	12-14	33	278D	4
10/16	0300-0700	ACN-MIL	12-15	32	289A	1
	0300-0700	ACN-MIL	12-14	33	289B	2
10/22	0950-1430	ACN-MIL	12-17	31	295A	4
	0950-1430	ACN-MIL	12-16	34	295B	2
10/25	1140-1600	MAD-MIL	12-15	32	298A	1
	1140-1600	MAD-MIL	12-14	33	298B	2
11/2	1500-2200	MAD-ACN	12-17	31	306A	4
	1905-2230	MAD-MIL	12-17	31	306B	4
	1500-2200	MAD-ACN	12-14	33	306C	2
	1905-2230	MAD-MIL	12-14	33	306D	2
11/5	2320-0600	MIL-GDS	16-17	47	309A	2
	2325-0600	MIL-GDS	16-15	48	309B	1,3
11/7	0000-0700	MIL-GDS	16-17	47	311A	2
	0000-0700	MIL-GDS	16-15	48	311B	1,3
	2130-0300	MAD-MIL	12-17	31	311C	4
	0030-0550	MIL-GDS	12-17	31	311D	4
	2130-0300	MAD-MIL	12-14	33	311E	4
	0030-0800	MIL-GDS	12-14	33	311F	2
11/8	1832-0415	MAD-ACN	12-15	32	312A	4
	2150-0500	MAD-MIL	12-15	32	312B	4
	0030-0700	MIL-GDS	12-15	32	312C	4
	1832-0415	MAD-ACN	12-14	33	312D	4
	2150-0500	MAD-MIL	12-14	33	312E	2
	0030-0700	MIL-GDS	12-14	33	312F	2

Date (mm/dd)	Times (hhmm)	Stations	ALSEPS	Obs. Lib. Tape	Series Name	Notes
11/9	1934-0500	MAD-ACN	12-16	34	313A	4
	2202-0400	MAD-MIL	12-16	34	313B	2
	0045-0600	MAD-GDS	12-16	34	313C	2
	1945-0500	MAD-ACN	12-15	32	313D	4
	2202-0400	MAD-MIL	12-15	32	313E	1
	0045-0600	MAD-GDS	12-15	32	313F	1
11/27	0500-1830	MAD-MIL	12-15	44	331A	1
	1500-1830	MAD-MIL	12-14	42	331B	2
11/28	1545-1945	MAD-MIL	12-17	41	332A	2
	1545-1940	MAD-MIL	12-16	43	332B	2
11/29	1700-2000	MAD-ACN	12-17	41	333A	5
	1700-2200	MIL-ACN	12-17	41	333B	5
	2155-0115	MIL-GDS	12-17	41	333C	2
	1756-2000	MAD-ACN	12-16	43	333D	5
	1756-2115	MIL-ACN	12-16	43	333E	5
	2155-0115	MIL-GDS	12-16	43	333F	5
11/30	1750-2130	MAD-MIL	12-15	44	334A	1
	2145-0230	MIL-GDS	12-15	44	334B	1
	1745-2130	ACN-MAD	12-14	42	334C	4
	1715-2130	MAD-MIL	12-14	42	334D	5
	2145-0230	MIL-GDS	12-14	42	334E	5
12/1	1645-2100	ACN-MAD	12-15	44	335A	1
	1645-2100	ACN-MAD	12-14	42	335B	2
12/3	2305-0400	MIL-GDS	15-17	46	337A	4
	2305-0400	MIL-GDS	15-16	45	337B	4
12/4	1915-0030	MIL-MAD	15-17	46	338A	4
	2315-0600	MIL-GDS	15-17	46	338B	4
	1915-0030	MIL-MAD	15-16	45	338C	4
	2309-0600	MIL-GDS	15-16	45	338D	4
12/6	0218-0650	MIL-GDS	15-16	45	340A	4
	0218-0650	MIL-GDS	15-16	45	340B	1,3

Date (mm/dd)	Times (hhmm)	Stations	ALSEPS	Obs. Lib. Tape	Series Name	Notes
12/7	0230-0645	MIL-GDS	12-17	41	340C	4
	0230-0645	MIL-GDS	12-14	42	340D	4
12/20	1426-1830	MIL-GDS	12-17	41	354A	5
	1426-1830	MIL-GDS	12-14	42	354B	2
12/21	1330-1915	MIL-GDS	12-15	44	355A	1
	1321-1915	MIL-GDS	12-16	43	355B	2
1974						
01/9	0345-1515	MAD-MIL	12-17	41	009M	4
	0345-1515	MAD-MIL	12-17	41	009N	4
	0530-1200	MIL-GDS	12-17	41	009P	5
	0530-1200	MIL-GDS	12-17	41	009Q	2
01/10	0215-0600	MAD-MIL	15-16	45	010M	1,3
	0455-1100	MIL-GDS	15-16	45	010N	1,3
	0215-0600	MAD-MIL	15-12	44	010P	1
	0500-1100	MIL-GDS	15-12	44	010Q	1
01/11	0200-0600	MAD-MIL	14-12	42	011M	2
	0605-1100	MIL-GDS	14-12	42	011N	4
	0200-0600	MAD-MIL	14-12	42	011P	4
	0605-1100	MIL-GDS	14-12	42	011Q	2
01/28	2215-0230	MIL-GDS	12-16	43	028M	2
	2215-0230	MIL-GDS	12-14	42	028N	2
01/30	1800-2400	MAD-MIL	12-17	41	030M	5
	2112-0400	MIL-GDS	12-17	41	030N	4
	1800-2400	MAD-MIL	12-14	42	030P	2
	2112-0400	MIL-GDS	12-14	42	030Q	2
02/1	1850-2400	MAD-MIL	16-17	47	032M	4
	2100-0145	MIL-GDS	16-17	47	032N	4
	2100-0145	MIL-GDS	16-15	45	032P	4
02/2	1746-2200	MAD-ACN	16-17	47	033M	5
	1900-2200	MAD-ACN	16-15	45	033N	5
02/15	0515-1000	ACN-MAD	12-17	41	046M	5
	0447-1000	ACN-MAD	12-16	43	046N	4
02/16	0430-1000	ACN-MAD	15-17	46	047M	5
	0425-1000	ACN-MAD	15-16	45	047N	4

Date (mm/dd)	Times (hhmm)	Stations	ALSEPS	Obs. Lib. Tape	Series Name	Notes
02/20	1405-1710	MIL-GDS	12-15	44	051N	5
02/21	1015-1700	MAD-ACN	12-17	41	052M	5
	1400-1800	ACN-MIL	12-17	41	052N	2
	1500-2200	MIL-GDS	12-17	41	052P	2
	1135-1700	MAD-ACN	12-16	43	052Q	4
	1352-1800	ACN-MIL	12-16	43	052R	2
	1454-2200	MIL-GDS	12-16	43	052S	2
02/22	1200-1745	ACN-MAD	12-15	44	053M	1
	1400-1800	ACN-MIL	12-15	44	053N	1
	1509-2200	MIL-GDS	12-15	44	053P	4
	1200-1745	ACN-MAD	12-14	42	053Q	2
	1400-1800	ACN-MIL	12-14	42	053R	2
	1500-2200	MIL-GDS	12-14	42	053S	2
02/23	1200-1830	ACN-MAD	12-17	41	054M	5
	1200-1830	ACN-MAD	12-14	42	054N	5
02/25	1348-2030	ACN-MIL	12-17	41	056M	2
	1700-0100	MIL-GDS	12-17	41	056N	2
	1348-2030	ACN-MIL	12-16	43	056P	2
	1700-0100	MIL-GDS	12-16	43	056Q	2
02/26	2317-0200	MIL-GDS	12-15	44	057M	4
	2317-0200	MIL-GDS	12-16	43	057N	4
02/27	1745-0300	MIL-GDS	12-15	44	058M	1
	1745-0300	MIL-GDS	12-14	42	058N	2
02/28	1615-2007	ACN-MIL	12-17	41	059M	5
	2010-0300	MIL-GDS	12-17	41	059N	2
	1615-2100	ACN-MIL	12-14	42	059P	4
	1824-0300	MIL-GDS	12-14	42	059Q	2
03/4	2235-0300	MIL-GDS	15-17	46	063M	5
	2235-0300	MIL-GDS	15-16	45	063N	1,3
03/15	0240-0745	ACN-MAD	12-17	50	074M	5
	0240-0910	ACN-MAD	12-14	51	074N	2

Date (mm/dd)	Times (hhmm)	Stations	ALSEPS	Obs. Lib. Tape	Series Name	Notes
03/22	1300-1630	MAD-MIL	12-15	52	081M	1
	1300-1630	MAD-MIL	12-16	53	081P	2
03/26	0955-1425	ACN-MAD	16-17	54	085M	2
	1315-1715	MAD-MIL	16-17	54	085N	2
	0955-1425	ACN-MAD	16-15	55	085P	1,3
	1315-1715	MAD-MIL	16-15	55	085Q	1,3
03/27	1720-2200	MAD-MIL	15-14	56	086M	1
	1110-1630	MAD-ACN	15-16	55	086N	1,3
	1400-2200	MAD-MIL	15-16	55	086P	1,3
04/1	2136-0200	ACN-MAD	16-17	54	091M	5
	2040-0200	ACN-MIL	16-17	54	091N	5
	2136-0200	ACN-MAD	16-15	55	091P	4
	2040-0200	ACN-MIL	16-15	55	091Q	1,3
04/2	2010-0200	MAD-ACN	16-17	54	092M	5
	2010-0200	MAD-MIL	16-17	54	092N	2
	2010-0200	MAD-ACN	16-15	55	092P	1,3
	2010-0200	MAD-MIL	16-15	55	092Q	1,3
04/9	0000-0630	ACN-MAD	14-12	51	099M	4
	0000-0630	ACN-MAD	14-15	56	099N	4
	2300-0415	ACN-MAD	12-14	51	099P	2
	2315-0415	ACN-MAD	12-17	50	099Q	5
04/16	0400-1230	MAD-ACN	17-16	54	106M	2
	0400-1230	MAD-ACN	17-15	57	106N	4
04/22	1320-1845	MAD-MIL	17-15	57	112M	5
	1250-1845	MAD-MIL	17-16	54	112N	5
04/23	1445-2330	GDS-MIL	15-12	52	113M	1
	1445-2330	GDS-MIL	15-14	56	113N	1
04/24	1500-1930	ACN-MAD	17-15	57	114M	1
	1455-1904	ACN-MAD	17-16	54	114N	2
04/29	1845-2312	ACN-MAD	16-12	53	119M	5
	1845-2400	MAD-MIL	16-12	53	119N	5
	1845-2312	ACN-MAD	16-17	54	119P	5
	1845-2400	MAD-MIL	16-17	54	119Q	5

Date (mm/dd)	Times (hhmm)	Stations	ALSEPS	Obs. Lib. Tape	Series Name	Notes
04/30	1715-2300	ACN-MAD	16-12	53	120M	4
	1715-2300	ACN-MAD	16-17	54	120N	4
05/1	1955-2400	MAD-MIL	16-15	55	121M	5
	1955-2400	MAD-MIL	16-17	54	121N	5
05/11	0128-0800	ACN-MAD	14-12	51	131M	5
	0128-0800	ACN-MAD	14-15	56	131N	5
05/12	0145-0800	ACN-MAD	12-15	52	132M	5
	0150-0800	ACN-MAD	12-17	50	132N	5
05/13	0126-0700	ACN-MAD	12-14	51	133M	5
	0126-0700	ACN-MAD	12-17	50	133N	5
05/15	0228-0850	ACN-MAD	16-15	55	135M	5
	0228-0850	ACN-MAD	16-17	54	135N	5
05/17	1300-1845	GDS-MIL	12-15	52	137M	5
	1627-1845	GDS-MIL	12-17	50	137N	5
05/20	1155-1600	MAD-ACN	16-17	54	140M	5
	1830-2200	MIL-GDS	16-17	54	140N	5
	1155-1600	MAD-ACN	16-12	53	140P	4
	1830-2200	MIL-GDS	16-12	53	140Q	2
05/21	1908-2315	MIL-GDS	15-16	55	141M	5
	1908-2315	MIL-GDS	15-14	56	141N	1
05/22	1115-1800	MAD-ACN	15-16	55	142M	4
	1115-1800	MAD-ACN	15-14	56	142N	1
05/27	1240-2000	MAD-ACN	12-14	51	147M	5
	1245-2000	MAD-ACN	12-15	52	147N	1
05/28	1830-2200	MAD-MIL	12-14	51	148M	5
	1830-2200	MAD-MIL	12-16	53	148N	5
05/30	2100-0100	MAD-MIL	16-15	55	150M	1,3
	2210-0210	MIL-ACN	16-15	55	150N	1,3
	2100-0100	MAD-MIL	16-17	54	150P	5
	2210-0210	MIL-ACN	16-17	54	150Q	2

Date (mm/dd)	Times (hhmm)	Stations	ALSEPS	Obs. Lib. Tape	Series Name	Notes
06/5	0110-0400	ACN-MAD	16-15	55	156M	5
	0110-0400	ACN-MAD	16-15	55	156N	4
06/7	0005-0600	ACN-MAD	16-15	55	158M	4
	0005-0600	ACN-MAD	16-12	53	158N	2
06/11	0215-0935	MAD-ACN	12-15	52	162M	1
	0215-0935	MAD-ACN	12-14	51	162N	2
06/13	0215-1115	ACN-MAD	12-17	50	164M	5
	0215-1115	ACN-MAD	12-16	53	164N	2
06/17	1300-2000	MIL-GDS	16-17	54	168M	5
	1300-2000	MIL-GDS	16-12	53	168N	2
06/18	0725-1430	MAD-ACN	16-17	54	169M	4
	0725-1430	MAD-ACN	16-12	53	169N	4
06/19	0700-1335	MAD-ACN	15-14	56	170M	1
	0700-1330	MAD-ACN	15-17	57	170N	4
06/20	1830-2230	MIL-GDS	15-14	56	171M	5
	1830-2230	MIL-GDS	15-17	57	171N	1

A.3 Derivation of Terms in the Differential N-Count Observable Resulting from the Moon's Horizontal Parallax

This appendix presents the derivation of Equation (2.2.8) which includes the effect of horizontal parallax in the differential N-count observable for the case where both the tracking stations and the ALSEPs lie in the plane of the earth's equator. Figure A.3.1 shows the geometry for a single station observing a single transmitter on the moon.

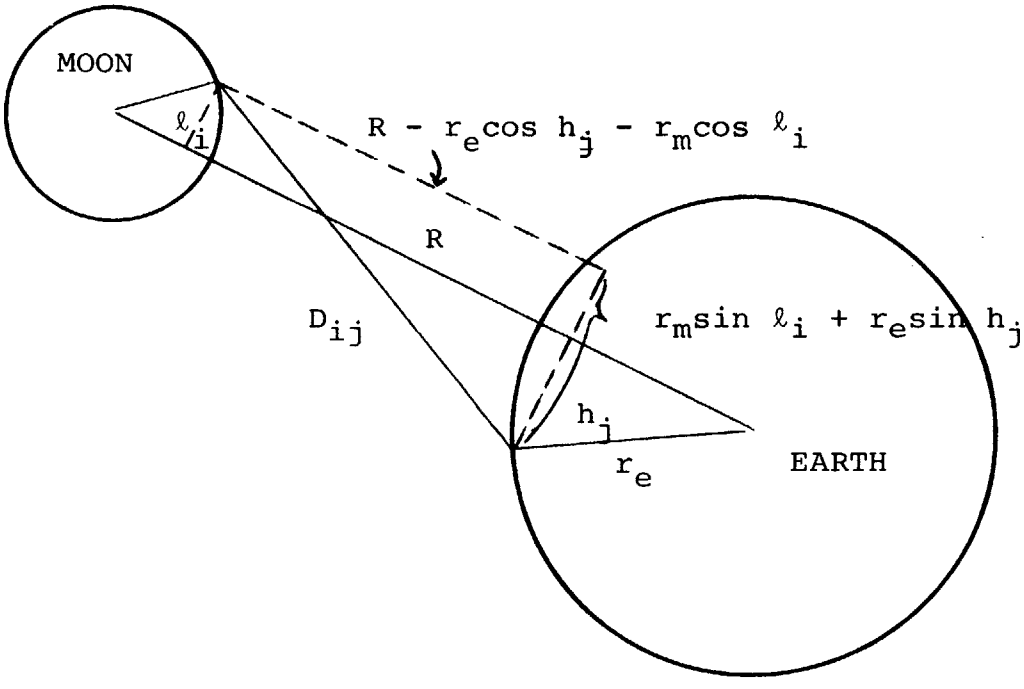


Figure A.3.1

In the figure, R is the earth-moon center-to-center distance, r_e is the earth's radius, r_m is the moon's radius, ℓ_i is the selenocentric longitude of the transmitter, and h_j is the hour angle of the moon at the tracking station. The differential fringe phase, or differential N-count, may be written

$$\Delta\phi(t) = \frac{\omega}{c}\{[D_{11}(t) - D_{12}(t)] - [D_{21}(t) - D_{22}(t)]\} \quad (A.3.1)$$

where $D_{ij}(t)$ is the distance from transmitter i to station j. Here, and in the remainder of this Appendix, the constant term $\Delta\phi_o$, which accounts for the initial counter readings is omitted for simplicity.

$$\begin{aligned} D_{11} &= (R - r_e\cos h_1 - r_m\cos \ell_1)^2 + (r_m\sin \ell_1 + r_e\sin h_1)^2 \\ &= R^2 + r_e^2\cos^2 h_1 + r_m^2\cos^2\ell_1 - 2Rr_e\cos h_1 - 2Rr_m\cos \ell_1 \\ &\quad + 2r_er_m\cos h_1\cos \ell_1 + r_m^2\sin^2\ell_1 + r_e^2\sin^2 h_1 \\ &\quad + 2r_mr_e\sin \ell_1\sin h_1 \end{aligned} \quad (A.3.2)$$

By combining terms and using the identities $\sin^2 x + \cos^2 x = 1$ and $\cos(x - y) = \cos x \cos y + \sin x \sin y$, Equation (A.3.2) can be written

$$\begin{aligned} D_{11}^2 = R^2[1 &+ (\frac{r_e}{R})^2 + (\frac{r_m}{R})^2 - 2(\frac{r_e}{R})\cos h_1 - 2(\frac{r_m}{R})\cos \ell_1 \\ &+ 2(\frac{r_er_m}{R^2})\cos(\ell_1 - h_1)] \end{aligned} \quad (A.3.3)$$

Since $(\frac{r_e}{R}) \approx .017$ and $(\frac{r_m}{R}) \approx .004$, the expression in brackets in Equation (A.3.3) has the form $(1 + x)$ with $|x| << 1$, and we can use the expansion $(1 + x)^{1/2} = 1 + \frac{1}{2}x - \frac{1}{8}x^2 + \frac{1}{16}x^3 \ldots$ for the square root of D_{11}. Expanding, and retaining all terms through order $(r/R)^3$, where r is r_e or r_m, we obtain

$$
\begin{aligned}
D_{11} = R[1 &+ \tfrac{1}{2}(\tfrac{r_e}{R})^2 + \tfrac{1}{2}(\tfrac{r_m}{R})^2 - (\tfrac{r_e}{R})\cos h_1 - (\tfrac{r_m}{R})\cos \ell_1 \\
&+ (\tfrac{r_e r_m}{R^2})\cos(\ell_1 - h_1) - \tfrac{1}{2}(\tfrac{r_e}{R})^2\cos^2 h_1 - \tfrac{1}{2}(\tfrac{r_m}{R})^2\cos^2 \ell_1 \\
&- (\tfrac{r_e r_m}{R^2})\cos h_1 \cos \ell_1 + (\tfrac{r_e^2 r_m}{R^3})\cos h_1 \cos(\ell_1 - h_1) \\
&+ (\tfrac{r_e r_m^2}{R^3})\cos \ell_1 \cos(\ell_1 - h_1) + \tfrac{1}{2}(\tfrac{r_e}{R})^3\cos h_1 \\
&+ \tfrac{1}{2}(\tfrac{r_m}{R})^3\cos \ell_1 + \tfrac{1}{2}(\tfrac{r_e r_m^2}{R^3})\cos h_1 + \tfrac{1}{2}(\tfrac{r_e^2 r_m}{R^3})\cos \ell_1 \\
&+ \tfrac{1}{2}(\tfrac{r_e}{R})^3\cos^3 h_1 - \tfrac{1}{2}(\tfrac{r_m}{R})^3\cos^3 \ell_1 - \tfrac{3}{2}(\tfrac{r_e^2 r_m}{R^3})\cos^2 h_1 \cos \ell_1 \\
&- \tfrac{3}{2}(\tfrac{r_e r_m^2}{R^3})\cos h_1 \cos^2 \ell_1] \qquad \text{(A.3.4)}
\end{aligned}
$$

Equation (A.3.4) may be used to write down the expression for D_{12}, D_{21}, and D_{22} simply by changing the subscripts on h and ℓ. When the double difference $[(D_{11} - D_{12}) - (D_{21} - D_{22})]$ is formed, all terms which contain only tracking station arguments, h_1 or h_2, or which contain

only ALSEP arguments, ℓ_1 or ℓ_2, will cancel. Retaining only the "mixed" terms of Equation (A.3.4) yields

$$\Delta\phi = \frac{\omega}{c}[(D_{11} - D_{12}) - (D_{21} - D_{22})]$$

$$= \frac{\omega R}{c}\{(\frac{r_e r_m}{R^2})[\cos(\ell_1 - h_1) - \cos(\ell_1 - h_2)$$

$$- \cos(\ell_2 - h_1) + \cos(\ell_2 - h_2) - \cos h_1 \cos \ell_1$$

$$+ \cos h_2 \cos \ell_1 + \cos h_1 \cos \ell_2 - \cos h_2 \cos \ell_2]$$

$$+ (\frac{r_e^2 r_m}{R^3})[\cos h_1 \cos(\ell_1 - h_1) - \cos h_2 \cos(\ell_1 - h_2)$$

$$- \cos h_1 \cos(\ell_2 - h_1) + \cos h_2 \cos(\ell_2 - h_2)$$

$$- \tfrac{3}{2}\cos^2 h_1 \cos \ell_1 + \tfrac{3}{2}\cos^2 h_2 \cos \ell_1 + \tfrac{3}{2}\cos^2 h_1 \cos \ell_2$$

$$- \tfrac{3}{2}\cos^2 h_2 \cos \ell_2] + (\frac{r_e r_m^2}{R^3})[\cos \ell_1 \cos(\ell_1 - h_1)$$

$$- \cos \ell_1 \cos(\ell_1 - h_2) - \cos \ell_2 \cos(\ell_2 - h_1)$$

$$+ \cos \ell_2 \cos(\ell_2 - h_2) - \tfrac{3}{2}\cos h_1 \cos^2 \ell_1$$

$$+ \tfrac{3}{2}\cos h_2 \cos^2 \ell_1 + \tfrac{3}{2}\cos h_1 \cos^2 \ell_2 - \tfrac{3}{2}\cos h_2 \cos^2 \ell_2]\} \qquad (A.3.5)$$

The expression can be simplified by defining the quantities

$$h = \frac{1}{2}(h_1 + h_2) \qquad \ell = \frac{1}{2}(\ell_1 + \ell_2)$$

$$\Delta h = h_2 - h_1 \qquad \Delta\ell = \ell_2 - \ell_1$$

By substituting in Equation (A.3.5) the expressions $h_2 = h_1 + \Delta h$ and $\ell_2 = \ell_1 + \Delta\ell$ and using the identities $\sin(x \pm y) = \sin x \cos y \pm \sin y \cos x$ and $\cos(x \pm y) = \cos x \cos y \mp \sin x \sin y$, we obtain after much algebra the result

$$\Delta\phi = \frac{4\omega r_e r_m}{cR}[\sin\Delta\ell/2 \sin\Delta h/2 \cos \ell \cos h + \frac{1}{4}(\frac{r_e}{R})\sin\Delta\ell/2 \sin\Delta h(2\cos \ell \cos 2h - \sin \ell \sin 2h) + \frac{1}{4}(\frac{r_m}{R})\sin\Delta\ell \sin\Delta h/2(2\cos h \cos 2\ell - \sin h \sin 2\ell)] \quad (A.3.6)$$

This expression may be rewritten in terms of the parameters of Equation (2.2.7) by noting that $2r_e \sin \Delta h/2 = B$, $2(\frac{r_m}{R})\sin \Delta\ell/2 \cos \ell = \Delta\alpha$, $\sin \Delta h = 2\sin \Delta h/2 \cos \Delta h/2 = PB/r^2$, and $\cos h = \sin(\alpha - A)$. Making these substitutions and making explicit the time dependence of the diurnally varying arguments allows Equation (A.3.6) to be written as

$$\Delta\phi(t) = \frac{\omega B\Delta\alpha}{c}\{\sin(\alpha - A(t)) + \frac{P}{R}[\sin 2(\alpha - A(t)) - \frac{1}{2}\tan \ell \cos 2(\alpha - A(t))] + \frac{r_m}{R}\frac{\cos \Delta\ell/2 \cos 2\ell}{\cos \ell}[\sin(\alpha - A(t)) - \frac{1}{2}\tan 2\ell \cos(\alpha - A(t))]\} \quad (A.3.7)$$

REFERENCES

1. Abbot, R. I., P. J. Shelus, J. D. Mulholland and E. C. Silverberg, 1973. "Laser Observations of the Moon: Identification and Construction of Normal Points for 1969-1971", Astron. J. 78, 784.

2. Ash, M. E., 1965. "Generation of Planetary Ephemerides on an Electronic Computer", Lincoln Lab. TR 391, Lexington, Mass.

3. Ash, M. E., 1965. "Generation of the Lunar Ephemeris on an Electronic Computer", Lincoln Lab. TR 400, Lexington, Mass., 36 pp.

4. Ash, M. E., I. I. Shapiro and W. B. Smith, 1967. "Astronomical Constants and Planetary Ephemerides Deduced from Radar and Optical Observations", Astron. J. 72, 338-349.

5. Ash, M. E., I. I. Shapiro and W. B. Smith, 1971. "The System of Planetary Masses", Science, 174, 551-556.

6. Ash, M. E., 1972. "Determination of Earth Satellite Orbits", Lincoln Lab. TN 1972-5, Lexington, Mass., 258 pp.

7. Bender, P. L., D. G. Currie, R. H. Dicke, D. H. Eckhardt, J. E. Faller, W. M. Kaula, J. D. Mulholland, H. H. Plotkin, S. K. Poultney, E. C. Silverberg, D. T. Wilkinson, J. G. Williams and C. O. Alley, 1973. "The Lunar Laser Ranging Experiment", Science 182, 229-238.

8. Cannell, W. D. 1975. Defense Mapping Agency Aerospace Center, private communication. The preliminary coordinates were determined by R. M. Batson, U.S.G.S. Center of Astrogeology, Flagstaff, Arizona.

9. Cassini, J., 1693. Traite de l'Origine et de Progres de L'Astronomie, reprinted in Memoires de l'Academie Royale des Sciences 8, p. 41, 1730.

10. Chao, C. C., 1971. "Improved Tables for Mapping Tropospheric Zenith Range Effects Down to Lower Elevation Angles", private communication.

11. Counselman, C. C., III, H. F. Hinteregger and I. I. Shapiro, 1972. "Astronomical Applications of Differential VLBI", Science 178, 607-608.

12. Counselman, C. C. III, and H. F. Hinteregger, 1973. "Digital Single-sideband Mixer", Proceedings of the IEEE 61, 478.

13. Counselman, C. C., III, H. F. Hinteregger, R. W. King and I. I. Shapiro, 1973. "Precision Selenodesy via Differential Interferometry", Science 181, 772.

14. Counselman, C. C.,III, H. F. Hinteregger, R. W. King and I. I. Shapiro, 1973. "Lunar Baselines and Libration from Differential VLBI Observations of ALSEPs", The Moon 8, 484-489.

15. Eckhardt, D. H., 1970. "Lunar Libration Tables", The Moon 1, 264-274.

16. Eckhardt, D. H., 1973. "Physical Librations Due to the Third and Fourth Degree Harmonics of the Lunar Gravity Potential", The Moon 6, 127-134.

17. Explanatory Supplement to the Ephemeris, 1961. H. M. Nautical Almanac Office, London, 505 pp.

18. Frankston, M. J., 1973. "Error Analysis of Differential Interferometric Determination of ALSEP Relative Positions and Lunar Libration", General Examination Paper, Department of Earth and Planetary Sciences, M.I.T., not published.

19. King, R. W., C. C. Counselman, III, H. F. Hinteregger and I. I. Shapiro, 1973. "Study of Lunar Librations Using Differential Very-Long-Baseline Observations of ALSEPs", Proceedings of 10th Anniversary Meeting of the Society for Engineering Science, Raleigh, N. C., Nov. 5-7, in print.

20. Koziel, K., 1962. "Libration of the Moon", in Physics and Astronomy of the Moon, Z. Kopal, ed., Academic Press, New York and London.

21. Liu, A. S. and P. A. Laing, 1971. "Lunar Gravity Analysis from Long-Term Effects", Science 173, 1017-1020.

22. Michael, W. H. and Blackshear, W. T., 1972. "Recent Results on the Mass, Gravitational Field and Moments of Inertia of the Moon", The Moon, 3, 388-401.

23. Moutsoulas, M. D., 1971, "Librations of the Lunar Globe", in Physics and Astronomy of the Moon, 2d Edition, ed. by Z. Kopal, Academic Press, New York, p. 29.

24. Moyer, T. D., 1971. "The Double Precision Orbit Determination Program, (DPODP)", Jet Propulsion Laboratory TR 32-1527, Pasadena, Calif., 160 pp.

25. Ondrasik, V. J. and K. H. Rourke, 1971. "Applications of Quasi-VLBI Tracking Data Types to the Zero Declination and Process Noise Problems", AAS Paper No. 71.399, presented at AAS/AIAA Astrodynamics Specialists Conference, Ft. Lauderdale, Fla., Aug 17-19.

26. Pfeiffer, G. W., 1969. "Calculation of the Phase Delay, Group Delay, and Doppler Shift of a Radio Wave Traversing the Ionosphere and the Non-Ionized Atmosphere", B. S. Thesis, Dept. of Physics, M.I.T., Cambridge, Mass.

27. Rogers, A. E. E., 1971. "Broad-Band Passive 90° RC Hybrid with Low Component Sensitivity for Use in the Video Range of Frequencies", Proceedings of the IEEE, 59, 1617.

28. Ryan, J. W., 1973. Private communication.

29. Salzberg, I. M., 1972. Private communication.

30. Schimerman, L.A., et al., 1975. "The Relative Position of the Apollo 15 Lunar Ranging Retroreflector and the ALSEP Central Station", NASA Contractor Report, Defense Mapping Agency Aerospace Center, St. Louis, Mo., in preparation.

31. Schimerman, L.A., 1975, Defense Mapping Agency, Aerospace Center, private communication.

32. Shapiro, I.I., R.D. Reasenberg, H.F. Hinteregger and C.C. Counselman, III, 1971. "Error Analysis for ALSEP Baseline Determination via the Double-Difference Technique", M.I.T., unpublished memo.

33. Shelus, P.J., J.D. Mulholland and E.C. Silverberg, 1975. "Laser Observations of the Moon: Normal Points for 1972", Astron. J., 80, 154.

34. Shelus, P.J., 1974. Normal Points from Lunar Laser Observations of the Moon, Jan 1973-July 1974, private communication.

35. Sjogren, W.L., 1971. "Lunar Gravity Estimate: Independent Confirmation", J. Geophys. Res., 76, 7021-7026.

36. Slade, M.A., 1971. "The Orbit of the Moon", M.I.T. Ph.D. Thesis, 280 pp.

37. Slade, M.A. and R.A. Preston, 1974, private communication.

38. Solloway, C.B., 1967. "Elements of the Theory of Orbit Determination", Jet Propulsion Lab. EPD-255, Pasadena, Calif., 120 pp.

39. "USB Frequency Offsets Relative to the U.S. Naval Observatory", 1972. In "STDN Metric Tracking Performance Apollo 16, Final Report", Document X-832-72-203, Goddard Space Flight Center, Greenbelt, Md., p. 135.

40. Williams, J.G., D.H. Eckhardt, W.M. Kaula, and M.A. Slade, 1973. "Lunar Physical Librations and Laser Ranging", The Moon, 8, 469.

41. Williams, J.G. and W.S. Sinclair, 1974. "Lunar Libration Tape 5", Jet Propulsion Laboratory, Pasadena, Calif., unpublished memo.

42. Williams, J. G., 1975. "Geodetic Results from Lunar Laser Ranging", EOS, 56, No. 4, p. 236.

43. Williams, J. G., 1975. Private communication.

44. Winn, F. B., 1969. "Lunar Landed Surveyor: SPODP Lunar Libration Sensitivities", in Space Programs Summary 37-56, Vol. II, Jet Propulsion Laboratory, Pasadena, Calif., p. 74.

45. Zielenbach, J. W., et al., 1973. "Differenced Radiometric Data as a Countermeasure for the Process Noise Problem", Tech. Rep. 32-1586, JPL, Pasadena, Calif., Nov. 13.

BIOGRAPHICAL NOTE

Robert Wilson King, Jr. was born in Fayetteville, North Carolina, on February 8, 1947. He attended public schools in that city until his graduation from high school in 1965. His undergraduate education was a combined program in physics and aerospace engineering at Davidson College (1965-1968) and North Carolina State University (1968-1970).

The author's graduate studies at M.I.T. have been with the Department of Aeronautics and Astronautics and in association with the Department of Earth and Planetary Sciences. His interests have been primarily in the fields of dynamical and positional astronomy, geodesy, spacecraft tracking, and estimation theory. In June 1974 he began active duty in the United States Air Force and has worked since that time in geodetic research at the Air Force Cambridge Research Laboratories, Bedford, Massachusetts.

He was married to Mary Etta Eyler of Wilmington, Delaware, in August, 1970. His wife is a resident in pediatrics at the Massachusetts General Hospital.